

Electronic Thesis and Dissertation Repository

4-8-2019 2:00 PM


Microwave and Ultrasonic Assisted Synthesis of zeolites from Coal Fly Ash in Batch and Circulating Batch Operation

Tahani Hassn Aldahri
The University of Western Ontario

Supervisor
Prof. Sohrab, Rohani
The University of Western Ontario

Graduate Program in Chemical and Biochemical Engineering
A thesis submitted in partial fulfillment of the requirements for the degree in Doctor of Philosophy
© Tahani Hassn Aldahri 2019

Follow this and additional works at: <https://ir.lib.uwo.ca/etd>

 Part of the [Chemical Engineering Commons](#), and the [Nanoscience and Nanotechnology Commons](#)

Recommended Citation

Aldahri, Tahani Hassn, "Microwave and Ultrasonic Assisted Synthesis of zeolites from Coal Fly Ash in Batch and Circulating Batch Operation" (2019). *Electronic Thesis and Dissertation Repository*. 6168.
<https://ir.lib.uwo.ca/etd/6168>

This Dissertation/Thesis is brought to you for free and open access by Scholarship@Western. It has been accepted for inclusion in Electronic Thesis and Dissertation Repository by an authorized administrator of Scholarship@Western. For more information, please contact wlsadmin@uwo.ca.

Abstract

Coal is one of the primary sources of energy worldwide. There are many countries that generate electricity from coal-fired power stations; however, today environmental pollution is considered to be the main issue threatening planet Earth. There are various sources of environmental pollutions, including the by-products of burned coal, such as coal fly ash (CFA). In the USA, about 20–80 million tonnes of CFA are produced per year. This value is expected to increase as population continues to grow and demand for energy increases. Although the building industry uses a percentage of CFA for cement and concrete, the majority of CFA is disposed of in landfill sites. Converting CFA from the waste stream into zeolite is of interest for researchers to recycle this material into an economic and environmental merit. Recently, microwave (MW) and ultrasound (UTS) energies have been used as novel heating sources for the zeolitization of CFA.

This research was focused on the production of zeolites from CFA through utilizing ultrasound and microwave power. A magnetic stirrer built into a single-mode microwave system. The initial conventional heating process of 6 h prior to microwave irradiation for samples with high solid-to-liquid (S/L) ratio (CFA mass/ NaOH solution volume, g/mL) led to a higher yield of zeolite and decreased the synthesis time and consumption of energy, while keeping the high quality of the synthesized zeolite intact. Ultrasound-assisted zeolitization CFA was also applied in this research. Ultrasound energy increased the pore diameter and surface area of the synthesized zeolitic product. The ultrasound-

assisted hydrothermal system enhanced the rate of nucleation and decreased the crystallization time during the synthesis process. The present technique could be considered an economic, eco-friendly, and fast conversion process.

This study has shown that zeolites were successfully synthesized from CFA by utilizing microwave and ultrasound irradiation. These novel energy sources significantly decreased the zeolitization process time. The single-mode microwave-assisted synthesis at high S/L ratio has been shown to be much more effective in producing the same results at a lower S/L ratio. On the other hand, utilization of an ultrasound probe produced a single-phase zeolite in a very short synthesis time compared to other conventional methods.

Keywords

Microwave, Ultrasound, Coal Fly Ash, Zeolite, Recycle, Solid/Liquid ratio, Coal

Dedicated

This thesis dedicated to the persons who supported me

To:

My dear parents

Mrs. Aliah Aldahri and Mr. Hassan Mohsen Aldahri

And

My dear husband and children

Wadee Abdullah Alkuhaili

Shahad, Raghad, Rafa and Saif

Co-Authorship Statement

Chapter 3

Article Title:

Synthesis of zeolite Na-P from coal fly ash by thermo-sonochemical Treatment

Authors

Tahani Aldahri, Jamshid Behin, Hossein Kazemian, Sohrab Rohani

Article Status

Published, Fuel.

T. Aldahri wrote the manuscript, conducted experiments and analyzed the product synthesized. J. Behin assisted in conducting experiments, collecting and compiling the data. The work was supervised by S. Rohani. Various drafts of the paper were reviewed by H. Kazemian and S. Rohani.

T. Aldahri, J. Behin, H. Kazemian, and S. Rohani, Synthesis of zeolite Na-P from coal fly ash by thermo-sonochemical treatment, Fuel 182 (2016) 494-501.

Chapter 4

Article Title:

Effect of microwave irradiation on crystal growth of zeolitized coal fly ash with different solid/liquid ratios

Authors

Tahani Aldahri, Jamshid Behin, Hossein Kazemian, Sohrab Rohani

Article Status

Published, Advanced Powder Technology

T. Aldahri wrote the manuscript, conducted experiments and analyzed the product synthesized. J. Behin assisted in collecting and compiling the data. The work was supervised by S. Rohani. Various drafts of the paper were reviewed by H. Kazemian and S. Rohani.

T. Aldahri, J. Behin, H. Kazemian, and S. Rohani, Effect of microwave irradiation on crystal growth of zeolitized coal fly ash with different solid/liquid ratios, Adv. Powder Technol. 28 (2017) 2865-2874.

Chapter 5

Article Title:

Response surface modeling of the removal of methyl orange dye from its aqueous solution using two types of zeolite synthesized from coal fly ash

Authors

Tahani Al-dahri¹, Adnan AbdulJabbar AbdulRazak, Intisar Hussain Khalaf, and Sohrab Rohani

Article Status

Published, Materials Express

All experiments were conducted by T. Aldahri with the assistance of A.A. AbdulRaza, and I. H. Khalaf. The manuscript was prepared and wrote by T. Aldahri, A.A. AbdulRaza, and I. H. Khalaf. The work was supervised by S. Rohani and various drafts of the paper were reviewed by S. Rohani.

T. Aldahri, A. A. AbdulRazak, I. H. Khalaf, and S. Rohani (2018). Response surface modeling of the removal of methyl orange dye from its aqueous solution using

two types of zeolite synthesized from coal fly ash, Mater. Express, 8(3), 234-244.

Chapter 6

Article Title:

Preparation and characterization of Linde-type A zeolite from coal fly ash: its application as adsorbent for removal of anionic dyes

Authors

Tahani Al-dahri¹, Adnan AbdulJabbar AbdulRazak, and Sohrab Rohani

Article Status

Under review by the Canadian J of Chem. Eng.

All experiments were conducted by T. Aldahri with the assistance of A. A. AbdulRazak.

The manuscript was prepared and wrote by T. Aldahri and A. A. AbdulRazak. The work was supervised by S. Rohani and various drafts of the paper were reviewed by S. Rohani.

Aldahri, T., AbdulRazak, A. A., Rohani, S. Preparation and characterization of Linde-type A zeolite from coal fly ash: its application as adsorbent for removal of anionic dyes.

The Canadian J of Chem. Eng. (Submitted 2018).

Chapter 7

Article Title:

Synthesis of Pure Zeolite-X in a FlowSynth Circulating Batch Microwave Reactor from Clear Solution Extracted from Coal Fly Ash

Authors

Tahani Aldahri and Sohrab Rohani

Article Status

Under review by Advance Powder Technology

This work was supervised by S. Rohani. Various drafts of the paper were reviewed by S. Rohani. All the experiments and data analysis were conducted by T. Aldahri.

T. Aldahri and S. Rohani. "Synthesis of Pure Zeolite-X in a Circulating Batch Flow Microwave Reactor from Clear Solution Extracted from Coal Fly Ash". Adv. Powder Technol. (Submitted 2018).

Appendix A

Article Title:

Highly Efficient Low-Cost Adsorbent for Anionic Dye Using a Synthesized Zeolite P from Waste Coal Fly Ash

Authors

I. Harizi, T. Aldahri, S. Rohani, D. Chebli, and A. Bouguettoucha.

Article Status

Published, the conference ISERD- 493rd International Conference on Chemical and Biochemical Engineering (ICCBE)

All experiments were conducted by Intissar Harizi with the assistance of T. Aldahri.

Analysis were conducted by I. Harizi and T. Aldahri. The manuscript was prepared by I. Harizi with the assistance of T. Aldahri. The work was supervised by S. Rohani and various drafts of the paper were reviewed by A. Bouguettoucha , D. Chebli and S. Rohani.

I. Harizi, T. Aldahri, S. Rohani, D. Chebli, and A. Bouguettoucha, "Highly Efficient Low-Cost Adsorbent for Anionic Dye Using a Synthesized Zeolite P from Waste Coal Fly Ash", the conference ISERD- 493rd International Conference on Chemical and Biochemical Engineering (ICCBE),2018-2019, Stockholm, Sweden.

Acknowledgments

Alhamdulillah, all praise be to Allah almighty for the blessing of completing this thesis.

Without his guidance and blessings, nothing is possible.

It has been a journey of four years and a half to complete this work. It is with pleasure that I write this page to express my sincerest gratitude and deep appreciation to my supervisor Dr. Sohrab Rohani who has supported me throughout my PhD study and gave me this unique opportunity to work in his group. His extensive knowledge, suggestions, encouragement, guidance, assistance and patience have been valuable resources.

Special thanks are extended to Dr. Hossein Kazemian for his constructive comments, inspirational talks, helpful suggestions, and excellent support in many aspects of this research. Also, Dr. Jamshid Behin who taught me the tricks and tools of research that benefited me a lot. Thanks to my colleagues who gave me a warm and friendly atmosphere in the lab to work and conduct experiments.

I am extremely grateful to my father, mother, sisters and brothers for their constant support, inspiration and encouragement over the years. Also, my lovely husband, Wadee Alkuhaili, for his Love, advice, support, and patient and my lovely children, Shahad, Raghad, Rafa and Saif, for their warm hugs and beautiful smiles.

Last but not least, I would like to thank Taibah University for supporting me in completing my PhD study. Also, I thank the Ministry of Education in Saudi Arabia and the Saudi Cultural Bureau in Canada for their support.

Table of Contents

Certificate of Examination.....	ii
Abstract	iii
Dedication.....	v
Co-Authorship Statement	vii
Acknowledgements	xi
List of tables	xvi
List of figures.....	xvii
Acronyms.....	xx
1 Introduction.....	1
1.1 Literature Survey	3
1.2 Scope of The Research.....	5
1.3 Outline and Organization of this Thesis	7
1.4 References	8
2 Experimental Process	13
2.1 CFA Zeolitization	13
2.2 Samples Preparations and Experimental Setups.....	14
2.2.1 Samples Preparations.....	14
2.2.2 Experimental Setups.....	15
2.2.2.1 Lab Scale Microwave Reaction.....	15
2.2.2.2 Ultrasound Reaction	16
2.2.2.3 Bench Scale Microwave Reaction	17
2.3 Evaluation Techniques and Analysis Instruments.....	18
2.3.1 X-ray fluorescence spectroscopy	18

2.3.2 X-Ray diffraction analysis.....	19
2.3.3 Zeolite percentage estimation (crystallinity)	19
2.3.4 Scanning electron microscope	19
2.3.5 Thermogravimetric analysis.....	20
2.3.6 Particle size distribution analysis	20
2.3.7 Brunauer-Emmett-Teller technique.....	20
3 Synthesis of Zeolite Na-P from Coal Fly Ash by Thermo-sonochemical	
Treatment.....	21
3.1 Introduction	22
3.2 Materials and Methods.....	24
3.3 Results and discussion	27
3.4 Conclusions	94
3.5 Acknowledgments	39
3.6 References	40
4 Effect of microwave irradiation on crystal growth of zeolitized coal fly ash with	
different solid/liquid ratios	46
4.1 Introduction	47
4.2 Materials and method	49
4.3 Experimental design.....	52
4.4 Results and discussion	52
4.4.1 Statistical analysis	64
4.4.2 Mechanism of microwave heating.....	68
4.5 Conclusions	71
4.6 References	72

5 Response surface modeling of the removal of methyl orange dye from its aqueous solution using two types of zeolite synthesized from coal fly ash.....	79
5.1 Introduction	80
5.2 Materials and Methods.....	82
5.2.1 Materials	82
5.2.2 Synthesis procedure	82
5.2.3 Characterization.....	83
5.2.4 Modification of the Synthesis Zeolites	84
5.2.5 Experimental Design.....	84
5.2.6 Removal Process.....	85
5.3 Results and discussion	86
5.3.1 Characterization of (LTA) and (ZP)	87
5.3.2 Dye Removal Regression Equations.....	91
5.3.3 Three-dimensional (3D) Response Surface and Contour Plots.....	95
5.3.4 Selection the Optimum Conditions.....	101
5.4 Conclusions	103
5.5 References	104
6 Preparation and Characterization of Linde-Type A zeolite From Coal Fly Ash by Microwave-Assisted Synthesis Method: its Application as Adsorbent for Removal of Anionic Dyes	110
6.1 Introduction	111
6.2 Materials and Methods.....	113
6.2.1 Materials	113
6.2.2 Preparation of (LTA)	114
6.2.3 Characterization of (LTA).....	114

6.2.4 Adsorption Study of (AR66) on (LTA).....	115
6.2.4.1 Batch experiments.....	115
6.2.4.2 Adsorption isotherm.....	116
6.3 Results and Discussion.....	116
6.3.1 Characterization of (LTA).....	116
6.4 Adsorption of (AR66)	120
6.4.1 Effect of pH on dye removal efficiency	120
6.4.2 The effect of contact time and initial dye concentration	121
6.4.3 Effect of (LTA) dosage on removal of dyes	123
6.5 Equilibrium isotherms.....	124
6.6 Kinetic models	128
6.7 Conclusions	131
6.8 References	132
7 Synthesis of Pure Zeolite-X in a FlowSynth Circulating Batch Microwave Reactor from Clear Solution Extracted from Coal Fly Ash.....	138
7.1 Introduction	139
7.2 Materials and method.....	140
7.2.1 Materials.....	140
7.2.2 Method	141
7.2.3 Extraction of silica (SiO ₂) and alumina (Al ₂ O ₃) from coal fly ash.....	141
7.2.4 Circulating Batch Microwave Experiments (Crystallization stage)	142
7.3 Results and discussion	149
7.4 Conclusions	155
7.5 References	156

8 Conclusions and recommendations	162
8.1 Conclusions	162
8.2 Recommendations and further research.....	165
8.2.1 Extraction of SiO ₂ and Al ₂ O ₃ from CFA.....	165
8.2.2 Aging step of CFA prior to crystallization process for zeolitization	165
8.2.3 Bench scale FlowSynth Circulating Batch MW reactor	166
8.2.4 Filtration of CFA prior to zeolitization	166
8.2.5 Other applications of zeolitized CFA.....	167
Appendix A.....	197
A Highly Efficient Low-Cost Adsorbent for Anionic Dye Using a Synthesized Zeolite P from Waste Coal Fly Ash.....	168
A.1 Introduction	169
A.2 Materials and Methods.....	171
A.2.1 Materials.....	171
A.2.2 Preparation of the adsorbent	172
A.2.3 Characterization	173
A.2.4 Sorption experiments.....	173
A.3 Results and discussion.....	175
A.3.1 Characterization of the materials	175
A.3.2 Adsorption results	177
A.3.2.1 The effect of the pH solution on dye adsorption	177
A.3.2.2 The effect of the adsorbent dosage	178
A.3.2.3 The effect of the Initial concentration and the contact time	179

A.3.2.4 The effect of temperature	181
A.3.3 Kinetic and equilibrium Modeling.....	183
A.4 Conclusions	184
A.5 References	185
Curriculum Vitae	188

List of Tables

Table 3.1 Chemical composition (XRF analysis) and mineral composition (XRD analysis) of the CFA used in this study (particle size 600 m) *	21
Figure 3.2 Two different treatment approaches for conversion of CFA to NaP zeolite with total reaction time of 4 hours. a) UTS irradiation followed by conventional heating b) Conventional heating followed by UTS irradiation.....	23
Table 3.3 Crystallinity of CFA-ZP synthesized by conventional heating followed by UTS irradiation for 4 hours.....	28
Table 4.1 Range and levels of experimental variables.....	48
Table 4.2 Central composite design matrix for three test variables in coded units along with the observed and predicted responses (microwave power: 250 W).....	51
Table 4.3 BET surface area of CFA and synthesized CFAZP	58
Table 4.4 Crystal size of synthesized CFAZP at different microwave time	59
Table 4.5 Analysis of variance (ANOVA) for prediction of relative peak intensity by the quadratic model*	60
Table 5.1 Process-independent variables and their levels	81
Table 5.2 CCD for three independent variables and the obtained % Dye removal	82
Table 5.3 BET surface area of CFA and synthesized ZP and LTA.....	84
Table 5.4 Zeta Potential of Modified Zeolite LTA and ZP vs. pH.....	86
Table 5.5 The results of ANOVA analysis for MZP and MLTA	88
Table 5.6 The percentage of contributions (PC) for MZP and MLTA	91
Table 6.1 Langmuir and Freundlich constants for (AR66) dye adsorption isotherms	

on (LTA) at 25, 4 pH and 250 mg /L adsorbent dosage. Freundlich parameters Langmuir parameter	117
Table 6.2 Comparison of q_m appears in references with this work.....	118
Table 6.3 The kinetic results of Intra- particle diffusion and Pseudo- second order. ...	120
Table 7.1 BET surface area of CFA and synthesized Na-X.....	143
Table 7.2 Yield, crystallinity and crystal size of synthesized Na-X.....	144
Table A-1 Pseudo second order fitting results to kinetics data	151
Table A-2 The parameters of the Langmuir and Sips model of the isotherm modeling of CR adsorption on zeolite P.....	151
Table A- 3 Thermodynamic parameters of the adsorption of CR on zeolite P	152

List of Figures

Figure 3.1 Photograph of experimental set-up	19
Figure 3.2 XRD patterns of CFA and zeolitized CFA a) with 1M NaOH and b) with 1.5M NaOH (CH: conventional heating, UTS: UTS irradiation, Q: quartz, M: mullite, C: cancrinite, H: hematite, P: zeolite Na-P, S: hydroxyl-sodalite)	26
Figure 3.3 XRD patterns of CFA and zeolitized CFA (CH: conventional heating, UTS: UTS irradiation, Q: quartz, M: mullite, C: cancrinite, H: hematite, P: zeolite Na-P, S: hydroxyl-sodalite).....	29
Figure 3.4 Thermogravimetric curves of the raw CFA and CFA-ZP produced under optimized condition (heating rate: 10 C/min, under 40 mL/min N ₂).	30
Figure 3.5 SEM images of the raw CFA and UTS-assisted synthesized zeolites samples after 4 hours.	32
Figure 3.6 The particle size distribution of raw CFA and CFA-ZP.....	33
Figure 3.7 Isothermal plot of synthesized CFA-ZP.	34
Figure 4.1 Schematic diagrams of experimental procedure and microwave set-up	46
Figure 4.2 XRD patterns (a) Raw CFA and CFAZP synthesized hydrothermally at 90 C for 24 h, (b) CFAZP synthesized hydrothermally for 6 h and CFAZP synthesized hydrothermally (6 h) followed by microwave irradiation for 30 min, where C: calcite, M:mullite, P: zeolite Na-P, Q: quartz, and S: hydroxyl-sodalite	49
Figure 4.3 TGA/DTA of (a) Raw CFA; (b) CFAZP synthesized hydrothermally and hydrothermally followed by microwave	53
Figure 4.4 Particle size distribution of raw CFA and synthesized CFAZP.....	54

Figure 4.5 The SEM images of the CFA and microwave-assisted synthesized zeolites samples after 30 min irradiation (a) Raw CFA (b) CFAZP synthesized hydrothermally for 6 h (c) CFAZP synthesized hydrothermally for 6 h followed by 30 min microwave irradiation	56
Figure 4.6 Adsorption/desorption isotherms of CFAZP synthesized under optimized condition (Run 5)	58
Figure 4.7 Diagnostic plots for relative peak intensity (a) normal probability, (b) predicted vs. actual values, and (c) residuals vs. predicted values.	61
Figure 4.8 3D response surface and 2D contours showing the interaction effects of the variables on the relative peak intensity	63
Figure 5.1 Methyl Orange chemical structure	78
Figure 5.2 The adsorption /desorption of (ZP) and LTA synthesized from CFA	83
Figure 5.3 The XRD patterns of CFA, ZP, and LTA. (A = zeolite Na-A, Q = quartz, M = mullite, H = hematite, M = magnetite, P = zeolite Na-P, H = hydroxy-sodalite and C= cristobalite)	84
Figure 5.4 The SEM of (a) CFA, synthesized (b) ZP, and (c) LTA zeolites	85
Figure 5.5 The TGA of CFA and synthesized zeolite ZP and LTA zeolite.	86
Figure 5.6 Actual vs. predicted values of %MO dye removal: (a) MLTA and (b) MZP.....	89
Figure 5.7 Pareto chart for (a) MLTA and (b) MZP	93
Figure 5.8 Response surface for MO removal (a) and (b) constant mass of adsorbent 1000mg/L by (a) MLTA and (b) MZP, respectively	94
Figure 5.9 Response surface for MO removal at constant mass of adsorbent 20 mg/L by (a) MLTA and (b) MZP, respectively	94
Figure 5.10 Response surface for MO removal at constant pH 6 by (a) MLTA and	

(b) MZP, respectively.....	95
Figure 5.11 Bar-graph showing the desirability values of %MO dye removal for both adsorbents; MLTA and MZP.....	101
Figure 5.12 The mechanism of anionic dye adsorption onto modified zeolite	102
Figure 6.1 acid red 66 chemical structures	104
Figure 6.2 The XRD pattern of (CFA) and microwave-assisted zeolitized coal fly ash (LTA).	108
Figure 6.3 The SEM image of a) raw (CFA) and b) (LTA) from (CFA).....	109
Figure 6.4 The adsorption and desorption isotherms of (LAT) from (CFA).	110
Figure 6.5 The (PSD) of raw (CFA) and (LAT) from (CFA).	111
Figure 6.6 Zeta potential of (LTA) vs. the pH of solution.	112
Figure 6.7 % dye removal vs. the pH of	112
Figure 6.8 The effect of contact time on a) % dye removal and b) adsorption capacity of (LTA).....	114
Figure 6.9 % dye removal vs. mass of adsorbent.	115
Figure 6.10 Freundlich isotherm of (AR66) on (LTA)	116
Figure 6.11 Langmuir isotherm of (AR66) on (LTA).....	117
Figure 6.12 Pseudo second order model for (AR66) dye adsorption onto (LTA).....	119
Figure 6.13 Intra- particle diffusion for (AR66) adsorption onto (LTA).	120
Figure 7.1 Process ow diagram of the microwave-assisted FlowSynth reactor	134
Figure 7.2 The XRD patterns of Na-X zeolite synthesized by MW-assisted in the circulating batch flow reactor, hydrothermally- synthesized, and raw CFA.....	137
Figure 7.3 XRD patterns of the mixture after aging and without aging.....	138
Figure 7.4 Zeolites produce after 4-h at a) 75 C, b) 85 C, and c) 95 C.....	139
Figure 7.5 The XRD patterns of Na-X zeolites synthesized by the microwave heating at 85 °C after 1-h, 2-h, 3-h, and 4-h crystallization time.....	10

Figure 7.6 SEM images of the CFA and zeolite.	141
Figure 7.7 EDAX images and elemental composition of synthesized zeolite Na-X by MW-assisted synthesis a) 4-h, and b) 2-h of crystallization time.	142
Figure 7.8 Isothermal plot of synthesized zeolite Na-X.	143
Figure 7.9 Schematic representation of the (a) nucleation rate and (b) crystal growth rate of zeolites described with a typical S-shaped curve, and (c) related rearrangements from amorphous particles into crystalline zeolite during the synthesis.	145
Figure A-1 Chemical structure of Congo red molecule	146
Figure A-2 The XRD patterns of CFA and Zeolite P (Q: Quartz, M: mullite, H: Hematite, C: cristobalite, P: zeolite P)	147
Figure A-3 SEM images of (a) Raw CFA (b) Zeolite P.	147
Figure A-4 pH effect on CR adsorption onto zeolite P	148
Figure A-5 Zeta potential of zeolite P at different pH	148
Figure A-6 The Adsorbent dosage effect on the adsorption of CR	149
Figure A-7 The effect of the contact time and the initial concentration on the adsorption of CR on zeolite P	150
Figure A-8 The effect of the temperature on the adsorption of CR on zeolite P.	150
Figure A-9 Experimental and modeling data of the adsorption isotherm of Cr on zeolite P	151
Figure A-10 Kinetics data points regression with pseudo second order model	152

Acronyms

CFA	Coal Fly Ash
UTS	Ultrasound Waves
MW	Microwave Irradiation
BET	Brunauer-Emmett-Teller for Surface Area
PSD	Particles Size Distribution
SEM	Scanning Electron Microscope
EDX	Energy Dispersive X-Ray
TGA	Thermogravimetric Analyzer
XRD	X-Ray Diffraction
XRF	X-Ray Florescence
CEC	Cation-exchange Capacity
CFAZP	Synthesized Zeolite P from Coal Fly Ash
CCD	Central Composite Design
S/L	Solid/Liquid Ratio (CFA mass/ NaOH solution volume, g/mL)
MZP	Modified Zeolite P
MLTA	Modified Zeolite Linde-Type A
ZP	Zeolite P
LTA	Zeolite Linde-Type A
MO	Methyl Orange
AR66	Acid Red 66
DI	Deionized Water

HDTMA Cationic Surfactant; hexadecyltrimethylammonium Bromide

RSM Response Surface Method

Chapter 1

INTRODUCTION

Zeolite is a mineral known for losing water upon heating and, as such, is called a 'boiling stone' because this mineral starts to lose water upon heating. Zeolites are crystalline aluminosilicates with a three-dimensional fully cross-linked open framework structure that develop uniformly-sized pores of molecular dimensions [1]. As crystalline aluminosilicates, zeolites are made up of primary units, where Si and Al atoms are located at the centre of a tetrahedra and surrounded by four oxygen atoms at the corners of the tetrahedra. Si and Al are linked by sharing one oxygen atom. Zeolites are commercially viable for several industrial applications. They are used as adsorbents, as they have the appropriate pore size for adsorbing different sized molecules. The net charge of zeolite is negative because within the framework of zeolite 4^+ Si is replaced by 3^+ Al at many places. The negative charge is balanced by an exchangeable alkali metal cation which is located within the cavities. These alkali metal cations have ion-exchange properties that allow them to react reversibly with polar molecules [1].

Coal is one of the main sources of energy, generating approximately 41% of the world's electricity [2]. Coal fly ash is a waste generated during the coal combustion process in thermal power stations. Millions of tonnes of CFA have been stored in landfills as a waste product and is an environmental pollutant. Researchers have found that zeolitization of CFA is promising in terms of converting a waste material, that is, CFA, into a value-added material. Zeolites are utilized in different areas, such as adsorption, catalysis, removal of heavy metal elements from water [3], in the health field, and

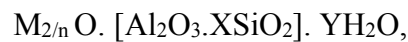
petrochemical and agricultural industries [4]. Zeolites are utilized in diverse ways, such as for adsorption, catalysis, removal of heavy metal elements from water, and processes in the healthcare, petrochemical, and agricultural industries. Zeolite's properties, such as adsorption, catalysis, and ion-exchange, make them highly valuable in biology, medicine, and pharmacology due to the strong relationship between the mineral's properties and biochemical processes. Also, zeolites possess size and shape selectivities and have known biological properties, along with long-term chemical and biological stability [5].

With coal being one of the main sources of energy worldwide, many countries generate electricity from coal-fired power stations. The rapid developments being made in technology and the human reliance on a continuous stream of energy will not only increase demand for energy but add to the threat of environmental pollution [1–3]. Coal fly ash (CFA) is defined as a by-product of coal-fired power plants, therefore with the high use of coal as a source of energy, billions of tonnes of CFA are produced every year around the world. Although CFA has been used in the building industry as a concrete and cement additive, a huge amount of CFA (~> 60 %) is disposed of in landfills with a high environmental and financial cost [1]. In order to decrease the environmental pollution and cost of disposal, CFA has been reused in methods which could lead to economic and environmental benefits. For example, extraction of valuable metals such as Si, Fe, Al, and synthesis of high CEC (cationic exchange capacity) zeolites. These materials; zeolites, could be reused for many different applications such as in environmental protection field. They could be used as heavy metals adsorption and water decontamination. In petrochemistry field they could be used as catalysis, and in construction field they could be used as concrete additive [1].

1.1 Literature Survey

With coal being one of the main sources of energy worldwide, many countries generate electricity from coal-fired power stations. The rapid developments being made in technology and the human reliance on a continuous stream of energy will not only increase demand for energy but add to the threat of environmental pollution [6-8]. Coal fly ash (CFA) is defined as a by-product of coal-fired power plants, therefore with the high use of coal as a source of energy, billions of tonnes of CFA are produced every year around the world. Although CFA has been used in the building industry as a concrete and cement additive, a huge amount of CFA (~> 60 %) is disposed of in landfills with a high environmental and financial cost [6]. In order to decrease the environmental pollution and cost of disposal, CFA has been reused in methods which could lead to economic and environmental benefits. For example, extraction of valuable metals such as Si, Fe, Al, and synthesis of high CEC (cationic exchange capacity) zeolites. These materials; zeolites, could be reused for many different applications such as in environmental protection field. They could be used as heavy metals adsorption and water decontamination. In petrochemistry field they could be used as catalysis, and in construction field they could be used as concrete additive [6]. Zeolites are molecular sieve materials containing void spaces that can host cations, water, or other molecules [9]. Zeolite is a value-added product with superior characteristics, such as adsorption, ion-exchange, and catalysis. There are 40 natural types of zeolite, such as analcime, chabazite, erionite, mordenite, clinoptilolite, and phillipsite [9]. There are more than 140 synthetic zeolitic types: Na-X, Na-Y, ZMS-5 and Na-A. Zeolites have been used for heavy metal adsorption in the areas of environmental sciences and protection, catalysis in the petrochemical field, drying of

gases in gas treatment, and in the agriculture, nuclear fields [8]. The chemical formula of zeolite is:



where the formula between square brackets is the framework composition, M is the exchangeable cations, n is the cation valence, X equals 2 or more as an alumina tetrahedral does not cover the adjacent tetrahedral. Y represents the hydration degree [9].

Many studies have been conducted to produce zeolites hydrothermally from different sources of raw materials. Dalai et al. [10] synthesized zeolites Na-X, Na-P, and hydroxysodalite hydrothermally from husk rice at a temperature of 500 °C–900 °C for 18 h. Also, some zeolites were produced hydrothermally from clear aluminosilicate solutions in the presence of organic templates, such as ZSM-5 [11, 12], Na-Y [13, 14], Na-A [15, 16], Na-X [16, 18]. In addition, CFA was successfully converted to zeolite P hydrothermally at a high temperature: ~ 200 °C for 8–100 h [19, 22].

Studies have been conducted on synthesis of zeolites utilizing either microwave (MW) or ultrasound (UTS) energy as a novel heating source rather than conventional heating, as MW and UTS energy reduces the overall synthesis time. CFA was converted to CFAZP utilizing a MW heating method assisted by hydrothermal heating in alkaline medium and batch processing at high S/L ratio for 6 h [8]. Pure zeolite Na-X was successfully produced using MW irradiation for 3 h by Ansari et al. [23]. Their results showed that MW heating increased the surface area and crystallinity of the product. Using UTS energy, Aldahri et al. [7] synthesized CFAZP from CFA via the thermo-sonication technique at low temperature and atmospheric pressure. Results

showed a strong reduction in synthesis process time over 4 h instead of 24 h. Bukhari et al. [24] converted CFA into CFAZA utilizing UTS energy for the crystallization step. They revealed that UTS enhanced the formation of the zeolitic product at low temperature within 60 min.

There have been several studies conducted on synthesized zeolites on a large scale in a batch system and via continuous flow. Moriyama et al. [22] and Querol et al. [26] produced zeolite P using 0.6 L and 10,000 L reactors respectively. The experiment conditions were 153 °C, 0.48 MPa, 3 M of NaOH solution, S/L is 0.91 kg/L and ~150 °C, 0.33 MPa, 2.4 M of NaOH solution, S/L is 0.60 kg/L respectively. Bukhari et al. synthesized zeolite-A at bench-scale utilizing continuous flow MW reactor of 0.2 L volume and recycled waste liquid from a synthesis process stream [27]. They observed that the crystallinity of the product increased as the MW power increased and reached the maximum at 2:30 h. In addition, results revealed that crystallinity and cation-exchange capacity were decreased by using recycled waste from the zeolitization process due to the decreasing amount of Si and Al in the waste after crystallization. To the best of our knowledge, synthesis of pure zeolite Na-X at bench-scale by using a FlowSynth circulating batch flow microwave reactor from CFA has not been investigated. In the present study, pure Na-X zeolite was produced from a clear solution that was extracted from CFA in alkaline medium with a high crystallinity [28].

1.2 Objectives of the research

The research aims have been to develop and optimize a novel, energy-efficient, and environmentally sustainable approach to synthesizing valuable zeolites from coal fly ash using either ultrasound or microwave technologies as the sources of energy.

This project involves three main parts: (1) Batch-wise synthesis of zeolite crystals using the selected optimized reaction compositions by utilizing microwave (MW) and ultrasound (UTS) assisted methods; (2) Developing and testing a mini-pilot circulating batch synthesis set-up (FlowSynth) from 1 g/h to 1 kg/h using MW energy sources to decrease crystallization and production time. The synthesis of zeolite from CFA is a hydrothermal reaction. It is widely known that a ton of CFA used in the cement mixture preserves the use of almost one barrel of oil; ~159 liters [29]. Since the pioneering work of zeolitization [24, 30- 32] of CFA utilizing two conventional heating methods, there have been many reports of CFA zeolitization with microwave (MW) and ultrasound (UTS) energies. This project has focused on the CFA zeolitization from laboratory-scale to large-scale. CFA has been previously zeolitized using MW and UTS energies; however, that work has been largely limited to small laboratory-scale experiments using altered household microwave [24, 29- 32] and ultrasound baths [6, 33].

(3) Test the synthesized zeolitic products as adsorbents for environmental applications. Also, verify the adsorption capacity of the synthesized zeolites adsorbents for the removal of environmental pollutants such as Anionic and Methyl Orange dye from contaminated aqueous solution.

The focus of this thesis was to consider more efficient methods of microwave and ultrasound irradiation for the zeolitization of coal fly ash. In the case of microwave experiments, a laboratory-scale single-mode microwave unit manufactured by CEM Corporation (Discover, USA) was used. In a single-mode microwave device, electromagnetic waves are directed through a designed waveguide that generates a wave, unlike an altered home microwave system, which produces waves with various

phase shifts resulting in multimode microwave irradiation. A single-mode microwave device results in a higher energy field density that is also uniform, compared with a multimode microwave system. This thesis also introduces the use of an ultrasound probe to directly irradiate the zeolitization reaction with ultrasound energy, unlike the previously conducted works that have used an ultrasound water bath [4].

1.3 Outline and Organization of the Thesis

This thesis is organized in an integrated article format as specified by The School of Postgraduate Studies at the University of Western Ontario.

Chapter 1 introduces the conversion process of CFA into zeolites with utilizing Microwave (MW) and Ultrasound (UTS) energies as novel energy sources.

Chapter 2 describes the methodology followed during conducting the research which include samples preparation, description for the zeolite synthesis process, and technique used to evaluate the synthesized zeolites which included X-Ray diffraction analysis (XRD), X-ray fluorescence spectroscopy (XRF), Scanning electron microscopy (SEM), Thermogravimetric analysis (TGA), Brunauer-Emmett-Teller technique (BET), and Particle size distribution analysis (PSD).

Chapter 3 describes the synthesis of zeolite Na-P from coal fly ash by thermo-sonochemical treatment.

The effect of microwave irradiation on crystal growth of zeolitized coal fly ash with different solid/liquid ratios is investigated in **Chapter 4**.

Chapter 5 contains the experiments done by response surface modeling for the removal of methyl orange dye from its aqueous solution using two types of zeolite synthesized from coal fly ash.

Chapter 6 discusses the preparation and characterization of Linde-Type A zeolite (LTA) from coal fly ash by microwave-assisted synthesis method: its application as an adsorbent for removal of anionic dyes is also discussed.

Bench scale experiments in a FlowSynth circulating batch flow microwave reactor from clear solution extracted from coal fly ash is discussed in **Chapter 7**.

Chapter 8 presents the general conclusions of the thesis based on the experimental results. Major findings are summarized and further recommendations for future work are provided.

1.4 References

- [1] Zaidi S. S. A.; A Step towards Continuous Production of NaY Zeolite in Amorphous Silica Particles using a Dry Process, University of Western, Ph.D. thesis, (2010) p.1,2.
- [2] Internet. EPA (US Environmental Protection Agency) Tier 2 Regulations., <http://www.bunkerportsnews.com/News.aspx?ElementId=2ccc6135-c559-4034-b1d1-c53787b27cf9.php>, 2010a.
- [3] Attari M., Bukhari S.S., Kazemian H., Rohani S.; Mercury Removal from Aqueous Solution by Zeolitized Coal Fly Ash: Equilibrium and Kinetic Study. *Chemosphere* n.d.
- [4] Bukhari S.S., Behin J., Kazemian H., Rohani S.; Conversion of coal fly ash to zeolite utilizing microwave and ultrasound energies: A review. *Fuel* 2015; 140:250–66.
- [5] Joughehdousta, S., & Manafib, S. Application of Zeolite in Biomedical Engineering: A Review. *Iran International Zeolite Conference (IIZC'08)*. 2008.
- [6] Querol X., Moreno N., Uman A. J.C., Alastuey A., Hernandez E., Lopez-Soler A.; Synthesis of Zeolites from coal fly ash: an overview. *Int. J. Coal Geol.* 2002; 50:413–

23.

[7] Aldahri T., Behin J., Kazemian H., and Rohani S.; Synthesis of zeolite Na-P from coal fly ash by thermo-sonochemical treatment; *Fuel* 182, 494 (2016).

[8] Aldahri T., Behin J., Kazemian H., and Rohani S.; Effect of microwave irradiation on crystal growth of zeolitized coal fly ash with different solid/liquid ratios; *Adv. Powder Technol.* 28, 2865 (2017).

[9] Sánchez A.; Computational Study of Adsorption and Diffusion in Zeolites with Cations, PhD thesis, Universidad Pablo de Olavide (Seville, Spain), November 2011.

[10] Dalai A. K., Pradhan N. C., Raob M. S., and Gokhale K. V. G. K.; Synthesis and characterization of NaX and Cu-exchanged NaX zeolites from silica obtained from rice husk ash; *Indian Journal of Engineering & Materials Sciences.* 12, (2005), 227-234.

[11] Karimi R., Bayati B., Aghdam N.C., Ejtemae M., Babaluo A.A.; Studies of the effect of synthesis parameters on ZSM-5 nanocrystalline material during template-hydrothermal synthesis in the presence of chelating agent, *Powder Technol.* 229 (2012) 229–236.

[12] Chauhana N.L., Dasb J., Jasrab R.V., Parikha P.A., Murthya Z.V.P.; Synthesis of small-sized ZSM-5 zeolites employing mixed structure directing agents, *Mater. Lett.* 74 (2012) 115–117.

[13] Holmberg B.A., Wang H., Yan Y.; High silica zeolite Y nanocrystals by dealumination and direct synthesis, *Microporous Mesoporous Mater.* 74 (2004) 189–198.

[14] Sang Sh., Liu Zh., Tian P., Liu Z., Qu L., Zhang Y.; Synthesis of small crystals zeolite NaY, *Mater. Lett.* 60 (2006) 1131–1133.

[15] Zhang X., Tang D., Jiang G.; Synthesis of zeolite NaA at room temperature: the

effect of synthesis parameters on crystal size and its size distribution, *Adv. Powder Technol.* 24 (2013) 689–696.

[16] Wang H., Holmberg B.A., Yan Y.; Synthesis of template-free zeolite nanocrystals by using in situ thermoreversible polymer hydrogels, *J. Am. Chem. Soc.* 125 (2003) 9928–9929.

[17] Zhan B.Z., White M.A., Robertson K.N., Cameron T.S., Gharghourib M.; A novel organic additive free synthesis of nanometer sized NaX crystals, *Chem. Commun.* 13 (2001) 1176–1177.

[18] Zhan B.Z., White M.A., Lumsden M., Mueller-Neuhaus J., Robertson K.N., Cameron T.S., Gharghour M.; Control of particle size and surface properties of crystals of NaX zeolite, *Chem. Mater.* 14 (2002) 3636–3642.

[19] Steenbruggen G., Hollman G.G.; The synthesis of zeolites from fly ash and the properties of the zeolite products, *J. Geochem. Explor.* 62 (1998) 305–309.

[20] Berggaut V., Singer A.; High capacity cation exchanger by hydrothermal zeolitization of coal fly ash, *Appl. Clay Sci.* 10 (1996) 369–378.

[21] Juan R., Hernández S., Andrés J.M., Ruiz C.; Synthesis of granular zeolitic materials with high cation exchange capacity from agglomerated coal fly ash, *Fuel* 86 (2007) 1811–1821.

[22] Ma W., Brown P.W., Komarneni S.; Characterization and cation exchange properties of zeolite synthesized from fly ashes, *J. Mater. Res.* 13 (1998) 3–7.

[23] Ansaria M., Aroujaliana A., Raisia A., Dabira B., Fathizadeha M.; Preparation and characterization of nano-NaX zeolite by microwave assisted hydrothermal method, *Adv. Powder Technol.* 25 (2014) 722–727.

[24] Bukhari S.S., Rohani S., and Kazemian H.; Effect of ultrasound energy on the zeolitization of chemical extracts from fused coal fly ash. *Ultrason. Sonochem.* 2016;

28:47–53. doi: 10.1016/j.ultsonch.2015.06.031.

[25] Moriyama R., Takeda S., Onozaki M., Katayama Y., and Shiota K.; Large-scale synthesis of artificial zeolite from coal fly ash with a small charge of alkaline solution. *Fuel*, (2005) 84: 1455-1461. DOI: 10.1016/j.fuel.2005.02.026.

[26] Querol X., Umaña J.C., Plana F., Alastuey A., and Lopez-Soler A.; Synthesis of zeolites from fly ash at pilot plant scale. Examples of potential applications. *Fuel*, (2001) 80: 857-865. DOI: 10.1016/S0016-2361(00)00156-3.

[27] Bukhari S., and Rohani S.; Continuous Flow Synthesis of Zeolite-A from Coal Fly Ash Utilizing Microwave Irradiation with Recycled Liquid Stream. *American Journal of Environmental Sciences* 2017, 13 (3): 233.244. DOI: 10.3844/ajessp.2017.233.244

[28] Aldahri T., Rohani S.; Synthesis of Pure Zeolite-X in a FlowSynth Circulating Batch Microwave Flow Reactor from Clear Solution Extracted from Coal Fly Ash. (Submitted 2018).

[29] Inada M., Tsujimoto H., Eguchi Y., Enomoto N., Hojo J.; Microwave-assisted zeolite synthesis from coal fly ash in hydrothermal process. *Fuel* 2005; 84:1482–6.

[30] Querol X., Alastuey A., López-Soler A., Plana F., Andrés JM., Juan R.; A fast method for recycling fly ash: microwave-assisted zeolite synthesis. *Environ. Sci. Technol.* 1997; 31:2527–33.

[31] Bukhari S.S., Behin J., Kazemian H., Rohani S.; A comparative study using direct hydrothermal and indirect fusion methods to produce zeolites from coal fly ash utilizing single-mode microwave energy. *J. Mater. Sci.* 2014; 49:8261–71.

[32] Belviso C., Cavalcante F., Lettino A., Fiore S.; Effects of ultrasonic treatment on zeolite synthesized from coal fly ash. *Ultrason. Sonochem.* 2011; 18:661–8.

[33] Bukhari S.S., Behin J., Kazemian H., Rohani S.; Synthesis of zeolite NA-A using

single mode microwave irradiation at atmospheric pressure: The effect of microwave power. *Can. J. Chem. Eng.* 2015; 93:1081- 90.

Chapter 2

Experimental Procedure

This chapter presents detailed descriptions of the techniques, analysis instruments, chemicals, and experimental setups used in the present research work to evaluate the synthesis process of zeolite from coal fly ash utilizing MW and UTS energy as heating sources in batch and batch circulating systems. This chapter is divided into two major sections. The first section describes sample preparations and experimental procedures, including the process followed to synthesize zeolite from coal fly ash utilizing MW and UTS energy as heating sources in batch and batch circulating systems, as well as different conditions used during the synthesis process. The second section focuses on the instrumentation technique used to evaluate results obtained for each studied case.

2.1 CFA Zeolitization

Coal fly ash (CFA) zeolitization using both MW and UTS as energy sources was examined. The raw CFA was hydrothermally treated to extract Si and Al to form alumina-silicate gel and zeolite nuclei. The MW and UTS energies were used in the crystallization stage to accelerate nuclei growth rate and form zeolite crystals. In the present work, zeolite P was produced by applying the MW and/or UTS energy post to the hydrothermal treatment of the CFA. Findings showed that MW-assisted synthesis of zeolite P led to higher crystallinity in the production of zeolite P. In addition, UTS-assisted synthesis of zeolite P increased the rate of nucleation and decreased crystallization time during the zeolitization process.

2.2 Samples Preparations and Experimental Setups

2.2.1 Samples preparations

Coal fly ash was obtained from the Nanticoke coal-fired power plant in Ontario, Canada (owned by Ontario Power Generation [OPG]). The CFA sample was stored in a sealed container before use. Sodium hydroxide (Alphachem, Canada), the sole chemical used in the research, was analytically graded and used as received without further purification. Deionized water (DI) was used for washing synthesized zeolite. Alkali solution was prepared by dissolving 0.8 g of NaOH into 20 ml of deionized water to form 1 M solution. For each experiment, 2 g of CFA was added to 20 ml of the alkali solution. The alkali solution was treated hydrothermally prior to MW and UTS irradiation as described in the following section.

In chapters 5 and 6, the used synthesized zeolites were prepared using the microwave-assisted synthesis method with (CFA) as raw materials; 2 g of (CFA) was dissolved in 20 ml of HCL solution (0.1 M). The mixture was agitated at 250 rpm and heated at 90 °C for 3 hours. Subsequently, the sample was filtrated, and the solid product was washed and dried overnight at room temperature. HCl treatment helps to remove impurities from the raw coal fly ash [1]. Zeolitization of coal fly ash involving a hydrothermal treatment step was conducted as follows: 1.5 molar of NaOH granules with 2 g of acid treated coal fly ash were dissolved in 20 ml of distilled water (CFA/NaOH ratio of 1.67), and then 0.4 g of sodium aluminate and 1 g of sodium meta-silicate were added to the reaction solution. Thereafter, the mixture was introduced to microwave radiation energy for crystallization using microwave source (self-adjusting type) (2.45 GHz, single mode, CEM cooperation, USA), the experiment conducted at atmospheric pressure. A cylindrical tube PTEE (28 mm ID X 108 mm) was fixed at the microwave chamber and equipped with a total reflux condenser. The radiation time was

30 minutes and microwave power 250W. Later, the solid product was filtered and washed with distilled water before being dried at room temperature overnight.

2.2.2 Experimental setups

Zeolite synthesis was studied under at different conditions by varying solid/liquid ratio, reaction temperature, reaction time, and concentration of NaOH in the reaction solution. Three different types of experiments were performed to synthesize zeolite from coal fly ash as described below.

2.2.2.1 Laboratory-scale microwave reaction

The process of CFA zeolitization included 30 minutes of microwave irradiation after a conventional hydrothermal treatment for 6 hours at a relatively low temperature (~90 °C). Then zeolite-P was synthesized from CFA at atmospheric pressure. Two g of CFA and 0.8 g of sodium hydroxide granules were dissolved in 20 ml deionized water to form an alkaline slurry of 1 M (solid/liquid ratio of 0.10 g/ml). The mixture was subjected to conventional heating under atmospheric pressure at 90 °C for 6 hours and stirred continuously using a heater stirrer (Thermo Scientific, China) at 170 rpm. After hydrothermal treatment for 6 hours in a 125-ml glass flask reactor in which Si and Al were extracted into the liquid, and achieving a desired solid/liquid ratio, a certain amount of the liquid was withdrawn by a syringe filter to adjust the solid/liquid ratio range. The latter was chosen in a way to allow the solids to form a wet bed for the safe irradiation of microwave and to avoid hot spots. The residual mixture was poured into a cylindrical PTFE vessel (40 ml, 28 mm ID) attached to a reflux condenser. The suspension was subjected to microwave radiation for crystal growth at 105 °C for 15-

30 minutes. Then, the filtered solid products were washed and dried overnight at room temperature. Microwave power was constant at 250W during the experiments.

The microwave treatment was performed in a self-adjusting microwave oven (single-mode microwave apparatus equipped with a magnetic stirrer, 2.45 GHz, CEM cooperation, Discover, USA), where the reaction temperature and power were monitored automatically.

In this experiment, zeolite P was produced using a small scale (laboratory scale) single mode microwave, for which the sample volume was 20 ml.

2.2.2.2 Ultrasound Reaction

CFA was converted to zeolite CFAZP at a low temperature ~ 100 °C, using atmospheric pressure via conventional hydrothermal heating prior to a sonochemical technique for 4 hours. Alkali solution was prepared by dissolving 0.8 g of NaOH into 20 ml of deionized water to form 1 M solution. For each experiment, 2 g of CFA was added to 20 ml of the alkali solution. Then, the mixture was subjected to conventional heating, ultrasound radiation, and a combination of the two at different durations to study the effect of irradiation time on crystallization of zeolite Na-P. A jacketed cylindrical glass reactor with an ID of 4 cm and length of 10 cm was used to conduct the reaction inside the ultrasound proof enclosure under a controlled temperature condition using a circulating oil bath. The crystallization experiments were carried out using an ultrasonic processor (Sonics, Vibra-Cell, USA) with standard probe (i.e. tip diameter of 13 mm) for sonicating under atmospheric pressure. The ultrasound process produced acoustic waves at the frequency of 20 kHz. The delivered power of the ultrasound wave was 125W (35% max). During sonication, the temperature of the mixture raised from ambient temperature to a steady state of 90 °C within 5 minutes.

Using a circulating oil bath, the reactor temperature was kept constant at 100 °C (± 1 °C). At the end of the thermo-sonochemical reaction, the reactor was cooled down to room temperature; the zeolitized CFA (CFA-ZP) was filtered, thoroughly washed with deionized water to remove un-reacted and water-soluble components, and dried overnight at room temperature.

In this work, zeolite P was produced at small scale using an ultrasonic processor (Sonics, Vibra-Cell, USA), for which the sample volume was 20 ml.

2.2.2.3 Bench Scale Microwave Reaction

A mixture of 14.0 g of raw CFA and 5.6 g of sodium hydroxide granules was dissolved in 140- ml deionized water to form an alkaline solution of 1 M. The alkaline hydrothermal process was applied to break down the fly ash crystalline phases and release the SiO_2 and Al_2O_3 content. Therefore, the mixture was subjected to conventional heating under atmospheric pressure at 90 °C for 4 hours using a heater stirrer (Thermo Scientific, China). After hydrothermal treatment for 4 hours in a 1,000 ml glass flask reactor, SiO_2 and Al_2O_3 were dissolved into liquid and extra deionized water was added while stirring the mixture at 200 rpm for 18 hours. The mixture was filtered, and the supernatant was collected as an aluminum silicate gel.

An appropriate amount of filtrate solution was mixed with Na_2SiO_4 and Na_2AlO_3 to render a molar ratio of the sample: 3.0 Na_2SiO_4 : 0.5 Na_2AlO_3 : 192 H_2O . The resulting solution was left in an aging feed tank for 6 hours at 85 °C. The aging feed tank was equipped with a heating jacket and a condenser for controlling reaction temperature. For the crystallization step, the mixture was then pumped into the microwave FlowSynth reactor for crystal growth at different temperatures: 78 °C, 85 °C, and 95 °C, for 270 minutes. The reaction time was 4 hours, and the mixture flow rate was 5

ml/minute. The system was kept at atmospheric pressure at 85 °C with the use of a reflux condenser and a recycle stream.

The solution was pumped into the FlowSynth MW reactor via a peristaltic pump (Masterflex L/S, Cole Parmer) with tubing (L/S 15, Tygon Chemical) with an inner diameter of 4.8 mm; it was then recirculated at a constant flow rate of 5 ml/minute. The system took about 10 minutes to reach steady-state. After reaching the steady-state, 5 ml samples were withdrawn from the mixing/feed tank every hour. Microwave power was constant at 125 W during the experiments. Subsequently, the filtrate solid products were washed and dried overnight at room temperature.

In this study, zeolites P, A, and X were produced using Milestone FlowSynth circulating batch MW reactor (large or bench scale), for which the sample volume was 0.5–1 kg.

2.3 Evaluation Techniques and Analysis Instruments

Zeolite phase formation and the physical properties of the produced zeolitic materials were evaluated using x-ray diffraction analysis (XRD), X-ray fluorescence spectroscopy (XRF), scanning electron microscopy (SEM), thermogravimetric analysis (TGA), Brunauer-Emmett-Teller technique (BET), and particle size distribution analysis (PSD).

2.3.1 X-ray fluorescence spectroscopy

The chemical and mineral compositions of the CFA used as starting materials was performed using X-ray fluorescence spectroscopy (XRF); PANalytical PW2400 Wavelength Dispersive.

2.3.2 X-Ray diffraction analysis

Synthesized zeolite was evaluated primarily using the x-ray diffraction technique using Rigaku-MiniFlex powder diffractometer (Japan) to collect XRD data of the synthesized samples using Cu K α ($k = 1.54059 \text{ \AA}$) over the range of $5^\circ < 2\theta < 40^\circ$ with a step width of 0.02° . The XRD patterns of the synthesized zeolite samples were compared with the characteristic peaks of Na-P from Ref.[2].

2.3.3 Zeolite percentage estimation (crystallinity)

The percentages of the produced zeolites were determined by “peak fitting” algorithm in the MDI-Jade v 7.5 software. For example, the characteristic peak for the CFA-ZP main peak was found at 2θ of 28° ; the crystallinity and crystal size were then calculated as follows:

$$\text{Crystallinity(\%)} = \frac{\text{Peak intensity of sample at } 2\theta: 28^\circ}{\text{Peak intensity of standard sample at } 2\theta: 28^\circ} \times 100$$

The crystal size was calculated using Scherrer's equation:

$$d(2\theta) = \frac{K \cdot \lambda}{\beta \cos \theta}$$

where d is average crystal size (nm), K is the Scherrer's constant, λ is the wavelength of the X-rays (nm), θ is the value of the Bragg angle, and β is the full width at half-maximum (FWHM) of the broad peak in radians.

2.3.4 Scanning electron microscope

Morphology of the produced zeolite was studied by scanning electron microscope (SEM) using a JSM 600F (Joel, Japan) operating at 10 keV of acceleration voltage.

2.3.5 Thermogravimetric analysis

Thermal analysis (TGA) was performed using a Mettler Toledo TGA/DTA 851e model (Switzerland) with version 6.1 Stare software by heating the samples from 25 °C to 600 °C with a heating rate of 10 °C/minute under nitrogen purge of 40 ml/minute.

2.3.6 Particle size distribution analysis

The Mastersizer 2000 (Malvern Instruments Ltd., UK) was used for particle size distribution (PSD) analysis.

2.3.7 Brunauer-Emmett-Teller technique

The Brunauer-Emmett-Teller (BET) technique was used to measure the specific surface area, pore size, and pore volume of selected synthesized zeolites using a Micrometrics Accelerated Surface Area and Porosimetry (ASAP 2010) surface area analyzer. Synthesized zeolites samples were degassed for 6–8 hours at 150 °C, before the analysis.

2.4 References

- [1] K. Yetilmezsoy, S. Demirel, and R. J. Vanderbei. Response surface modeling of Pb(II) removal from aqueous solution by *Pistacia vera* L.: Box–Behnken experimental design . *J. Hazard. Mater* . 171,551 (2009).
- [2] MMJ. Treacy, JB. Higgins. Collection of simulated XRD powder patterns for zeolites. Elsevier. (2007).

Chapter 3

SYNTHESIS OF ZEOLITE Na-P FROM COAL FLY ASH BY THERMO-SONOCHEMICAL TREATMENT²

Abstract

In the present work, coal fly ash (CFA) was transformed to Na-P zeolite (CFA-ZP) experimentally at atmospheric pressure and low temperature (~ 100 °C) via conventional hydrothermal heating followed by sonochemical energy in 4 hours. The synthesized products were characterized using XRD, TGA/DTA, SEM, PSD, and BET techniques. The effect of ultra-sonication time on crystallinity of the synthesized zeolite was studied. Crystallinity of Na-P zeolite as high as 87 % was achieved at the optimum experimental conditions of NaOH/CFA of 0.27 and 1 hour conventional heating followed by 3 h ultrasound irradiation. Experimental results revealed that sonochemical treatment shortened the crystallization time from 24 hours to 4 hours. Increasing the conventional heating time and decreasing the ultra-sonication time resulted in a lower crystallinity of the synthesized zeolite.

Keywords: Coal fly ash; Rapid crystallization; Ultrasound energy; Zeolite Na-P

² This Chapter is published in the Fuel. Tahani Aldahri, Jamshid Behin, Hossein Kazemian, Sohrab Rohani, Fuel 182, 494 (2016)

3.1. Introduction

Coal fly ash (CFA) is a by-product of coal fired power plants which is considered as residual solid waste [1,2]. CFA is mainly used in concrete production as pozzolan [3]. However, more than 50% of the world's CFA are disposed into landfills at significant cost to producers of this solid waste [4]. Efficient disposal of CFA is a worldwide issue because of its massive production and its harmful effects on the environment [5].

In order to overcome this issue, numerous approaches have been studied and tested, in which using of CFA as a raw material for the production of different valued added products has been considered. In the past four decades, researchers have focused on using CFA as a source of silicon and aluminum for manufacturing different types of synthetic zeolites such as Na-P zeolite [6-15]. Na-P zeolite is one of the most interesting synthesized zeolite because of its high cation exchange and adsorption capacity. This synthetic zeolite can be used in different application such as gas separation application; removal of heavy metal, ammonium, toxic and radioactive waste species; extraction of potassium from sea water; water-softening; and as a builder and water-softening agent for eco-friendly detergent [16, 17].

Conventional hydrothermal method of synthesis of NaP zeolite is an energy- and time-consuming process, in which the crystallization time might be as long as 8 to 100 h, requiring relatively high temperature up to 200°C [18-24]. The conventional hydrothermal method has been optimized in terms of the operating alkaline process variables to achieve higher yield, purity, cation exchange capacity and crystallinity [25-27].

To make the process more cost effective, novel sources of energy such as microwave (MW) radiation energy were used along with conventional hydrothermal

process to shorten synthesis time. There are several reports on microwave-assisted hydrothermal conversion of CFA to different synthetic zeolites (e.g. Na-A) [28-36].

Ultrasound (UTS) is an alternative energy source, which is considered to be safer compared to microwave because of its wave frequencies that are lower than the microwave [37]. UTS assisted synthesis is a straightforward and simple technique that has been used by our research group to manufacture different zeolites and zeolite-like porous materials [38-40]. The chemical effects of ultrasound originate from acoustic cavitation and collapsing of generated micro-bubbles in liquid medium, which leads to a micro-mixing effect. This phenomenon increases the secondary nucleation rates and enhances mass transfer that eventually increases crystal growth rates [37, 41].

It has been suggested that using microwave and ultrasound as energy sources could lead to homogenous nucleation and uniform distribution of heat leading to a decrease in the reaction time from days down to hours and even minutes. The use of alternative energy sources can lead to an economically viable zeolitization process [42]. Azizi et al. [43] synthesized zeolite Na-P under ultrasonic and microwave ageing process prior to the hydrothermal crystallization using perlite. The optimum conditions for maximum zeolite crystallinity (97%) were obtained in 55 min using microwave-assisted ageing and 4 hours for the hydrothermal crystallization time. Recently, Pal et al. [44] synthesized zeolite Na-P from pure chemicals by sonochemical method and compared the results with conventional hydrothermal technique. The precursors were mixed at room temperature for 1 hour and then sonicated for 3 hours. During the sonication, the temperature of bulk reaction mixture raised up to 80 °C. According to their study, sonochemical treatment followed by hydrothermal treatment does not show any significant effect on crystallization and phase formation of zeolite under the studied conditions.

The short-time zeolitization is preferable for efficient industrial production [13]. To the best of the authors' knowledge, so far, the sonochemical conversion of CFA into zeolite Na-P has not been reported. In this study, CFA was converted into zeolite Na-P by means of ultrasound irradiation in an alkali medium as a facile method of synthesis. Furthermore, the effectiveness of ultrasound (UTS) and UTS-assisted hydrothermal method are compared.

3.2. Materials and Methods

Coal fly ash was obtained from Nanticoke coal fired power plant, Ontario, Canada (owned by Ontario Power Generation; OPG). The CFA sample was stored in a sealed container before use. The chemical and mineral compositions of the CFA used as starting materials and the main source of Si and Al are given in Table 3-1. The content of unburnt carbon determined by a loss on ignition (LOI) test. The $\text{SiO}_2/\text{Al}_2\text{O}_3$ ratio was found to be 2.13, which is suitable for synthesis of zeolite Na-P under the mild concentration of NaOH without adding extra aluminate or silicate precursors for adjusting the batch composition. The sodium hydroxide (Alphachem, Canada), as the sole chemical used in the experiments, was analytical grade and used as received without further purification. Deionized water was used for washing of synthesized zeolite.

Table 3-1: Chemical composition (XRF analysis) and mineral composition (XRD analysis) of the CFA used in this study (particle size $\leq 600 \mu\text{m}$) *

Parameter	Weight percent (%)
<i>Major oxide</i>	
SiO ₂	41.78
Al ₂ O ₃	19.61
CaO	13.64
Fe ₂ O ₃	5.79
MgO	3.23
TiO ₂	1.39
K ₂ O	1.10
Na ₂ O	0.94
P ₂ O ₅	0.71
BaO	0.36
SrO	0.25
Cr ₂ O ₃	0.01
MnO	0.02
<i>Loss On Ignition</i>	10.89
Total	99.72
<i>Phases analysis</i>	
Amorphous aluminosilicate	88
Quartz (SiO ₂)	8
Mullite (3Al ₂ O ₃ .2SiO ₂)	3
Others	1

*SiO₂/Al₂O₃: 2.13

Alkali solution was prepared by dissolving 0.8 g of NaOH into 20 mL of deionized water to form 1 M solution. For each experiment, 2 g of CFA was added to 20 mL of the alkali solution. Then, the mixture was subjected to conventional heating, ultrasound radiation and their combination at different durations to study the effect of irradiation

time on crystallization of zeolite Na-P. A jacketed cylindrical glass reactor with an ID of 4 cm and length of 10 cm was used to conduct the reaction inside the ultrasound proof enclosure under controlled temperature condition using a circulating oil bath. The crystallization experiments were carried out using an ultrasonic processor (Sonics, Vibra-Cell, USA) with standard probe (i.e. tip diameter of 13 mm) for sonicating under atmospheric pressure. The ultrasound process produces acoustic waves at the frequency of 20 kHz. The delivered power of ultrasound wave was 125 W (35% max). During sonication, the temperature of mixture raised from ambient temperature to a steady state of 90 °C within 5 min by immersing UTS probe (Vibra Cell VCX-500, Sonics & Materials, USA) into the reaction mixture. Using a circulating oil bath, the reactor temperature was kept constant at 100 °C (± 1 °C). The photographs of the experimental setup and the jacketed glass reactor are illustrated in Figure 3-1.



Figure 3-1: Photograph of experimental set-up

At the end of thermo-sonchemical reaction, the reactor was cooled down to room temperature; the zeolitized CFA (CFA-ZP) was filtered, thoroughly washed with deionized water to remove un-reacted and water soluble components, and dried overnight at room temperature.

Rigaku-MiniFlex powder diffractometer (Japan) was used to collect XRD data of the synthesized samples using $\text{CuK}\alpha$ ($\lambda = 1.54059 \text{ \AA}$) over the range of $5^\circ < 2\theta < 40^\circ$ with a step width of 0.02° . The XRD patterns of the synthesized zeolite samples were compared with the characteristic peaks of NaP from references [45]. The characteristic peak intensity (crystallinity) percentage of the synthesized zeolite was determined by "peak fitting" algorithm in the MDI-Jade v 7.5 software. Area of the characteristic peaks were found for the CFA-ZP main peaks at 2θ of 12.5° , 21.3° , and 28° and the average crystallinity was then calculated. The effect of ultrasound on the yield of CFA-ZP estimated from mass of the final product multiplied by the average crystallinity as shown in Table 3-3. Morphology of the produced zeolite were studied by scanning electron microscope (SEM) using a JSM 600F (Joel, Japan) operating at 10 keV of acceleration voltage. Thermal analysis was performed using a Mettler Toledo TGA/DTA 851e model (Switzerland) with version 6.1 Stare software by heating the samples from 25°C to 600°C with a heating rate of $10^\circ\text{C}/\text{min}$ under nitrogen purge of $40 \text{ mL}/\text{min}$. Mastersizer 2000 (Malvern Instruments Ltd., UK) was used for particle size distribution (PSD) analysis. Burnauer-Emmett-Teller (BET) technique was used to measure the specific surface area, pore size and pore volume of selected CFA-ZP using a Micrometrics Accelerated Surface Area and Porosimetry (ASAP 2010) surface area analyzer. CFA-ZP samples were degassed for 6-8 hours at 150°C , before the analysis. X-ray fluorescence spectroscopy (XRF) was used to determine the chemical composition of the CFA sample using PANalytical PW2400 Wavelength Dispersive.

3.3. Results and discussion

Synthesis time, energy consumption and risk of leaching harmful components of CFA should be considered as three main factors limiting the commercialization of CFA zeolitization process. Therefore, the main objective of this work was to synthesize zeolite under mild and cost effective conditions. The temperature of alkaline reaction mixture raised from ambient to ~ 90 °C solely as a result of the energy supplied by ultrasound irradiation alone. In order to ensure reproducibility at a controlled temperature, all of the tests were conducted at 100 °C by using a circulating oil bath. At constant temperature of 100 °C, the energy supplied by the oil as the external source of energy will be the lowest. The NaOH to CFA mass ratio was set at a minimum value of 0.27 (1 M).

In order to determine whether or not the ultrasound irradiation affect the zeolite formation process, the overall crystallization time at 100 °C was kept constant for 4 hours for all the tests while the sonication and conventional hydrothermal duration was varied. Therefore, in order to find the optimized synthesis procedure, two combinations of sonication and conventional heating were studied. First, the UTS irradiation (named early sonication) followed by conventional heating was performed. For a 4 hour time, the UTS irradiation time was decreased as the conventional heating was increased. Results are illustrated in Table 3-2. As it can be seen from Table 3-2a, when ultrasonic energy was applied at first; neither 4 hours of ultra-sonication nor the combination of ultrasonic and conventional heating resulted in any zeolitic product. This set of experiments revealed that under the tested conditions, apparently continuous UTS irradiation retards the recrystallization process of CFA to NaP zeolite. According to de Castro and Priego Capote [46], ultrasound irradiation enhances the dissolution of solid

particles suspended in liquid phase as a result of the mechanical effect. Thus, the deposited product was an amorphous aluminosilicate gel. This means that the UTS heating enhanced the dissolution of CFA but inhibited the crystallization of zeolite from the intermediate gel. Partial UTS irradiation exhibits various influences in the course of conventional heating process. The early-stage UTS heating doesn't enhance the zeolite formation, which is caused by the retardation of nucleation in the intermediate aluminosilicate gel.

Conventional heating followed by UTS irradiation (named late sonication) was also performed for a total of 4 hours treatment time. Late sonication resulted in successful synthesis of zeolite. This finding is in agreement with those reported in [46]; the cavitation phenomenon of UTS accelerates the rate of nucleation and crystallization. When bubbles collapsed, precursors are distributed in the liquid and grow up to form crystalline structure. It is noteworthy that no zeolitic product was obtained by conventional heating alone after 4 hours (Table 3-2b). However, late UTS heating successfully shortened the crystallization time compared to the conventional heating. Therefore, conventional heating followed by late UTS heating should be considered as an effective approach to enhance the zeolitization of coal fly ash.

Table 3-2: Two different treatment approaches for conversion of CFA to NaP zeolite with total reaction time of 4 hours. a) UTS irradiation followed by conventional heating. b) Conventional heating followed by UTS irradiation

Experimental run (-)	First treatment: UST irradiation (h)	Second treatment: Conventional heating (h)	Remarks
1	0.0	4.0	No Zeolitization
2	3.0	1.0	No Zeolitization

3	2.0	2.0	No Zeolitization
4	1.0	3.0	No Zeolitization

(a)

Experimental run (-)	First treatment: Conventional heating (h)	Second treatment: UST irradiation (h)	Remarks
1	1.0	3.0	Zeolite Na-P
2	2.0	2.0	Zeolite Na-P
3	3.0	1.0	Zeolite Na-P
4	4.0	0.0	No Zeolitization

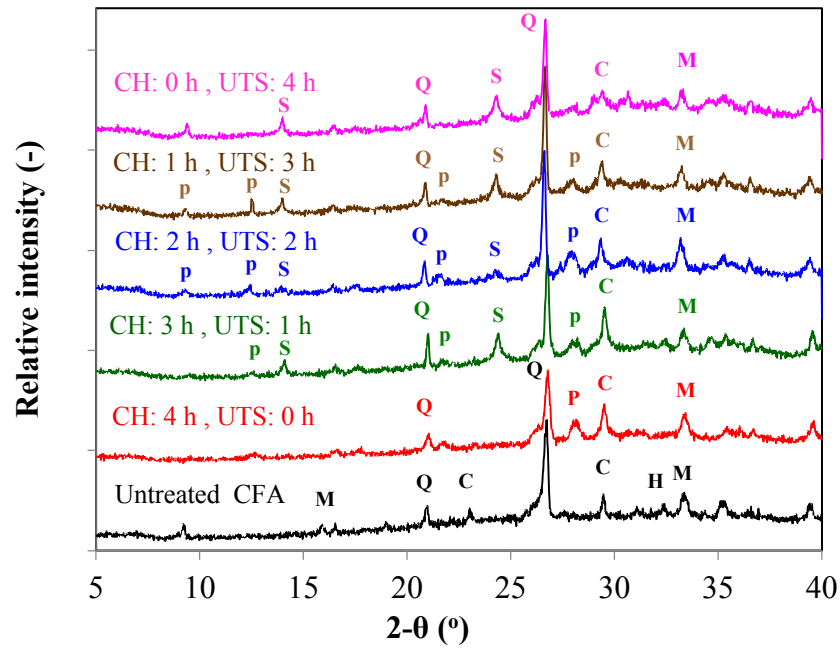
(b)

Figure 3-2 illustrates the XRD patterns of the raw coal fly ash before and after subjecting to treatment at the 2θ ranging from 5 to 40 degrees. Quartz, mullite, calcite and hematite are the main crystalline phases presented in raw CFA. During the conventional heating process of CFA with sodium hydroxide for 4 hours, hematite and calcite phases were partially dissolved; therefore, the intensities of some relevant peaks (i.e. $2\theta = 23^\circ, 32.3^\circ$) were decreased. No noticeable dissolution of quartz was observed at the mild alkaline conditions indicating the resistance of quartz during direct hydrothermal treatment. Mullite appeared to be a less-active crystalline component for zeolite formation. There is no significant difference between XRD patterns of the raw CFA and the products after 4 hours treatment solely with ultrasound energy or conventional heating. The XRD patterns of the zeolite synthesized by thermo-sonochemical crystallization showed at least three main characteristic peaks at 2θ :

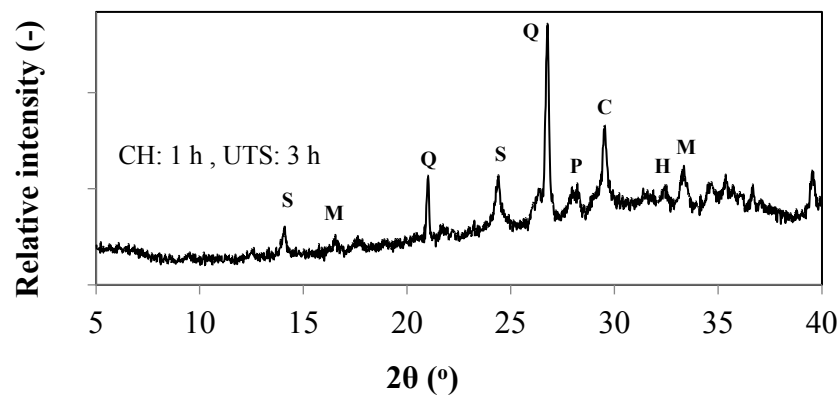
12.46°, 21.67°, 28.10° confirming the successful formation of zeolite Na-P as the major crystalline phase of the zeolitized CFA (Figure 3-2a).

The diffraction peak intensity of crystalline zeolite P increases with an increase in UTS irradiation time (below 3 hours) while the conventional heating time was decreased. Ultrasonic irradiation heating for 4 hours, however, led to the formation of a more stable phase of hydroxysodalite as a side product without any NaP zeolite. The relatively high temperature of the reaction mixture can be considered as another reason for the formation of hydroxyl-sodalite [9].

To study the effect of NaOH/CFA ratio on zeolitization process, one experiment was conducted with 1.5 M NaOH at the optimum heating condition of 1 hour conventional heating followed by 3 hours UTS heating. The XRD pattern of the product, which is illustrated in Figure 3-2b, revealed that increasing the NaOH concentration from 1 M to 1.5 M favors the formation of hydroxysodalite phase instead of NaP. It seems hydrothermal conversion to zeolite from CFA at higher concentration of NaOH will result in conversion of NaP zeolite crystals to a more stable crystalline phase of hydroxysodalite phase. This trend and observation are in strong agreement with the previous work reported by Murayama et al. [22].



a) NaOH: 1 M



b) NaOH: 1.5 M

Figure 3-2: XRD patterns of CFA and zeolitized CFA a) with 1M NaOH and b) with 1.5M NaOH (CH: conventional heating, UT: S UTS irradiation, Q: quartz, M: mullite, C: cancrinite, H: hematite, P: zeolite Na-P, S: hydroxyl-sodalite)

In order to optimize the CFA zeolitization process, late sonication was performed at shorter time intervals of 0.5 hour by keeping the overall synthesis time at 4 hours. The results are shown in Table 3-3. The maximum crystallinity of the NaP zeolitic phase of 87 %, was achieved in 1 hour conventional heating followed by 3 hours of

UTS irradiation. Increasing hydrothermal treatment time to 3.5 hours and decreasing the UTS irradiation time to 0.5 hour resulted in decreasing the peak intensity (crystallinity) of product to 78 %. The results showed that the late sonication including hydrothermal treatment (at least 1 hour) and UTS irradiation (at least 0.5 hour) are necessary for successful conversion of CFA to NaP zeolite. On the other hand, late irradiation is effective rather than the overall irradiation during the zeolitization.

Table 3-3: Crystallinity of CFA-ZP synthesized by conventional heating followed by UTS irradiation for 4 hours

Experimental run (-)	First treatment: Conventional heating (h)	Second treatment: UST irradiation (h)	Peak intensity (%)
1	0.5	3.5	0.0
2	1.0	3.0	87.05
3	1.5	2.5	82.91
4	2.0	2.0	80.32
5	2.5	1.5	79,34
6	3.0	1.0	78.89
7	3.5	0.5	78.44

In order to investigate the effect of UTS irradiation time on the crystallinity of CFA-ZP, experiments were conducted using 1 hour of conventional heating plus 4 hours, 5 hours, and 6 hours of ultrasonication. The XRD patterns of the products are illustrated in Figure 3-3, which reveal the absence of NaP zeolite. These results

ascertain that in order to produce NaP zeolite from CFA using ultrasonic-assisted approach, the order of treatment is important.

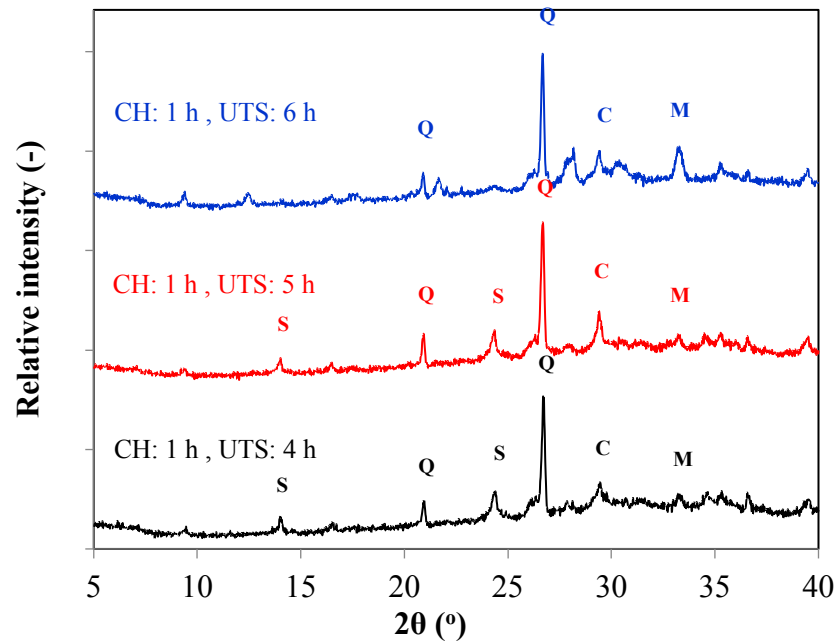


Figure 3-3: XRD patterns of CFA and zeolitized CFA (CH: conventional heating, UTS: UTS irradiation, Q: quartz, M: mullite, C: cancrinite, H: hematite, P: zeolite Na-P, S: hydroxyl-sodalite).

Raw CFA and the CFA-ZP with highest crystallinity of 87.05 % were analyzed using TGA/DTA technique to measure their water adsorption capacities. In Figure 3-4, the single inflection point at 105 °C corresponds to an endothermic weight loss of ~ 4.5 % which is attributed to the removal of physically adsorbed water. The TGA curve of CFA-ZP sample showed higher adsorption capacity (~ 14 %) than CFA sample. The two step weight losses at 90 °C and 130 °C indicated the desorption of un-bond moisture on the surface of non zeolitized CFA and bond moisture on CFA-ZP, respectively. It was found that UTS heating promotes the rate of increase of the adsorption capacity of the produced NaP zeolite.

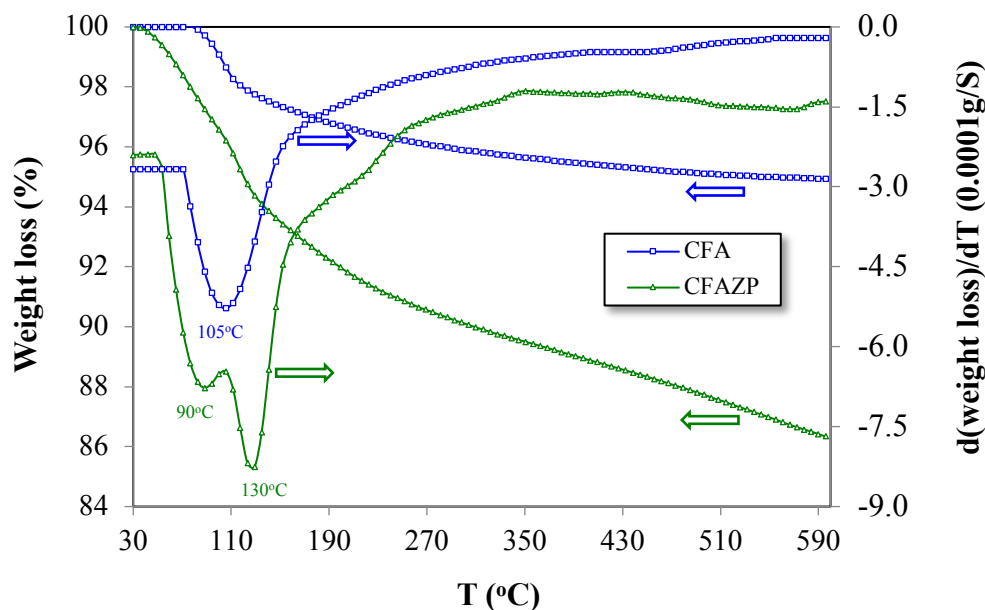


Figure 3-4: Thermogravimetric curves of the raw CFA and CFA-ZP produced under optimized condition (heating rate: 10°C/min, under 40mL/min N₂).

Figure 3-5 shows the SEM micrographs of raw CFA and the zeolitized CFA under the optimum conditions (i.e. CH: 1 hour and UTS: 3 hours) with highest crystallinity of 87%. It reveals that the CFA used in this study is quasi-spherical with a smooth surface. Very significant changes can be observed on the surface of CFA during zeolitization process. The NaP zeolite crystallites deposit on partially activated fly ash spheres which is in agreement with literature [9, 22]. The micrographs of CFA-ZP demonstrate regular morphology of the synthesized crystals. Zeolite NaP can be identified by pseudo-spherical forms constituted by small plates. This typical morphology, which comprises most of the samples, displays well-defined NaP crystal faces [19].

The X-ray patterns indicate the presence of hydroxysodalite in acicular shapes in zeolitic products. The characteristic and morphological shapes of hydroxysodalite crystals, predominantly as randomly oriented rods, indicate that the crystal growth using the UTS energy was somewhat lower than the hydrothermal case. The product changes from zeolite P to hydroxysodalite via co-crystallization between zeolite P and

hydroxysodalite, under prolonged UTS irradiation. Similar results were observed with increasing alkali concentration in hydrothermal conversion of CFA to zeolite P [22].

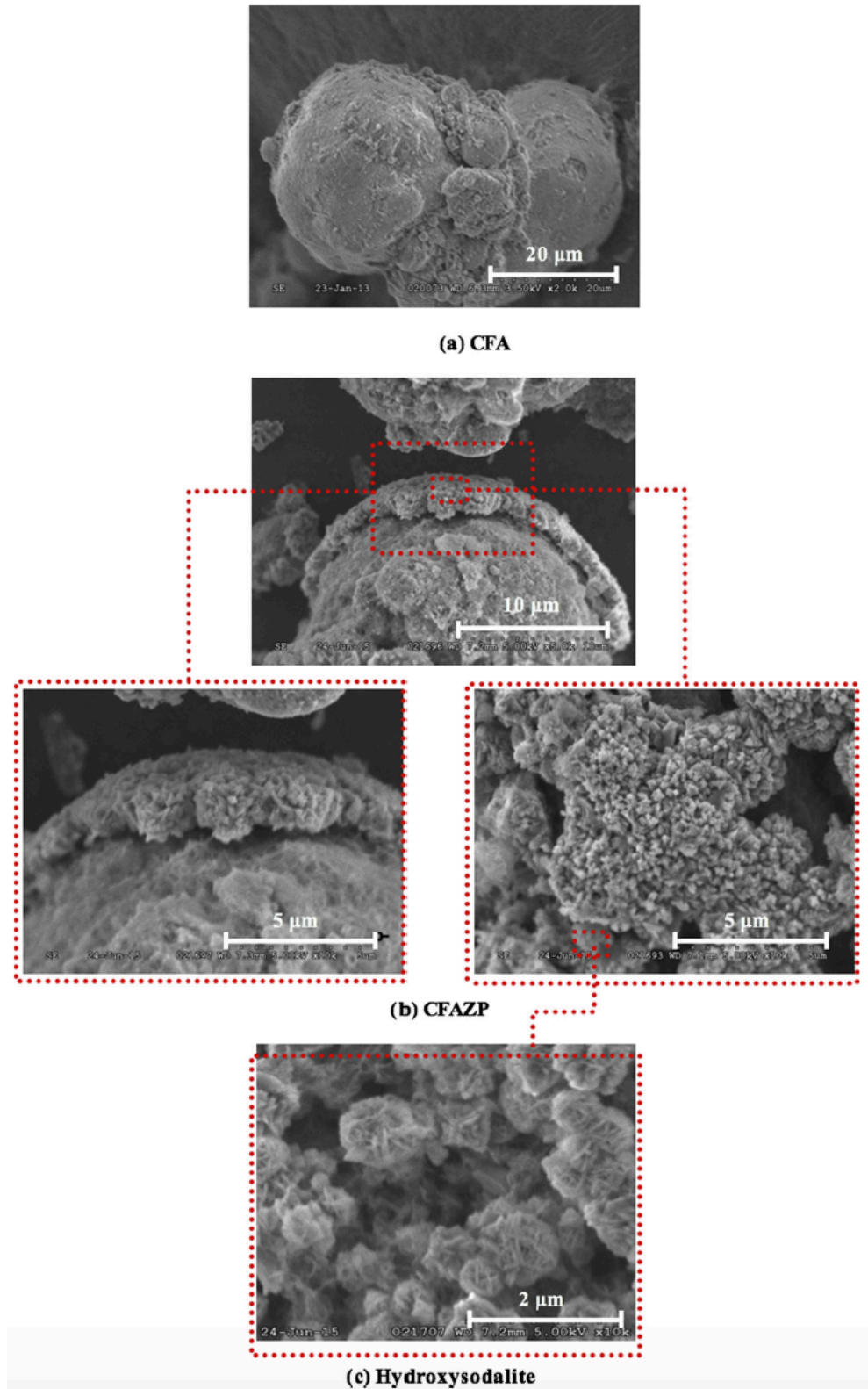


Figure 3-5: SEM images of the raw CFA and UTS-assisted synthesized zeolites samples after 4 hours.

The particle size analysis using a Malvern Mastersizer 2000, revealed that both raw CFA and the CFA-ZP products show similar particle size distribution from 0.2 μm to 200 μm with the maximum volumetric population of 5.5 vol.% at 35 μm . The particle size distribution curves of both raw CFA and the CFA-ZP product that are illustrated in Figure 3-4. That shows no significant changes during zeolitization process. Apparently, the thermo-sonochemical treatment at mild alkali condition has little influence on the particle size distribution. Using ultrasonication for reducing solid particle size is common due to the ability of ultrasonic energy to destroy agglomeration and/or the structure of particles. However, in this work, it seems using ultrasonic treatment under the tested condition doesn't have a strong influence on the particle size reduction.

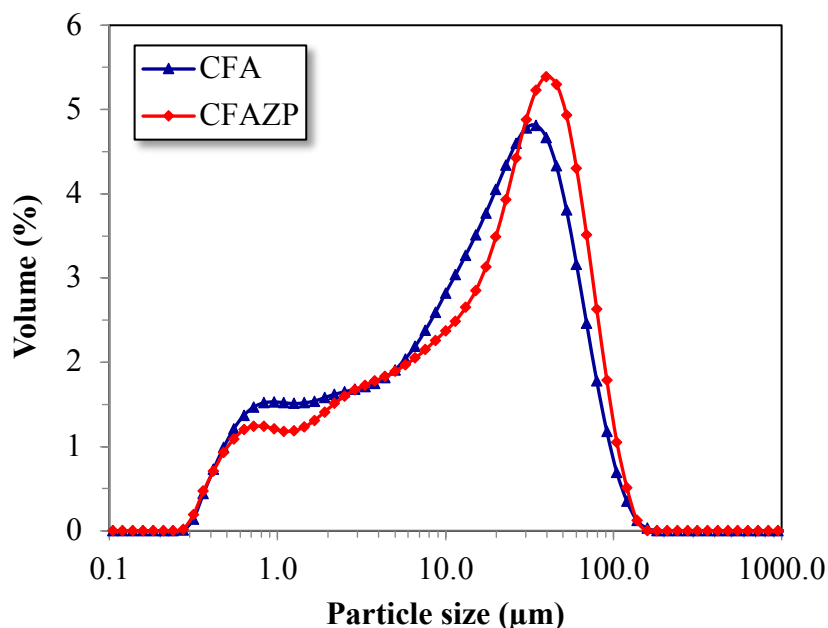


Figure 3-6: The particle size distribution of raw CFA and CFA-ZP.

The BET surface area of the raw CFA and the CFA-ZP sample synthesized under optimized condition was 15.47 m^2/g and 68.81 m^2/g , respectively. A remarkable

increase of the surface area is achieved by zeolitization of CFA. Micro-pore area and mesoporous area of the produced sample were 8.99 m²/g and 59.38 m²/g, respectively. According to the XRD and SEM results, the synthetic zeolite (CFA-ZP) was formed on the surface of CFA, which attributes to the increase of the surface area due to the higher porosity of CFA-ZP. The pore volume and the mean pore diameter of the best sample were 0.132 cm³/g and 10.92 Å, respectively. Nitrogen adsorption/desorption isotherm of the CFA-ZP product, which is illustrated in Figure 3-7 indicates a type II isotherm. A type II isotherm is known for the microporous zeolites that could be assigned to impurities occupying the pores and channels of CFA-ZP which limit the adsorption of N₂ inside the pores.

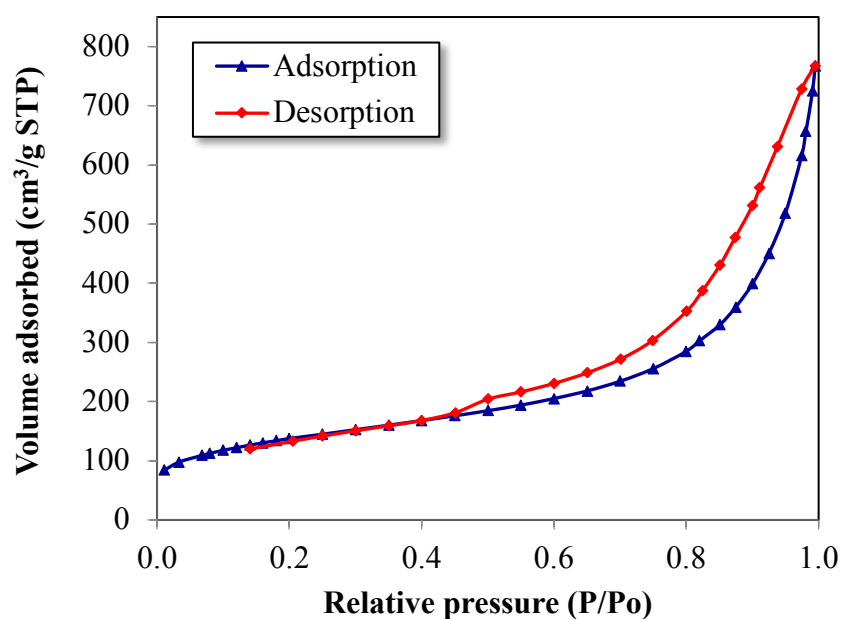


Figure 3-7: Isothermal plot of synthesized CFA-ZP

3.4. Conclusions

The experimental results of this research revealed that CFA could be converted successfully to zeolite Na-P by the thermo-sonochemical treatment at low temperature (i.e. 100°C) and atmospheric pressure in 4 hours. The main synthesized zeolitic phase

was Na-P zeolite with traces of hydroxysodalite with 1 hour conventional heating followed by 3 hours of sonochemical treatment. When ultrasound was applied in the course of hydrothermal treatment, zeolitization was promoted by later stage irradiation. On the other hand, the ultrasound irradiation in the early-stage retarded the crystallization of zeolite. Thermo-sonochemical zeolitization of CFA leads to an increase in the surface area and pore diameter. It can be concluded that the ultrasound-assisted hydrothermal technique facilitates formation of NaP zeolite from CFA by enhancing the rate of nucleation and shortening the crystallization time during the conversion process. The developed method can be considered as a fast and eco-friendly zeolitization process with lower energy demands.

3.5. References

- [1] X. Querol, N. Moreno, J.C. Umaña, A. Alastuey, E. Hernández, A. López-Soler, F. Plana, Synthesis of zeolites from coal fly ash: an overview. *Int. J. Coal Geol.* 2002, 50: 413-423.
- [2] R.S. Blissett, N.A. Rowson, A review of the multi-component utilization of coal fly ash, *Fuel*, 2012, 97: 1-23.
- [3] C. Heidrich, H. Feuerborn, A. Weir, Coal combustion products: a global perspective. World Coal Ash WOCA, Lexington, KY: 2013.
- [4] M. Ahmaruzzaman, A review on the utilization of fly ash, *Progress in Energy and Combustion Science*, 2010, 36: 327-363.
- [5] I. Twardowska, J. Szczepanska, Solid waste, terminological and long-term environmental risk assessment problems exemplified in a power plant fly ash study, *Sci. Total Environ.* 2002, 285: 29-51.

- [6] V. Berkgaout, A. Singer, High capacity cation exchanger by hydrothermal zeolitization of coal fly ash, *Appl. Clay Sci.* 1996, 10: 369-378.
- [7] X. Querol, F. Plana, A. Alastuey, A. López-Soler, Synthesis of Na-zeolites from fly ash, *Fuel*, 1997, 76: 793-799.
- [8] G.G. Hollman, G. Steenbruggen, M. Janssen-Jurkovičová, A two-step process for the synthesis of zeolites from coal fly ash, *Fuel*, 1999, 78: 1225-1230.
- [9] M. Park, C.L. Choi, W.T. Lim, M.C. Kim, J. Choi, N.H. Heo, Molten-salt method for the synthesis of zeolitic materials: II. Characterization of zeolitic materials. *Microporous Mesoporous Mater.* 2000, 37: 91-98.
- [10] N. Moreno, C.F. Pereira, M. Janssen- Jurkovičová, Utilization of zeolites synthesized from coal fly ash for the purification of acid mine waters, *Environ. Sci. Technol.* 2001, 35: 3526-3534.
- [11] X. Querol, J.C. Umaña, F. Plana, A. Alastuey, A. Lopez-Soler, A. Medinaceli, A. Valero, M.J. Domingo, E. Garcia-Rojo, Synthesis of zeolites from fly ash at pilot plant scale. Examples of potential applications, *Fuel*, 2001, 80: 857-865.
- [12] N. Moreno, X. Querol, F. Plana, J.M. Andres, M. Janssen, H. Nugteren, Pure zeolite synthesis from silica extracted from coal fly ashes. *J. Chem. Technol. Biotechnol.* 2002, 77: 274–279.
- [13] M. Inada, Y. Eguchi, N. Enomoto, J. Hojo, Synthesis of zeolite from coal fly ashes with different silica-alumina composition, *Fuel*, 2005, 84: 299-304.
- [14] M. Wdowin, M. Franus, R. Panek, L. Badura, W. Franus, The conversion technology of fly ash into zeolites, *Clean Technol. Envir.* 2014, 16: 1217-1223.
- [15] T.T. Walek, F. Saito, Q. Zhang, The effect of low solid/liquid ratio on hydrothermal synthesis of zeolites from fly ash, *Fuel*, 2008, 87: 3194-3199.

- [16] B.R. Albert, A.K. Cheetham, J.A. Stuart, C.J. Adams, investigation on P zeolite: Synthesis, characterization, and structure of highly crystalline low-silica Na-P, *Microporous and Mesoporous Materials* 21 (1998) 133-142.
- [17] Z. Huo, X. xu, Z. Lü, J. Song, M. He, Z. Li, Q. Wang, L. Yan, Synthesis of zeolite NaP with controllable morphologies, *Microporous and Mesoporous Materials* 158 (2012) 137-140.
- [18] V. Berkgaot, A. Singer, High capacity cation exchanger by hydrothermal zeolitization of coal fly ash. *Appl. Clay Sci.* 10 (1996) 369-378.
- [19] W. Ma, P.W. Brown, S. Komarneni, Characterization and cation exchange properties of zeolite synthesized from fly ashes, *J. Mater. Res.* 13 (1998) 3-7.
- [20] G. Steenbruggen, G.G. Hollman, The synthesis of zeolites from fly ash and the properties of the zeolite products. *J. Geochem. Explor.* 62 (1998) 305-309.
- [21] R. Juan, S. Hernández, J.M. Andrés, C. Ruiz, Synthesis of granular zeolitic materials with high cation exchange capacity from agglomerated coal fly ash, *Fuel* 86 (2007) 1811-1821.
- [22] N. Murayama, H. Yamamoto, J. Shibata, Mechanism of zeolite synthesis from coal fly ash by alkali hydrothermal reaction, *Int. J. Miner. Process* 64 (2002) 1-17.
- [23] N. Murayama, T. Takahashi, K. Shuku, H. Lee, J. Shibata, Effect of reaction temperature on hydrothermal syntheses of potassium type zeolites from coal fly ash, *Int. J. Miner. Process* 87 (2008) 129-133.
- [24] N.M. Musyoka, Hydrothermal synthesis and optimisation of zeolite Na-P1 from South African coal fly ash, University of Western Cape (2009).
- [25] H. Tanaka, A. Fujii, S. Fujimoto, Y. Tanaka, Microwave-assisted two-step process for the synthesis of a single-phase Na-A zeolite from coal fly ash, *Adv. Powder Technol.*, 2008, 19: 83-94.

- [26] N.M. Musyoka, L.F. Petrik, W.M. Gitari, G. Balfour, E. Hums, Optimization of hydrothermal synthesis of pure zeolite Na-P1 from South African coal fly ashes, *J. Environ. Sci. Health Part A*, 47, 2012, 337-350.
- [27] D. Mainganye, T. V. Ojumu, L. Petrik, Synthesis of zeolites Na-P1 from South African coal fly ash: Effect of impeller design and agitation, *Materials*, 2013, 6: 2074-2089.
- [28] J. Behin, S.S. Bukhari, V. Dehnavi, H. Kazemian, S. Rohani, Using coal fly ash and wastewater for microwave synthesis of LTA zeolite, *Chemical Engineering and Technology* 37 (2014) 1532-1540.
- [29] S.S. Bukhari, J. Behin, H. Kazemian, S. Rohani, A comparative study using direct hydrothermal and indirect fusion methods to produce zeolites from coal fly ash utilizing single-mode microwave energy, *Journal of Materials Science* 49 (2014) 8261-8271.
- [30] S.S. Bukhari, J. Behin, H. Kazemian, S. Rohani, Synthesis of zeolite Na-A using single mode microwave irradiation at atmospheric pressure: The effect of microwave power, *The Canadian Journal of Chemical Engineering*, DOI 10.1002/cjce.22194.
- [31] M. Inada, H. Tsujimoto, Y. Eguchi, N. Enomoto, J. Hojo, Microwave-assisted zeolite synthesis from coal fly ash in hydrothermal process, *Fuel*, 2005, 84: 1482-1486.
- [32] R. Juan, S. Hernández, J.M. André, C. Ruiz, Synthesis of granular zeolitic materials with high cation exchange capacity from agglomerated coal fly ash, *Fuel*, 2007, 86: 1811-1821.
- [33] K. Fukui, M. Katoh, T. Yamamoto, H. Yoshida, Utilization of NaCl for phillipsite synthesis from fly ash by hydrothermal treatment with microwave heating, *Adv. Powder Technol.*, 2009, 20: 35-40.
- [34] C. Belviso, F. Cavalcante, A. Lettino, S. Fiore, Effects of ultrasonic treatment on zeolite synthesized from coal fly ash, *Ultrason. Sonochem.* 2011, 18: 661-668.

- [35] S.S. Bukhari, S. Rohani, H. Kazemian, Effect of ultrasound energy on the zeolitization of chemical extracts from fused coal fly ash, *Ultrason. Sonochem.* 2016, 28: 47-53.
- [36] P.M. Slangen, J.C. Jansen, H. Van Bekkum, The effect of ageing on the microwave synthesis of zeolite NaA, *Microporous Mater.* 1997, 9: 259-65.
- [37] O. Andac, M. Tatlier, A. Sirkecioglu, I. Ece, A. Erdem-Senatarlar, Effect of ultrasound on zeolite-A synthesis, *Microporous and Mesoporous Materials* 79 (2005) 225-233.
- [38] M. Abrishamkar, S.N. Azizi, H. Kazemian, Synthesis of borosilicate MFI type zeolite using different ageing techniques, *Chem. Met. Alloys* 3 (2010) 12-17.
- [39] R. Sabouni, H. Kazemian, S. Rohani, A novel combined manufacturing technique for rapid production of IRMOF-1 using ultrasound and microwave energies, *Chemical Engineering Journal* 165 (2010) 966-973.
- [40] J. Gordon, H. Kazemian, S. Rohani, Rapid and efficient crystallization of MIL-53 (Fe) by ultrasound and microwave irradiation, *Microporous and Mesoporous Materials* 162 (2012) 36-43.
- [41] S. Askari, Sh. Miar Alipour, R. Halladj, M.H. Davood Abadi Farahani, Effects of ultrasound on the synthesis of zeolites: a review, *J. Porous Mater.* 20 (2013) 285-302.
- [42] S.S. Bukhari, J. Behin, H. Kazemian, S. Rohani, Conversion of coal fly ash to zeolite utilizing microwave and ultrasound energies: A review, *Fuel* 140 (2015) 250-266.
- [43] S.N. Azizi, N. Asemi, the effect of ultrasonic and microwave-assisted aging on the synthesis of zeolite P from Iranian perlite using Box-Behnken experimental design, *Chem. Eng. Comm.* 2014, 201: 909-925.

[44] P. Pal, J.K. Das, N. Das, S. Bandyopadhyay, Synthesis of NaP zeolite at room temperature and short crystallization time by sonochemical method, *Ultrasonics Sonochemistry* 20 (2013) 314-321.

[45] M.M.J. Treacy, J.B. Higgins, *Collection of simulated XRD powder patterns for zeolites*, Elsevier (2007).

[46] M. D. Luque de Castro, F. Priego-Capote Ultrasound-assisted crystallization (sonocrystallization), (2007 b) *Ultrasonics Sonochemistry*. 14: 717-724.

Chapter 4

EFFECT OF MICROWAVE IRRADIATION ON CRYSTAL GROWTH OF ZEOLITED COAL FLY ASH WITH DIFFERENT SOLID/LIQUID³

Abstract

In the present work, coal fly ash (CFA) was converted to zeolite (CFAZP) experimentally at atmospheric pressure via a conventional hydrothermal heating for 6 h at low temperature (90 ± 3 °C) followed by microwave irradiation for 30 min. The synthesized products were characterized using XRD, TGA/DTA, SEM, PSD, BET, and cation-exchange capacity (CEC) techniques. The effect of microwave on the crystal growth of nucleated CFAZP at different solid/liquid ratios (suspended CFA mass to NaOH solution volume, g/mL) was studied. A three-variable, three level central composite statistical experimental design was applied to investigate the effect of the independent variables on the response function defined as the ratio of the characteristic peak intensity at $2\theta: 28^\circ$ of a sample to that of the same peak of a sample run for 24 h with conventional heating. The relative peak intensity of CFAZP as high as 97 % was achieved under optimum experimental conditions with 1 M of NaOH concentration, 6 h of conventional heating followed by 30 min microwave irradiation with a solid/liquid

³ "This Chapter is published in the Advance Powder Technology. Tahani Aldahri, Jamshid Behin, Hossein Kazemian, Sohrab Rohani, Advance Powder Technol. 28, 2865(2017)".

ratio of 0.40 g/mL. Under constant microwave energy, higher solid/liquid ratios led to higher relative peak intensity of the product.

Keywords: Coal fly ash; Crystallization; Na-P Zeolite; Microwave energy; CFA/NaOH ratio

4.1. Introduction

Coal fly ash (CFA), as a by-product of coal fired power plants, is considered as one of the biggest industrial waste streams in the world [1,2]. About 50% of the world's electricity energy is produced by burning coal [3]. Treatment of CFA is a worldwide priority due to several reasons, including but not limited to its harmful effects on the environment. In addition, disposing this solid waste, in landfills is a financial liability for the coal burning power plants [4]. In order to overcome this problem, numerous investigations have been conducted on the zeolitization of CFA as a source of silicon and aluminum. CFAZP is an interesting synthesized zeolite with high cation exchange capacity (CEC) [5-11].

Successful conversion of CFA to CFAZP was conducted using a conventional hydrothermal process at relatively high temperatures up to 200°C for 8-100 h [12-15]. The synthesized product had a relatively high cation exchange capacity and crystallinity [16-18]. The characteristics of zeolites such as purity and CEC were strongly influenced by the hydrothermal heating methods and the synthesis parameters such as the reaction time, temperature, etc. [19-22]. Conventional hydrothermal treatment is an energy-intensive and time-consuming process which is difficult to commercialize. Using microwave (MW) and ultrasound (UTS) as alternative energy sources could lead to homogenous nucleation and uniform distribution of thermal energy and decrease the reaction time remarkably from days down to hours, which can lead to an economically

viable zeolitization process [23-28]. Inductive energies can strongly affect the synthesis of zeolites by accelerating the crystallization process [29-36].

Querol et al. [37] synthesized CFAZP from CFA by conventional and microwave-assisted hydrothermal alkaline activation experiments. Synthesis yields obtained from both methods were similar, but the activation time needed was drastically reduced from 24-48 h to 30 min by using microwaves. All experiments were carried out using 0.5-5.0 M of NaOH, CFA mass to NaOH solution volume ratios of 0.05-0.1 g/ml and the highest microwave power available (1000 W) with temperature control. Inada et al. [38] investigated the effect of microwave irradiation on the yield of zeolite from CFA. The NaOH concentration was 2 M and the solid/liquid ratio was fixed at 0.125g/ml for safe irradiation of microwave. The microwave heating was performed by using a household oven (500 W) refurbished to equip the vessel with a condenser under the ambient atmosphere. CFAZP was formed after the conventional treatment at 100 °C, but no zeolitic product was obtained by microwave heating alone after 2 h. In the combined experiment, however, zeolitization was achieved when the microwave was applied for 15 min in the course of the conventional heating. The initial MW irradiation was more effective. This is due to the stimulated dissolution of SiO₂ and Al₂O₃ from CFA. On the other hand, the microwave irradiation in the middle to later stages of the process retarded the crystallization of zeolite. Especially, the microwave heating at 45-60 min into the process influenced the zeolitization negatively.

Fukui et al. [39] synthesized phillipsite from CFA with a solid to liquid ratio of 0.04g/ml at controlled temperature 100 °C (variable power) over 6 h of conventional heating and microwave heating. Microwave heating reduced the crystallization induction time compared to the conventional heating, but it retarded the crystal growth rate slightly leading to smaller particle size of the synthesized phillipsite. They showed

that the crystal structure and chemical composition of the product powder did not depend on the heating method [15]. To the best of our knowledge, utilizing MW energy after a period of conventional heating for the crystallization of CFAZP from CFA has not been reported. In this study, CFA was converted into CFAZP by means of microwave irradiation of CFA after hydrothermal treatment in an alkali medium. Furthermore, the effectiveness of the hydrothermal and microwave-assisted hydrothermal method is compared.

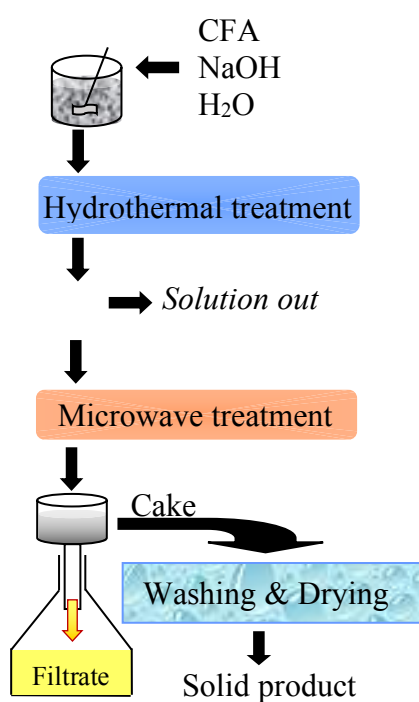
4.2. Materials and method

Coal fly ash, as a source of Al and Si, was supplied by a coal-fired power plant (OPG, Nanticoke) located in Ontario, Canada. Analytical grade sodium hydroxide (Alphachem, Canada) was used as received. Deionized water was used for the preparation of the solutions and washing.

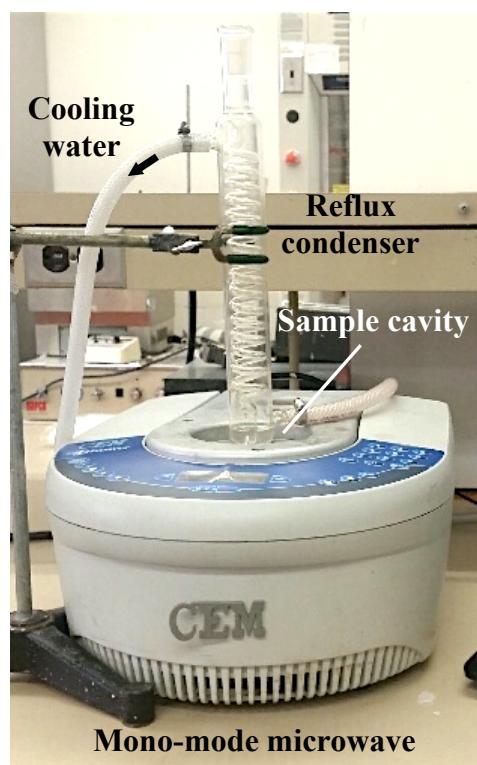
Two g of CFA and 0.8 g of sodium hydroxide granules were dissolved in 20 ml deionized water to form an alkaline slurry of 1M (solid/liquid ratio of 0.10 g/ml). The mixture was subjected to conventional heating under atmospheric pressure at 90 °C for 6 h and stirred continuously using a heater stirrer (Thermo Scientific, China) at 170 rpm. The schematic of the synthesis procedure and microwave setup are illustrated in Figure 4-1.

After hydrothermal treatment for 6 h in a 125-ml glass flask reactor in which Si and Al were extracted into the liquid, and achieving a desired solid/liquid ratio, a certain amount of the liquid phase was withdrawn by a syringe filter to adjust the solid/liquid ratio range. The latter was chosen in a way to allow the solids to form a wet bed for the safe irradiation of microwave and avoiding the hot spots issue. The residual mixture was poured into a cylindrical PTFE vessel (40 ml, 28 mm ID) attached to a reflux

condenser. The suspension was subjected to microwave radiation for crystal growth at 105 °C for 15-30 min. Then, the filtered solid products were washed and dried overnight at room temperature. Microwave power was constant at 250 W during the experiments. The microwave treatment was performed in a self-adjusting microwave oven (single-mode microwave apparatus equipped with a magnetic stirrer, 2.45 GHz, CEM cooperation, Discover, USA), where the reaction temperature and power were monitored automatically.



(a) High Solid/Liquid (S/L) ratio



(b) Microwave apparatus

procedure

Figure 4-1. Schematic diagrams of experimental procedure and microwave set-up

Rigaku-MiniFlex powder diffractometer (Japan) was used to collect XRD diffraction pattern data of the synthesized samples using $\text{CuK}\alpha$ (λ : 1.54059 Å) over the range of $5^\circ < 2\theta < 40^\circ$ with step width of 0.02° and scan speed: $2^\circ/\text{min}$. The XRD patterns of the synthesized zeolite samples were compared with the characteristic peaks of CFAZP from the literature [40]. The peak intensities were calculated by the "peak fitting" algorithm in the MDI-Jade v 7.5 software. Intensities of the characteristic peaks were found for CFAZP main peaks at 2θ of 12.5° , 21.3° , and 28° . The relative peak intensity was defined as the ratio of the characteristic peak intensity at 2θ : 28° of a sample to that of the same peak of a sample run for 24 h with conventional heating. Crystal morphology of the produced zeolite was studied by scanning electron microscope (SEM) using a JSM 600F (Joel, Japan) operating at 10 keV. Thermal analysis was performed using a Mettler Toledo TGA/DTA 851e model (Switzerland) with version 6.1 Stare software by heating the samples from 25°C to 600°C with a heating rate of $10^\circ\text{C}/\text{min}$ under nitrogen purge of $40\text{mL}/\text{min}$. Master-sizer 2000 (Malvern Instruments Ltd., UK) was used for the particle size distribution (PSD) analysis. Brunauer-Emmett-Teller (BET) technique was used to measure the specific surface area, pore size and pore volume of selected CFAZP using a Micrometrics Accelerated Surface Area and Porosimetry (ASAP 2010) analyzer (Micrometrics, USA). CFAZP samples were degassed for 6-8 h at 150°C , before the analysis. The cation-exchange capacities (CECs) values of the synthesized CFAZP samples were determined based on Bain and Smith procedure; using the ammonium acetate saturation standard method [41]. The crystal size was calculated using Scherrer's equation [42]:

$$d(2\theta) = \frac{K \cdot \lambda}{\beta \cos\theta} \quad (\text{Eq. 4-1})$$

where d is average crystal size (nm), K is the Scherrer's constant, λ is the wavelength of the X-rays (nm), θ is the value of the Bragg angle, and β is the full width at half-maximum (FWHM) of the broad peak in radians.

4.3 Experimental design

A central composition design (CCD) was considered with three variables, the molarity of alkaline solution, solid to liquid ratio, and microwave irradiation time as the independent variables in the zeolitization process. The experimental design was conducted in Design Expert Software (ver.7.1.5, USA). According to the CCD, all variables have three levels (-1, 0, +1) as shown in Table 4-1.

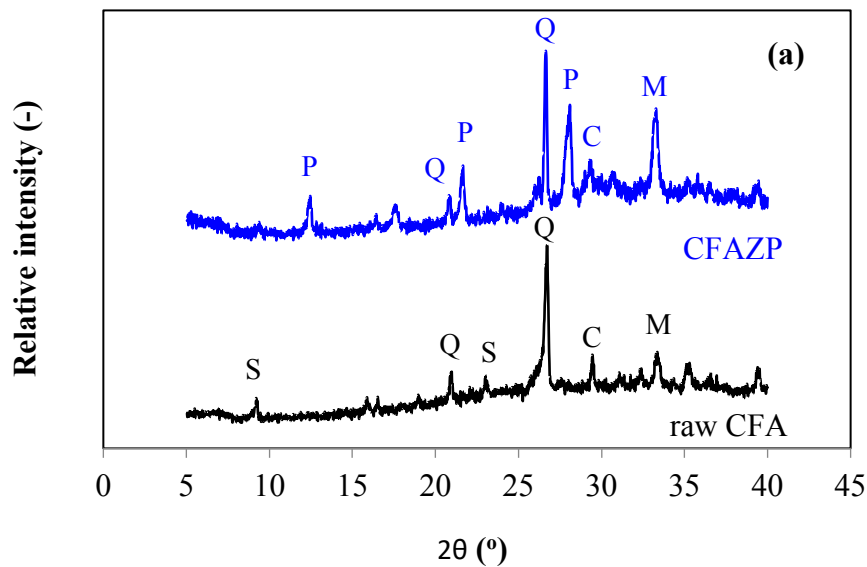
Table 4-1: Range and levels of experimental variables.

Independent variable	Unit	levels and Range		
		<i>-1</i>	<i>0</i>	<i>1</i>
A : Solution molarity	mol/L	1.00	1.15	1.30
B : Solid/liquid ratio	g/mL	0.10	0.25	0.40
C : Microwave time	min	15.00	22.5	30.00

4.4. Results and discussion

The results of XRD patterns are shown in Figure 4-2 a. For comparison, the XRD patterns of the raw coal fly ash are also shown for the 2θ ranging from 5 to 40 degrees. Quartz, mullite, calcite and hematite are the main crystalline phases present in the raw CFA. During the conventional heating process of the CFA with sodium hydroxide, hematite and calcite phases were partially dissolved; therefore, the intensities of peaks

(at 2θ : 23° , 32.3°) were decreased. No noticeable dissolution of quartz was observed at the mild alkaline conditions indicating high resistance of quartz under direct conventional hydrothermal conversion of CFA to CFAZP. Mullite appeared to be a reactive silica crystalline phase of CFA during the course of zeolite formation. The XRD patterns of the zeolite synthesized by hydrothermal crystallization showed at least three main characteristic peaks at 2θ : 12.46° , 21.67° , and 28.10° confirming the successful formation of zeolite CFAZP as the major crystalline phase of the zeolitized CFA. For comparison and in order to achieve the best quality of zeolitized CFA with the highest relative peak intensity at 2θ : 28° (the objective function) of Na-P zeolite product, a conventional hydrothermal synthesis was conducted at 90°C for 24 h. The alkaline-solution molarity and solid/liquid ratio were considered as 1 M and 0.10 g/ml, respectively.



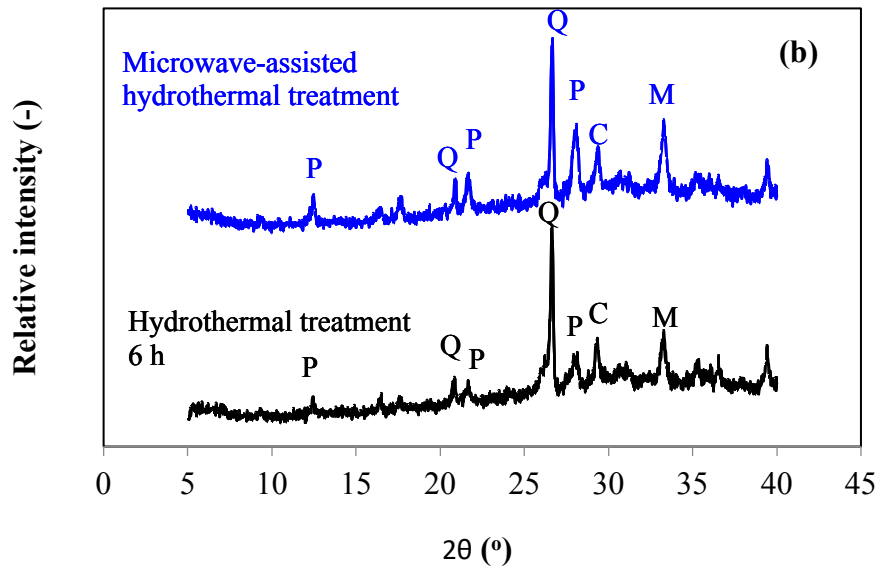


Figure 4-2: XRD patterns (a) Raw CFA and CFAZP synthesized hydrothermally at 90 °C for 24 h, (b) CFAZP synthesized hydrothermally for 6 h and CFAZP synthesized hydrothermally (6 h) followed by microwave irradiation for 30 min, where C: calcite, M:mullite, P: zeolite Na-P, Q: quartz, and S: hydroxyl-sodalite

To find the optimal conditions for maximum relative peak intensity at $2\theta: 28^\circ$ of the product under microwave-assisted hydrothermal procedure, the CCD experimental design was carried out. The effects of the molarity of alkaline solution, solid to liquid ratio, and microwave irradiation time on response factor as well as the observed and the CCD model predicted values of the peak intensity are presented in Table 4-2. As shown in Table 4-2, the percentage relative peak intensity ($I_{rel.}$) was calculated by dividing the peak intensity of a product at $2\theta: 28.1^\circ$ by the peak intensity of the standard sample run for 24 h using conventional hydrothermal synthesis with estimated errors ± 0.05 at the same 2θ of a sample.

$$I_{rel.}(\%) = \frac{\text{The peak intensity of the sample at } 2\theta: 28^\circ}{\text{The peak intensity of the standard sample at } 2\theta: 28^\circ} \times 100 \quad (\text{Eq. 4-2})$$

The best sample (Run 5 of Table 4-2) with the highest peak intensity, was obtained with 6 h of conventional heating followed by 30 min of MW irradiation, with solid to liquid ratio of 0.40g/ml, and 1 M of NaOH concentration. Figure 4-2 b shows the XRD pattern of the sample synthesized by means of conventional hydrothermal method at 90 °C for 6 h (1 M of NaOH and solid/liquid ratio: 0.10 g/ml) and the best sample synthesized under optimized condition at 30 min of MW irradiation. To synthesize CFAZP from CFA, it seems hydrothermal treatment time of at least 6 h prior to microwave treatment is necessary, which agrees with another work that reported continuous microwave irradiation could not initiate the nucleation of CFAZP from un-treated CFA as main source of Si and Al [38]. It seems nucleation starts under conventional hydrothermal treatment as was confirmed by the appearance of characteristic peaks CFAZP with low intensity. Microwave irradiation speeds up crystal growth leading to a zeolite product with higher relative peak intensity. The relative peak intensity of CFAZP obtained under higher solid/liquid ratio of 0.40g/ml was comparable with the zeolite obtained under lower solid/liquid of 0.10g/ml ratio; at 97.09 % and 93.51 %, respectively.

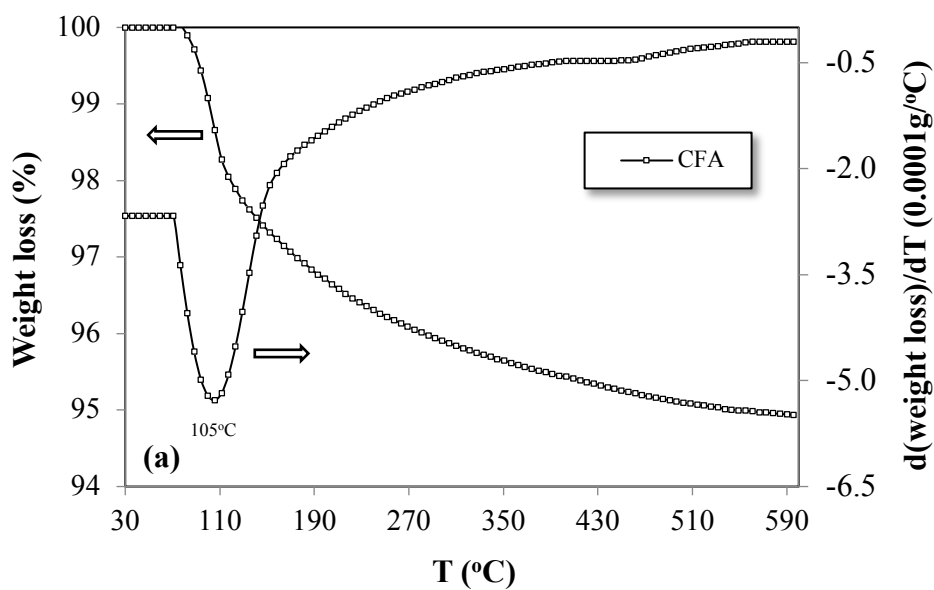
Table 4-2: Central composite design matrix for three test variables in coded units along with the observed and predicted responses (microwave power: 250 W)

Run order	Factors			Response factor	
	Molarity (mol/l)	Solid/liquid ratio (g/ml)	MW irradiation time (min)	Relative peak intensity at peak of 2θ: 28° (%)	
	A	B	C	observed	predicted
1	1.00	0.10	30.0	93.51	94.23
2	1.15	0.25	22.5	80.71	80.59
3	1.15	0.25	15.0	79.32	76.10
4	1.15	0.25	22.5	80.01	80.59
5	1.00	0.40	30.0	97.09	97.96

6	1.15	0.25	22.5	80.99	80.59
7	1.15	0.40	22.5	83.33	76.79
8	1.30	0.10	15.0	83.42	83.71
9	1.15	0.10	22.5	83.13	83.86
10	1.00	0.40	15.0	67.40	70.83
11	1.30	0.40	30.0	71.31	72.54
12	1.15	0.25	22.5	77.01	80.59
13	1.30	0.25	22.5	67.39	74.13
14	1.15	0.25	22.5	82.99	80.59
15	1.00	0.10	15.0	83.14	83.08
16	1.30	0.40	15.0	65.40	65.84
17	1.30	0.10	30.0	76.68	74.42
18	1.15	0.25	22.5	83.99	80.59
19	1.15	0.25	30.0	84.70	85.10
20	1.00	0.25	22.5	85.05	86.52

After 6 h conventional heating applied to all samples, small peaks of CFAZP crystals were observed. When that step was followed by either 30 min MW irradiation at ~ 105 °C under atmospheric pressure, or using oven heating for additional 18 h at 90 °C; high XRD peaks of zeolite CFAZP were observed as shown in Figure 4-2 (a, b). Following the initial conventional heating for 6 h, the required additional 18 h of oven heating was reduced to 30 min with MW irradiation. The samples of raw CFA and the CFAZP with highest peak intensity of 97 % (Run 5) were analyzed using thermogravimetric analysis (TGA/DTA) (Figure 4-3). In Figure 4-3a, the TGA curve of raw CFA shows a single inflection point at 105°C corresponding to an endothermic weight loss of ~ 5 %, which is attributed to the removal of physically adsorbed water from the solid sample. Figure 4-3b displays the TGA curves of zeolites synthesized by 6 h conventional hydrothermal heating and the zeolites synthesized hydrothermally for 6 h followed by microwave heating for 30 min. The TGA curves show 7% and 12% weight

losses corresponding to the point of inflection approximately 120 °C and 115 °C, respectively. These weight losses indicate that the water content in the produced zeolites is much higher than the raw CFA due to the higher micro porosity area and larger surface area. Shifting of dehydration temperature of the MW-assisted sample from 120 °C to 115 °C could be attributed to the larger micropore area and pore volume of the sample in comparison to the conventionally synthesized sample. [29]. These results were confirming the obtained BET micropore surface areas that are presented in Table 4-3. It was found that MW heating increases the water adsorption capacity of the produced CFAZP.



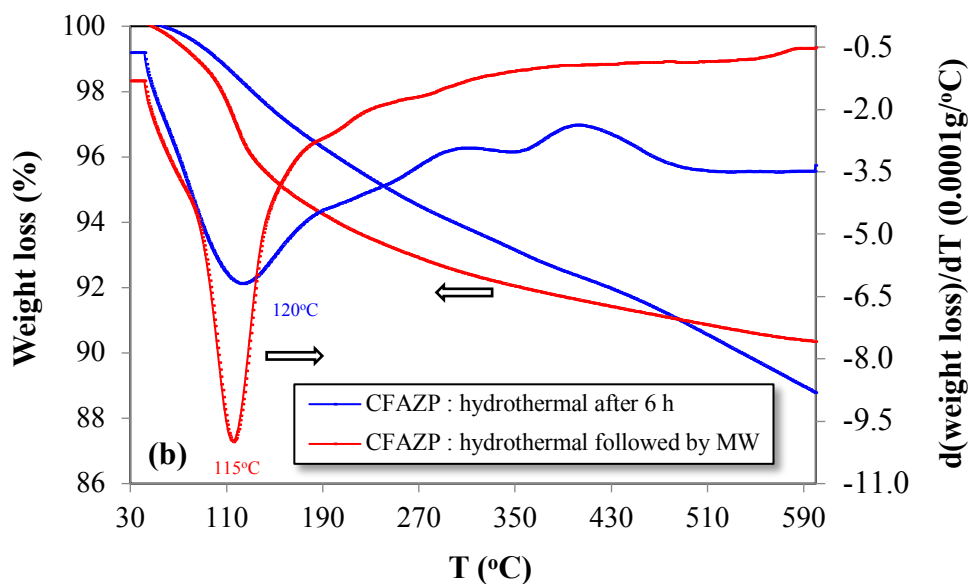


Figure 4-3: TGA/DTA of (a) Raw CFA; (b) CFAZP synthesized hydrothermally and hydrothermally followed by microwave

The particle size distribution curves of both raw CFA and the CFAZP product are illustrated in Figure 4-4. The particle size analysis reveals little change during zeolitization process during the conventional heating process. The small particles of CFA are consumed during alkaline hydrothermal treatment and the particles size of the final product is slightly increased that could be relate to agglomeration smaller particles. The microwave-assisted synthesis zeolite CFAZP resulted in particles with narrower particle size distribution. In this work, it seems using MW after hydrothermal treatment step (under the tested condition) have a strong effect on decreasing agglomeration and controlling of particle size. The particle size distribution corresponding to the sample processed hydrothermally for 6 h (0.8-1000 μm), became narrower for the sample processed with microwave (10-420 μm).

In microwave assisted synthesis of zeolites, the fast and homogenous nucleation and crystal growth results in reducing of agglomerates formation. Therefore, MW-

assisted synthesized zeolite has a narrower particle size distribution [43, 44]. However, according to Ansari et al. [45], with increasing crystallization temperature the simultaneous progress of generation and resolution of zeolite crystal in solution leads to generate of larger agglomerated zeolite particles.

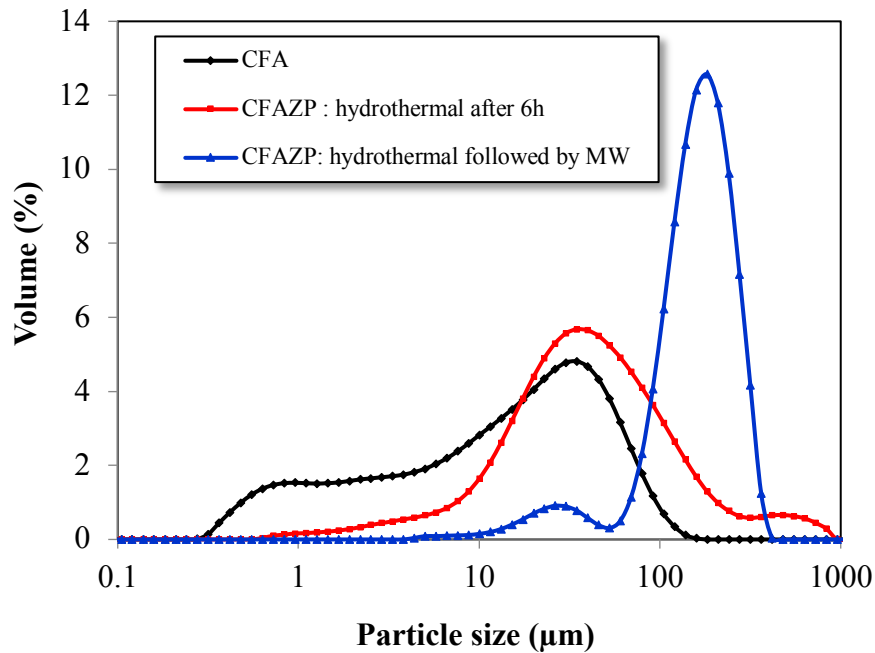
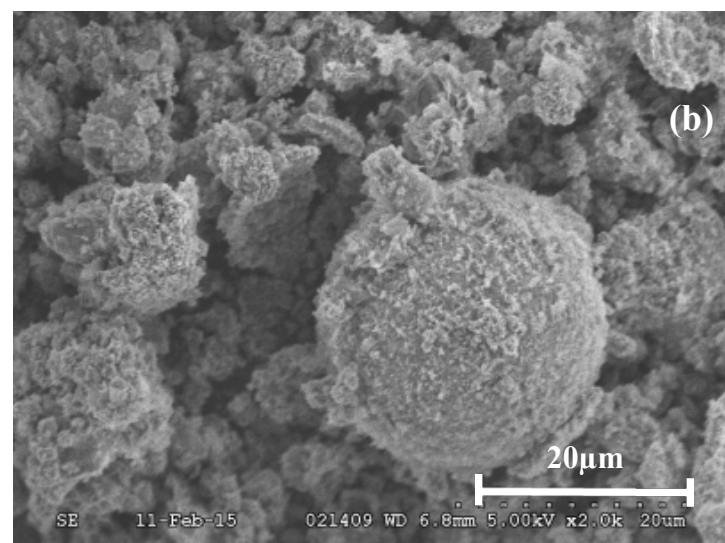
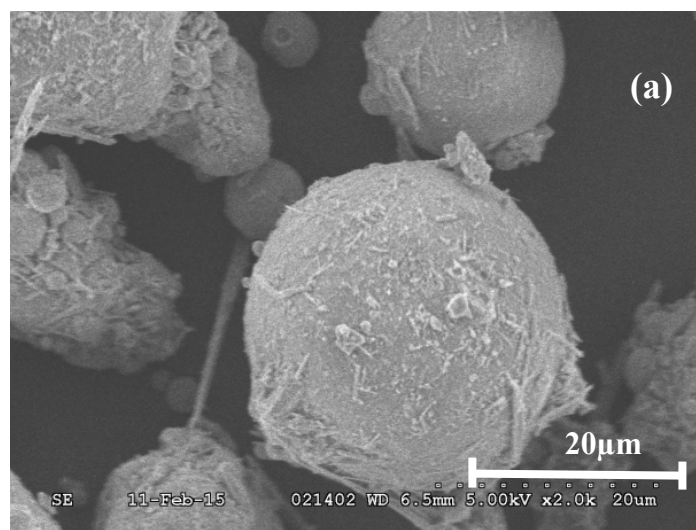


Figure 4-4: Particle size distribution of raw CFA and synthesized CFAZP

Figure 4-5 shows the SEM micrographs of raw CFA and the zeolitized CFA under the best conditions (i.e. M: 1; solid/liquid ratio: 0.40 g/ml and MW irradiation: 30 min) with highest relative peak intensity of 97%. It reveals that the CFA used in this study is quasi-spherical with a smooth surface. Significant changes occur on the surface of CFA during zeolitization process. Figure 4-5b displays the surface of CFA after 6 h hydrothermal treatment which shows that zeolite particles started to form on the CFA's surface, partially activating the fly ash spheres which agrees with the literature [38,46]. Figure 4-5c shows Na-P zeolite particles cover the whole surface of CFA due to applying the MW irradiation after conventional heating. MW heating enhances the rate

of crystal growth of zeolite CFAZP. The micrographs of CFAZP demonstrate uniform distribution of the zeolite particle sized and uniform morphology of its crystallites. Zeolite CFAZP can be identified on the surface of the CFA pseudo-spherical forms as small plates, which form polycrystals with an average size of approximately 1-1.5 μm . This typical morphology, which comprises most of the samples, displays well-defined CFAZP crystal faces [7].



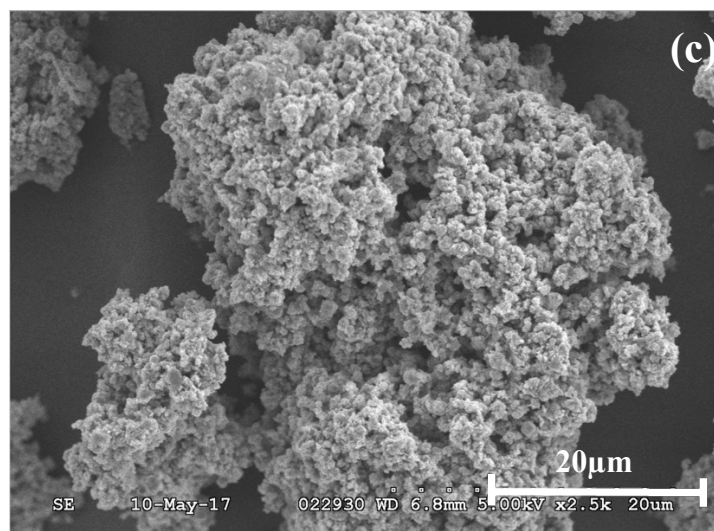


Figure 4-5: The SEM images of the CFA and microwave-assisted synthesized zeolites samples after 30 min irradiation (a) Raw CFA (b) CFAZP synthesized hydrothermally for 6 h (c) CFAZP synthesized hydrothermally for 6 h followed by 30 min microwave irradiation

Table 4-3 displays the BET surface area of the raw CFA and the best CFAZP sample synthesized under optimized condition as $15.47 \text{ m}^2/\text{g}$ and $72.05 \text{ m}^2/\text{g}$, respectively. A remarkable increase of surface area was achieved by zeolitization of CFA. The micro pore area of the produced samples was $17 \text{ m}^2/\text{g}$. According to the XRD and SEM results, the synthetic zeolite (CFAZP) was formed on the surface of CFA, which attributes to the increase of the surface area due to the higher microporosity of CFAZP. The pore volume and the mean pore diameter of the best sample were $0.134 \text{ cm}^3/\text{g}$ and 110.68 \AA , respectively. The proposed technique of synthesis allows to produce CFAZP with surface area of ~ 4.7 times higher than raw CFA and ~ 2 times higher than CFAZP; which was synthesized conventionally at $105 \text{ }^\circ\text{C}$ for 24h (with the BET surface area and pore volume of $39 \text{ m}^2/\text{g}$ and $0.015 \text{ cm}^3/\text{g}$, respectively) [47]. Higher loss on ignition of the MW- assisted synthesized sample could be explained

because of its larger surface area and larger pore volume, which leads to higher water sorption capacity [29]. The BET surface area of the CFAZP which was synthesized conventionally and CFAZP which was synthesized by MW-assisted synthesis were 39 m²/g and 72.05 m²/g, respectively. Furthermore, the pore volume of the MW-assisted and conventionally synthesized CFAZP were 0.134 cm³/g and 0.015 cm³/g, respectively [47]. Nitrogen adsorption/desorption isotherm of the CFAZP product, which is illustrated in Figure 4-6 indicates a type I isotherm. A type I isotherm is known for the microporous zeolites according to Applied Chemistry (IUPAC) isotherm classification and the International Union of Pure [48,49]. The limited adsorption of N₂ inside the pores, could be attributed to the impurities that occupy pores and channels of CFAZP.

The cation-exchange capacities (CECs) of the raw CFA and the best CFAZP sample which was synthesized under optimized condition were 0.30 meq/g and 0.48 meq/g, respectively. To compare, the CEC of the CFAZP synthesized by conventional heating was 0.22 meq/g [47]. The new synthesis technique enhances the CEC of the synthesized CFAZP by ~38% and ~54% compared to the CEC of the raw CFA and the CFAZP synthesized by conventional heating; respectively. Due to the high CEC, the product (CFAZP) could be very useful as an adsorbent for many environmental applications.

Table 4-3: BET surface area of CFA and synthesized CFAZP.

	CFA	CFAZP		
		MW: 0 min	MW:15 min	MW:30 min
BET surface area (m ² /g)	15.47	57.20	59.12	72.05
Micropore area (m ² /g)	3.38	6.38	7.36	17.10

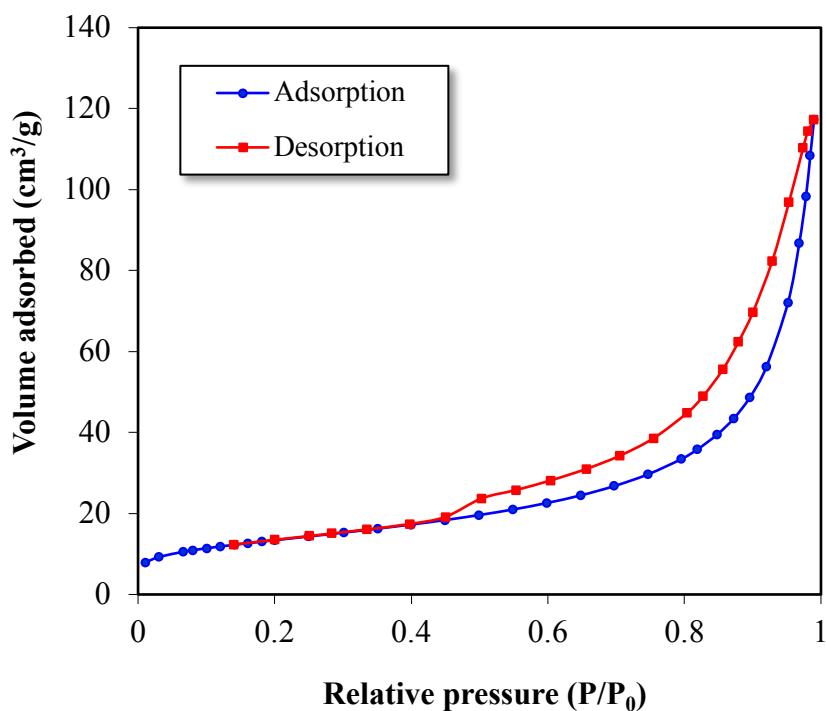


Figure 4-6: Adsorption/desorption isotherms of CFAZP synthesized under optimized condition (Run 5)

The crystal size of the prepared zeolites at various synthesis conditions was estimated using Scherrer's equation (Eq. 4-1) from the peak width of (310) reflection plane at 2θ : 28.1° . The full width at half-maximum (FWHM) of the broad peak calculated by "peak fitting" algorithm in the MDI-Jade v 7.5 software and the results are presented in Table 4-4. Results show that crystal size and relative peak intensity of synthesized zeolite CFAZP increases as MW time increase. This result agrees with the finding of literature [45] where authors found that zeolite LAT under longer time at 25°C has narrow particle size distribution with small crystal size up to $0.4\ \mu\text{m}$ [50].

Table 4-4: Crystal size of synthesized CFAZP at different microwave time.

Heating method	Temperature (°C)	Time (min)	Relative peak intensity (%)	Crystal size (nm)
Microwave- assisted	105	15	67.4	25
Microwave-assisted	105	22.5	85.0	29
Microwave-assisted	105	30	97.09	31

4.4.1 Statistical analysis

The statistical significance of the model was analyzed by the analysis of variance (ANOVA). The model F-value of 14.84 implies the model is significant. There is only a 0.01% chance that a model F-value this large could occur due to noise. Table 4-5 presents statistical characteristics of the selected model's parameters to describe the relative peak intensity as a function of the variables studied. The significance of the coefficients was determined by F-value and P-value (probability value). A small probability value ($p < 0.05$) indicates that the model was highly significant. The probability value (0.0001) shows that the effect of the variables on the relative peak intensity of CFAZP is significant. Also, the probability value (0.0001) shows the highest effect of NaOH concentration on the relative peak intensity of the CFAZP sample, while the probability value (0.0065) shows the lowest effect of solid/liquid ratio on the relative peak intensity of the CFAZP. The goodness of the fit for the model was validated by the determination correlation coefficient (R^2). Correlation coefficient (R^2) measures the amount of variations about the mean. Adjusted R^2 estimates the variations about the mean adjusted for the number of parameters in model. Predicted R^2 enunciates the predictive capability of model. Adequate precision compares the range of predicted

values at design points to the average prediction error and is a measure of the signal to noise ratio (S/N ratio) [51,52]. Correlation coefficient was 0.8726 which indicates the absence of variations about the mean. When the difference between R^2_{Adj} and R^2_{Pred} is less than 0.2, R^2_{Pred} would be in reasonable agreement with R^2_{Adj} . Difference between R^2_{Pred} of 0.638 and R^2_{Adj} of 0.8138 was found less than 0.2 which indicates the rational agreement between regression coefficients. Moreover, the adequate precision is a measure of the range of the predicted response relative to its associated error. The adequate precision greater than 4 (15.728 in this case) shows that the model could be used to navigate the design space defined by the CCD. From the analysis data that is shown in Table 4-5, the terms A, B, C, AC, BC are significant and other model's terms are not significant (with a probability value larger than 0.05).

Table 4-5: Analysis of variance (ANOVA) for prediction of relative peak intensity by the quadratic model*

Parameters	Statistics				
	Sum of squares	Degree of freedom	Mean squares	F-value	P-value
Model	1060.77	6	176.79	14.84	<0.0001
A: Molarity (mol/l)	384.28	1	384.28	32.25	<0.0001
B: S/L ratio (g/ml)	124.96	1	124.96	10.49	0.0065
C: MW time (min)	199.01	1	199.01	16.70	0.0013
AB	15.76	1	15.76	1.32	0.2708
AC	209.00	1	209.00	17.54	0.0011
BC	127.76	1	127.76	10.72	0.0060
Residuals	154.92	13	11.92		
Lack of fit	125.05	8	15.63	2.62	0.1521

*The model F-value implies the model is significant. A probability less than 0.05 indicates model terms are significant. In this case A, B, C, AC, BC are significant model terms.

In order to describe the effects of the variables studied, a quadratic model was fitted to the actual data. The quadratic model for predicting the relative peak intensity ($I_{rel,prd}$) of the zeolitized samples in terms of the coded variables with significance of 99.99% is as follow:

$$I_{rel,prd} = 4.849 + 76.496 A - 31.744 B + 4.932 C - 4.543 AC + 3.552 BC \quad \text{(Eq. 4-3)}$$

The negative coefficients of the model components indicate the unfavorable effects of B and AC on the relative peak intensity, while, the positive coefficients for A, C and BC indicate favorable effects on the response.

The main diagnostic plots were used to evaluate the response surface design, ensuring that the statistical assumptions fit the analyzed data. The predictions of the experimental data by developed quadratic model for the relative peak intensity are illustrated in Figure 4-7 that convey the general impression of a normal distribution of underlying errors. Since the relative peak intensity values fall near a straight line; there is no clear indication of non-normality of experimental results. Based on these plots, the relative peak intensity values appear to be randomly scattered; thus, the proposed model is adequate and the constant variance assumption is confirmed.

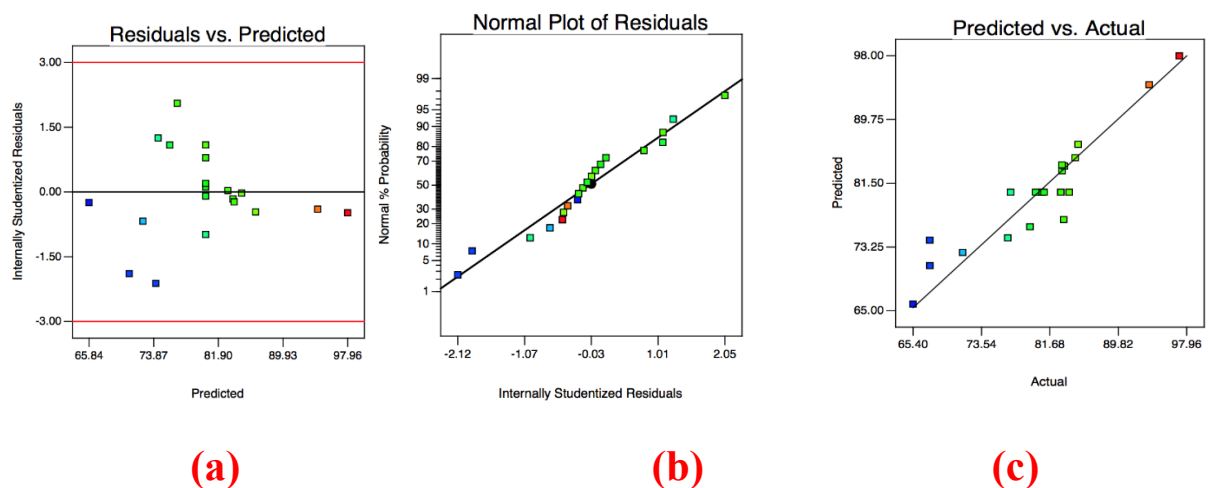
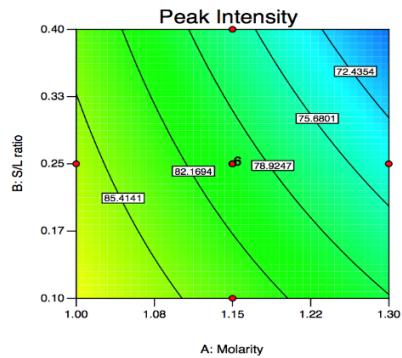
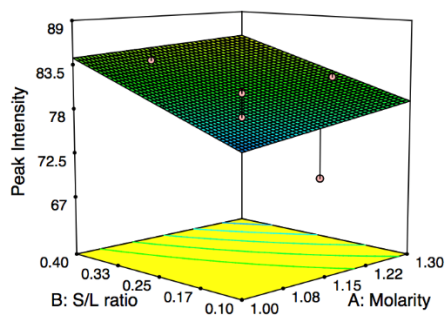
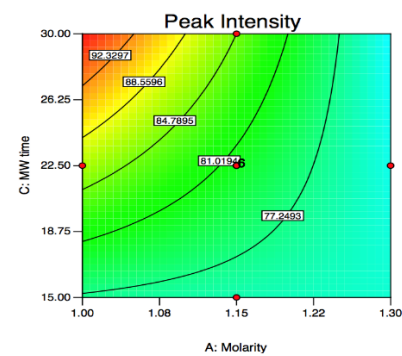
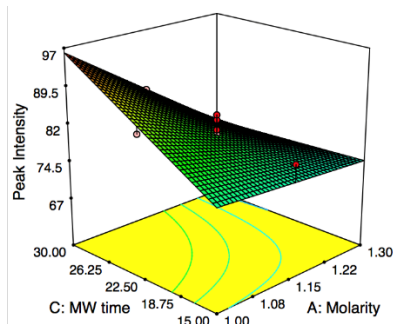


Figure 4-7: Diagnostic plots for relative peak intensity (a) normal probability, (b) predicted vs. actual values, and (c) residuals vs. predicted values.

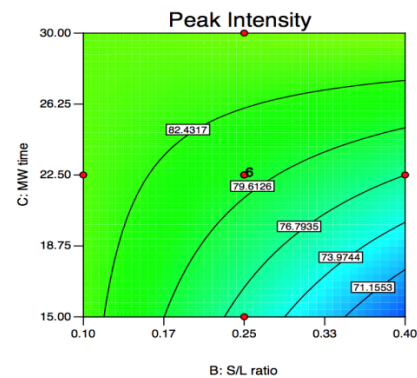
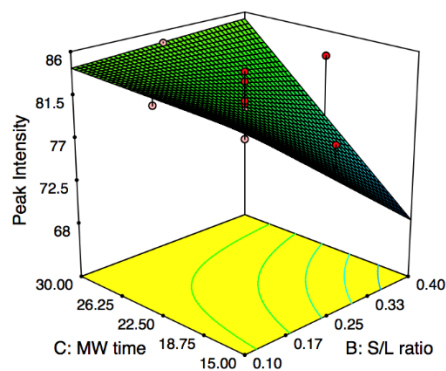
The contour and 3D plots of the relative peak intensity vs solid/liquid ratio, MW irradiation time and the molarity are shown in Figure 4-8. The relationship between solid/liquid ratio and molarity (Figure 4- 8a) is an inverse relationship where increasing both the molarity and the solid/liquid ratio of the sample mixture led to a decrease in the relative peak intensity. The time of MW irradiation and molarity led to a decrease in the relative peak intensity (Figure 4-8b). Increasing MW irradiation time and molarity led to a decrease in the relative peak intensity. The highest value of the relative peak intensity achieved at 30 min of MW irradiation time and 1 M. At 1.0-1.15 M NaOH concentration, a high relative peak intensity was observed when the time of MW irradiation was 26.25 to 30.0 min. Increasing the concentration of NaOH solution led to a decrease in the CFAZP's relative peak intensity. Moreover, the plot in Figure 4- 8c shows that increasing MW irradiation time and solid/liquid ratio led to an increase in the relative peak intensity. The highest relative peak intensity was achieved at a solid/liquid ratio equal to 0.40 g/ml and 30 min MW irradiation time. The experiments with a solid/liquid ratio higher than 0.40 g/ml weren't conducted to avoid the possible appearance of hot spots in the slurry solution and to keep a homogenous MW heating environment. The increase in the relative peak intensity at $2\theta: 28^\circ$ might be attributed to the higher dissolution of silica as sodium silicate and alumina as sodium aluminate when CFA reacts with the sodium hydroxide solution. In this figure, at a higher solid/liquid ratio (0.40 g/ml), the relative peak intensity of the product at $2\theta: 28^\circ$ is either at a minimum or a maximum depending on the time of MW irradiation.



(a) Molarity and Solid/Liquid (S/L) ratio



(b) Molarity and microwave irradiation (MW) time



(c) Solid/Liquid (S/L) ratio and microwave irradiation (MW) time

Figure 4- 8: 3D response surface and 2D contours showing the interaction effects of the variables on the relative peak intensity

4.4.2. Mechanism of microwave heating

In order to investigate the effect of the microwave irradiation on the relative peak intensity of the zeolite at 20: 28°, Inada et al. [38], Tanaka et al. [18], and Querol et al.

[37] obtained zeolite P1 from CFA by applying MW energy at a solid/liquid ratio 0.055-0.125 g/mL and found out that early stage MW irradiation is effective to produce zeolite CFAZP. Microwave irradiation breaks down the hydrogen bonds of H₂O molecules and enhances the dissolution of Si and Al from the CFA particles [38]. In the present work, hydrothermal treatment was applied in the first 6 h at a solid//liquid of 0.10 g/mL. During this step, aluminate ions and silicate ions dissolved from CFA into the solution and formed the precursor alumino-silicate gel. This precursor was attacked by sodium ions and it crystallized to CFAZP crystals. Figure 4-5b shows that the CFAZP particles start to deposit on the surface of the unreacted fly ash which confirms the XRD's result in Figure 4-2b. After hydrothermal treatment, the solid//liquid ratio of the synthesis mixture was changed to different values; 0.25 g/ml and 0.40 g/ml by withdrawing a certain amount of the liquid phase. Then, the mixture with higher solid/liquid ratio was exposed to MW irradiation (max 300 W) for 15 min to 30 min. Figure 4-5c shows the completion of the zeolitization process of the CFA after applying MW heating. The induction time of the crystallization in Figure 4-5b, was shortened by the microwave heating method. Microwave heating appears to help crystal growth, compared to the conventional heating which agrees with literature [53].

The proposed method, hydrothermal treatment prior to microwave irradiation, achieves the zeolitization of CFA in less time and leads to higher relative peak intensity of zeolite CFAZP. Table 4-2 shows that the relative peak intensity (~ 97 %) for the sample with a solid/liquid of 0.40 g/mL was higher than that (~ 93 %) for a sample with a solid/liquid of 0.10g/mL. This result shows that liquid phase retards the formation of CFAZP. This could be attributed to the MW irradiation characteristics. Since MW heating is generated via ionic conduction and dipolar polarization of water molecules, using microwave chemistry increases selectivity, raises thermal homogeneity, saves

time and increases the product yield [54]. The microwave assisted crystallization process mechanism is not fully understood, however; it is known to provide volumetric heating, rather than the conventional heating which heats by conduction and convection through a surface leading to a temperature profile within the reacting mixture. Microwave heating is generated when the irradiated molecules dipoles try to move quickly to arrange themselves with the electro-magnetic field. Also, during ions' oscillation with the oscillating field, they collide with other molecules in the solution and release large amounts of thermal energy. In addition, MW penetration depth is considered as an important factor that could affect the MW efficiency. Penetration depth depends on the dielectric properties of materials and the dielectric loss tangent; $\tan \delta = \frac{\epsilon''}{\epsilon'}$, where ϵ'' is the relative dielectric loss which is a measure of the ability of a dielectric material that converts MW irradiation to thermal energy, and ϵ' is the reflected or stored energy the relative dielectric constant which is a measure the ability of the dielectric material to reflect or store electrical energy [55,56]. In the present study; when an alkaline solution with a relatively large dielectric loss tangent ($\tan \delta$) was used, the reactant molecules in the solution with large $\tan \delta$ collide and raise the temperature [55]. When the MW irradiation introduced into the high solid/liquid ratio sample, a raise of temperature occurred on the surface of nuclei leading to an increase in the growth rate and crystal size. An increase in the intensity of X-ray diffraction peaks of CFAZP were observed which corresponded to an increase in the relative peak intensity at 2θ : 28.1° (Figure 4-5c). Recently, Gitari et al. [57] reported that decreasing the solid/liquid ratio could change the degree of the supersaturation which decreases the crystallization rate. Therefore, higher solid/liquid ratios increase the supersaturation faster leading to higher growth rate of the nano-particles. Formation of a zeolite structure consists of three stages including formation of building units,

nucleation by using the building units, and crystal growth followed the nucleation by adsorption of building units on the surface of zeolite nuclei [45]. In other word, zeolite crystals form on CFA's surface via precipitation method as a result of fast homogenous heating of particles. By using microwave heating after the hydrothermal treatment at higher solid/liquid ratios, the rate of crystal growth of zeolite increases due to the surface activation characteristic of MW irradiation which leading to a strong aggregation between zeolite particles and nuclei were formed during conventional heating step [57]. Increasing the solid/liquid ratio led to lower energy requirement due to a lower heating volume [58]. Thus, the present technique of zeolite synthesis significantly reduces the consumption of energy and increases the productivity of CFAZP.

4.5. Conclusions

The eco-friendly technique to synthesize zeolite P from coal fly ash by utilizing MW irradiation at high solid/liquid ratio after the initial conventional heating for 6 h, resulted in a higher yield of CFAZP and reduced the reaction time and energy consumption remarkably without decreasing the quality of the zeolite. The particle size distribution with MW irradiation was narrower and the SEM images and XRD data showed the product's relative peak intensity at $2\theta: 28.1^\circ$ was comparable with the zeolite obtained hydrothermally with 24 h of conventional heating. Post microwave heating enhanced the crystal growth of the existing nuclei formed during the initial 6 h of conventional heating.

4.6. References

- [1] R.S. Blissett, N.A. Rowson, A review of the multi-component utilization of coal flyash, *Fuel*, 97 (2012) 1–23.
- [2] X. Querol, N. Moreno, J.C. Umaña, A. Alastuey, E. Hernández, A. López-Soler, Synthesis of zeolites from coal fly ash: an overview, *Int Journal Coal Geol*, 50 (2002) 413–23.
- [3] M. Ahmaruzzaman, A review on the utilization of fly ash, *Progr Energy Combust Sci*, 36 (2010) 327-363.
- [4] I. Twardowska, J. Szczepanska, Solid waste terminological and long-term environmental risk assessment problems exemplified in a power plant fly ash study, *Sci. Total Environ*. 285 (2002) 29-51.
- [5] X. Querol, F. Plana, A. Alastuey, A. López-Soler, Synthesis of Na-zeolites from fly ash, *Fuel*, 76 (1997) 793-799.
- [6] G.G. Hollman, G. Steenbruggen, M. Janssen-Jurkovičová, A two-step process for the synthesis of zeolites from coal fly ash, *Fuel*, 78 (1999) 1225-1230.
- [7] M. Park, C.L. Choi, W.T. Lim, M.C. Kim, J. Choi, N.H. Heo, Molten-salt method for the synthesis of zeolitic materials: II. Characterization of zeolitic materials, *Microporous Mesoporous Mater*, 37 (2000) 91-98.
- [8] N. Moreno, X. Querol, F. Plana, J.M. Andres, M. Janssen, H. Nugteren, Pure zeolite synthesis from silica extracted from coal fly ashes, *J. Chem. Technol. Biotechnol*, 77 (2002) 274–279.
- [9] M. Inada, Y. Eguchi, N. Enomoto, J. Hojo, Synthesis of zeolite from coal fly ashes with different silica-alumina composition, *Fuel*, 84 (2005) 299-304.
- [10] T.T. Wałek, F. Saito, Q. Zhang, The effect of low solid/liquid ratio on hydrothermal synthesis of zeolites from fly ash, *Fuel*, 87 (2008) 3194-3199.

- [11] M. Wdowin, M. Franus, R. Panek, L. Badura, W. Franus, The conversion technology of fly ash into zeolites, *Clean Technol. Envir*, 16 (2014) 1217-1223.
- [12] V. Berggaut, A. Singer, High capacity cation exchanger by hydrothermal zeolitization of coal fly ash, *Appl. Clay Sci*, 10 (1996) 369-378.
- [13] W. Ma, P.W. Brown, S. Komarneni, Characterization and cation exchange properties of zeolite synthesized from fly ashes, *J. Mater. Res*, 13 (1998) 3-7.
- [14] G. Steenbruggen, G.G. Hollman, The synthesis of zeolites from fly ash and the properties of the zeolite products, *J. Geochem. Explor*, 62 (1998) 305-309.
- [15] R. Juan, S. Hernández, J.M. Andrés, C. Ruiz, Synthesis of granular zeolitic materials with high cation exchange capacity from agglomerated coal fly ash, *Fuel*, 86 (2007) 1811-1821.
- [16] N. Murayama, H. Yamamoto, J. Shibata, Mechanism of zeolite synthesis from coal fly ash by alkali hydrothermal reaction, *Int. J. Miner. Process*, 64 (2002) 1-17.
- [17] N. Murayama, T. Takahashi, K. Shuku, H. Lee, J. Shibata, Effect of reaction temperature on hydrothermal syntheses of potassium type zeolites from coal fly ash, *Int. J. Miner. Process*, 87 (2008) 129-133.
- [18] N.M. Musyoka, Hydrothermal synthesis and optimisation of zeolite Na-P1 from South African coal fly ash, University of Western Cape (2009), PhD thesis.
- [19] H. Tanaka, A. Fujii, S. Fujimoto, Y. Tanaka, Microwave-assisted two-step process for the synthesis of a single-phase Na-A zeolite from coal fly ash, *Adv. Powder Technol*, 19 (2008) 83-94.
- [20] N.M. Musyoka, L.F. Petrik, W.M. Gitari, G. Balfour, E. Hums, Optimization of hydrothermal synthesis of pure zeolite Na-P1 from South African coal fly ashes, *J. Environ. Sci. Health Part A*, 47 (2012) 337-350.

- [21] D. Mainganye, T. V. Ojumu, L. Petrik, Synthesis of zeolites Na-P1 from South African coal fly ash: Effect of impeller design and agitation, *Materials*, 6 (2013) 2074-2089.
- [22] R. Juan, S. Hernández, J.M. André, C. Ruiz, Synthesis of granular zeolitic materials with high cation exchange capacity from agglomerated coal fly ash, *Fuel*, 86 (2007) 1811-1821.
- [23] P.M. Slangen, J.C. Jansen, H. Van Bekkum, The effect of ageing on the microwave synthesis of zeolite NaA, *Microporous Mater*, 9 (1997) 259-65.
- [24] O. Andac, M. Tatlier, A. Sirkecioglu, I. Ece, A. Erdem-Senatarlar, Effect of ultrasound on zeolite-A synthesis, *Microporous and Mesoporous Materials*, 79 (2005) 225-233.
- [25] K. Fukui, M. Katoh, T. Yamamoto, H. Yoshida, Utilization of NaCl for phillipsite synthesis from fly ash by hydrothermal treatment with microwave heating, *Adv. Powder Technol*, 20 (2009) 35-40.
- [26] R. Sabouni, H. Kazemian, S. Rohani, A novel combined manufacturing technique for rapid production of IRMOF-1 using ultrasound and microwave energies, *Chemical Engineering Journal*, 165 (2010) 966-973.
- [27] J. Behin, S.S. Bukhari, V. Dehnavi, H. Kazemian, S. Rohani, Using coal fly ash and wastewater for microwave synthesis of LTA zeolite, *Chemical Engineering and Technology*, 37 (2014) 1532-1540.
- [28] S.S. Bukhari, J. Behin, H. Kazemian, S. Rohani, A comparative study using direct hydrothermal and indirect fusion methods to produce zeolites from coal fly ash utilizing single-mode microwave energy, *Journal of Materials Science*, 49 (2014) 8261-8271.

- [29] S.S. Bukhari, J. Behin, H. Kazemian, S. Rohani, Synthesis of zeolite Na-A using single mode microwave irradiation at atmospheric pressure: The effect of microwave power, *The Canadian Journal of Chemical Engineering*, 93 (2015) 1081-1090.
- [30] S.S. Bukhari, J. Behin, H. Kazemian, S. Rohani, Conversion of coal fly ash to zeolite utilizing microwave and ultrasound energies: A review, *Fuel*, 140 (2015) 250-266.
- [31] C. Belviso, F. Cavalcante, A. Lettino, S. Fiore, Effects of ultrasonic treatment on zeolite synthesized from coal fly ash, *UltrasonSonochem*, 18 (2011) 661-668.
- [32] J. Gordon, H. Kazemian, S. Rohani, Rapid and efficient crystallization of MIL-53 (Fe) by ultrasound and microwave irradiation, *Microporous and Mesoporous Materials*, 162 (2012) 36-43.
- [33] S. Askari, Sh. MiarAlipour, R. Halladj, M.H. DavoodAbadiFarahani, Effects of ultrasound on the synthesis of zeolites: a review, *J. Porous Mater*, 20 (2013) 285-302.
- [34] P. Pal, J.K. Das, N. Das, S. Bandyopadhyay, Synthesis of NaP zeolite at room temperature and short crystallization time by sonochemical method, *Ultrasonics Sonochemistry*, 20 (2013) 314-321.
- [35] T. Aldahri, J. Behin, H. Kazemian, S. Rohani, Synthesis of zeolite Na-P from coal fly ash by thermo-sonochemical treatment, *Fuel*, 182 (2016) 494–501.
- [36] S.S. Bukhari, S. Rohani, H. Kazemian, Effect of ultrasound energy on the zeolitization of chemical extracts from fused coal fly ash, *Ultrason. Sonochem*, 28 (2016) 47-53.
- [37] X. Querol, A. Alastuey, A. López-Soler, F. Plana, A Fast Method for Recycling Fly Ash: Microwave-Assisted Zeolite Synthesis *Environ. Sci. Technol*, 31 (1997) 2527-2533.

- [38] M. Inada, H. Tsujimoto, Y. Eguchi, N. Enomoto, J. Hojo, Microwave-assisted zeolite synthesis from coal fly ash in hydrothermal process, *Fuel*, 84 (2005) 1482-1486.
- [39] K. Fukui, K. Arai, K. Kanayama, H. Yoshida, Phillipsite synthesis from fly ash prepared by hydrothermal treatment with microwave heating, *Advanced Powder Technol*, 17 (2006) 369-382.
- [40] M.M.J. Treacy, J.B. Higgins, *Collection of Simulated XRD Powder Patterns for Zeolites*, Elsevier. (2007).
- [41] D.C. Bain, B.F.L. Smith, A handbook of determinative methods in clay mineralogy, Chemical analysis, in M.J. Wilson (ed.), Chapman and Hall, New York, NY, (1987) 248-274.
- [42] M.M.J. Treacy, J.B. Higgins, R.V. Ballmoos, *Collection of particle size is about 300 nm for the sample judged to simulated XRD powder patterns for zeolites (3rd ed.)*, Elsevier, New York. (1996).
- [43] M.N. Nadagouda, T. F. Speth, R.S. Varma, Microwave-assisted green synthesis of silver nanostructures, *Accounts of Chemical Research*, 44 (2011) 469-478.
- [44] X. H. Liao, J.J. Zhu, H.Y. Chen, Microwave synthesis of nanocrystalline metal sulfides in formaldehyde solution, *Materials Science and Engineering: B. Lett.*, 85.1 (2001) 85 – 89.
- [45] M. Ansaria, A. Aroujaliana, A. Raisia, B. Dabira, M. Fathizadeha, Preparation and characterization of nano-NaX zeolite by microwave assisted hydrothermal method, *Advanced Powder Technology*, 25 (2014) 722–727.
- [46] N. Murayama, H. Yamamoto, J. Shibata, Mechanism of zeolite synthesis from coal fly ash by alkali hydrothermal reaction, *Int. J. Miner. Process*, 64 (2002) 1-17.

- [47] A. Derkowski, W. Franus, E. Beran, A. Czímerová. Properties and potential applications of zeolitic materials produced from fly ash using simple method of synthesis, *Powder Technology*, 166 (1) (2006) 47 -54.
- [48] F. Rouquerol, J. Rouquerol, K. S. W. Sing, Adsorption by powders and porous solids, *Academic Press*, Waltham, USA (1999).
- [49] K. Sing, D. Everett, R. Haul, L. Moscou, R. Peirotti, J. Rouquerol, *Pure Appl. Chem.* 57 (1985) 603.
- [50] Y. Tatsuo, U. Shinji, I. Kazumi, K. Yasuo, Type Zeolite and Production thereof, *Jpn. Patent 1153514A*, (1989).
- [51] D.M. Allen, The relationship between variable selection and data augmentation and a method for prediction. *Technometrics*, 16 (1974) 125-7.
- [52] T. Tarpey, A note on the prediction sum of squares statistic for restricted least squares, *Am Stat*, 54 (2000) 116-8.
- [53] K. Fukui, K. Kanayama, T. Yamamoto, H. Yoshida, Effects of microwave irradiation on the crystalline phase of zeolite synthesized from fly ash by hydrothermal treatment, *Advanced Powder Technol*, 18 (2007) 381-393.
- [54] K. Fukui, M. Katoh, T. Yamamoto, H. Yoshida, Utilization of NaCl for phillipsite synthesis from fly ash by hydrothermal treatment with microwave heating, *Advanced Powder Technology*, 20 (2009) 35-40.
- [55] C. Gabriel, S. Gabriel, E.H. Grant, B.S.J. Halstead, D.M.P. Mingos, Dielectric parameters relevant to microwave dielectric heating, *Chem. Soc. Rev*, 27 (1998) 213-224.
- [56] J. Sun, W. Wang, Q. Yue, Review on Microwave-Matter Interaction Fundamentals and Efficient Microwave-Associated Heating Strategies, *Materials*, 9 (2016).

[57] J.R. Agger, N. Pervaiz, A.K. Cheetham, M.W. Anderson, Crystallization in zeolite A studied by atomic force microscopy, *J. Am. Chem. Soc.*, 120 (1998) 10754-10759.

[58] M.W. Gitari, L.F. Petrik, N. M. Musyoka, Hydrothermal conversion of South African coal fly ash into pure phase zeolite NaP1, *In Tech*, (2016).

Chapter 5

RESPONSE SURFACE MODELING OF THE REMOVAL OF METHYL ORANGE DYE FROM ITS AQUEOUS SOLUTION USING TWO TYPES OF ZEOLITE SYNTHESIZED FROM COAL FLY ASH⁴

ABSTRACT:

Coal fly ash (CFA) produced as a waste material in coal power plants was converted into Linde-type A (LTA) and Na-P type (ZP) zeolite using microwave irradiation. The prepared zeolites were characterized and modified using a cationic surfactant. The removal of methyl orange (MO) dyes from aqueous solution by LTA and ZP as adsorbent was studied by applying the response surface method (RSM). A quadratic model was developed to relate the MO removal rate to the main independent variables, namely the solution pH (in the 3–9 range), the initial MO concentration (in the 20–100 mg/L range), and the adsorbent mass (200–1000 mg/L). The modified MLTA was found to be a more effective adsorbent relative to the modified MZP. In addition, MLTA mass exerted the greatest influence on the MO removal process under the studied conditions. However, when MZP zeolite was used as an adsorbent, the pH of

⁴ This Chapter is published in the Materials Express Journal. Tahani Aldahri, Adnan A. AbdulRazak, Intisar H. Khalaf and Sohrab Rohani Sohrab, Materials Express 8 (2018) 234 - 244.

the solution was the most influential factor. The two quadratic models were found to be statistically significant.

Keywords: Methyl orange, Coal fly ash, Zeolite LTA, Zeolite Na-P, Microwave synthesis.

5.1 INTRODUCTION

Treatment of wastewater produced in the textile industry has been the subject of extensive research, due to the large volume of water required (up to 100 l/kg of finished textile product). These effluents have a significant detrimental impact on the water resources because they contain slowly- or non-biodegradable organic materials. At present, different treatment methods are utilized to remove the dyes from wastewater, including those based on biological treatment, floatation, coagulation, membrane filtration and adsorption techniques. However, the economic cost, effectiveness, and environmental impact of these methods differ significantly ^(1,2).

Adsorption is the most common dye removal method, because it does not produce dangerous byproducts, and some of the adsorbents can be easily regenerated. Methyl orange (MO) is a well-known anionic dye, frequently utilized in various industries, such as dye manufacturing plants and textile industries, and as acid and basic indicator. Discharge of effluents containing MO can have detrimental environmental consequences, as it can adversely affect human health and the ecosystem of other living organisms. Empirical evidence indicates that release of MO dyes without proper treatment can cause significant health problems. ⁽³⁾ In addition, presence of even a very low concentration of MO dye in water system may reduce the light penetration and affect the photosynthetic processes.

Recently, various adsorbents—such as zeolite,⁽³⁾ multiwall carbon nanotubes,⁽⁴⁾ graphene oxide,⁽⁵⁾ and calcined ZnMgAl hydrotalcite⁽⁶⁾ have been utilized for MO removal.

Coal fly ash (CFA) is a powder produced as a byproduct of burning coal to generate electricity. In the EU and the US, around 115 million tones of CFA are produced per year.⁽⁷⁾ Presently, fly ash is primarily used as additive in cement and concrete production. Due to its high silica and alumina content, CFA is also converted to different types of zeolite by hydrothermal treatment. Bukhari et al. recently reported on this hydrothermal conventional method, assisted by microwave and ultrasonic energy.⁽⁸⁾ Microwave energy is employed in the zeolite synthesis process because this can yield different zeolite morphologies, which not only leads to different zeolite types, but also accelerates nucleation, shortens the crystallization time, reduces the undesirable phases due to phase selectivity, and facilitates control of the particle size distribution.⁽⁹⁾ Zeolites are used in various applications as adsorbents, ion exchangers, catalysts, and membranes. The applications and utilization of synthetic zeolites from CFA were reviewed by Ahmaruzzaman.⁽¹⁰⁾

To the best of the authors' knowledge, zeolite extraction from CFA by using the microwave assisted method as a means of removing dyes from a wastewater stream has rarely been studied.

As zeolites possess a net negative charge, their adsorption of an anionic dye would be relatively low due to the repulsive forces between the zeolite surface and the dye. Thus, to make zeolites suitable for adsorption of anionic dyes, the negative surface charge must be modified by using cationic surfactants, such as hexadecyltrimethylammonium bromide (HDTMA).

The aim of this work was to synthesize Linde-type A (LTA) and Na-P type (ZP) from CFA by using the microwave assisted method. These zeolites were further modified by HDTMA before being utilized as adsorbent to eliminate the MO dye from the aqueous solution.

5.2 MATERIALS AND METHODS

5.2.1 Materials

Coal fly ash (CFA) was supplied by a coal-fired power plant (Ontario Power Generation, Nanticoke, Canada), and was stored in a sealed container until required. $\text{Na}_2\text{SiO}_3 \cdot 5\text{H}_2\text{O}$ (sodium met silicate), $\text{Na}_2\text{O} \cdot \text{Al}_2\text{O}_3 \cdot 3\text{H}_2\text{O}$ (sodium aluminate anhydrous) and HDTMA bromide were purchased from Sigma-Aldrich, USA, while NaOH (sodium hydroxide) was supplied by Alphachem, Mississauga, Canada. Methyl orange with an MW = 327.34 g/mole was purchased from Alfa Aesar, USA. The chemical structure of MO is shown in Figure 5.1. Deionized water (DI) was used for the preparation of the solutions and washing of synthesized zeolite. All chemicals (including those used for characterization tests) were of analytical grade and were used as received.

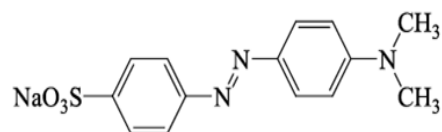


Figure 5.1. MO chemical structure.

5.2.2 Synthesis Procedure

The CFA zeolitization process of CFA commenced with dissolving 2 g of CFA in 0.1 M of HCl and heating the mixture for 3 hours at 90 °C, as acid treatment enhances

CFA purity by removing impurities.⁽¹¹⁾ Subsequently, the mixture was filtered and the solid phase was washed with deionized water and was left to dry overnight at room temperature. Next, 2 g of acid treated CFA, 1.5 M of NaOH granules, 0.4 g of NaAlO₃, and 0.07–1 g of NaSiO₄ were added to 20 mL of distilled water to produce the reaction solution of Linde-type A (LTA) and Na-P type (ZP) zeolite, respectively.^(9,12,13) The obtained samples were subjected to microwave irradiation for a certain period of time and a fixed power required for crystallization. A self-adjusting microwave (single-mode, 2.5 GHz, CEM cooperation, Discover, USA) was used to conduct experiments at atmospheric pressure. A reflux condenser was attached to a cylindrical batch PTFE vessel (28 mm ID × 108 mm) and was placed in the microwave chamber for 30 min, at 250 W microwave power. The samples were subsequently filtered and the solid phase was collected, washed with deionized water, and dried at room temperature overnight.

5.2.3 Characterization

Microscopic images revealing phase purity and morphology of the zeolitized CFA were obtained by using scanning electron microscope (SEM), Hitachi S 2600N SEM (Tokyo, Japan), operating at 5 kV accelerating voltage. Powder X-ray diffraction (XRD) images of the synthesized ZP and LTA zeolites were obtained by Rigaku–Miniflex powder diffractometer (Japan) with CuK_α (λ for K_α = 1.54059 Å) over the $5^\circ < 2\theta < 40^\circ$ range in 2° increments. The obtained crystalline phase was verified by comparing the characteristic peaks of ZP and LTA with the standard peaks reported in the pertinent literature.⁽¹⁴⁾ The thermogravimetric analysis (TGA) of the samples was performed using a Mettler Toledo TGA/SDTA 851e model (Switzerland) coupled with Stare software version 6.1. The samples were heated from 25 °C to 600 °C in 10 °C/min steps under nitrogen purge. Specific surface area and pore size of the synthesized zeolite

(ZP and LTA) were measured using a Micromeritics ASAP 2020 Surface Analyzer, while a Zetasizer Nano ZS 3000 HSA (Malvern, Worcestershire, UK) was used for measuring the zeta potential of the product particles.

5.2.4 Modification of the Synthesized Zeolites

For the modification of LTA and ZP, 500 mL of the solution of the cationic surfactant, HDTMA bromide, at a concentration of 55 mmol/L was strongly mixed with 10 g of LTA at 50 °C for 4 h. The reaction settings were chosen to assure proper surfactant loading. After being cooled to room temperature, the product was centrifuged, washed with doubly distilled water, dried in an oven at 60 °C and ground to pass through an 80-mesh sieve.

5.2.5 Experimental Design

Response Surface Method (RSM) was employed in this work, as it is a well-known statistical technique utilized for designing experiments in various engineering and research disciplines.(15,16) To investigate the influence of the independent variables, the solution pH, the initial dye concentration, and the adsorbent mass, on the adsorption process, a three-factorial, three-level central composite design (CCD) was adopted. Seventeen experimental runs were required, including five replicates at the center points. The experiments were designed using Design-Expert 7 software. Table 5.1 shows the low, center and high levels of the independent variables investigated in this study. A 3-9 pH range was chosen for the solution to cover both the acid and basic mediums. Also, no precipitation was formed below pH = 3. The Initial MO dye concentration range, 20-100 mg/L, was chosen based on information from the fabric factories. Also, mass of the adsorbent range chosen was between 200 and 1000 mg/L to achieve the minimum and maximum percentage of dye removal.

Table 5.1. Process-independent variables and their levels.

Variables	Levels and Range		
	(+1)	(0)	(-1)
pH of the solution (X_1)	9	6	3
Initial MO dye concentration (X_2) (mg/L)	100	60	20
Mass of the adsorbent (X_3) (mg/L)	1000	600	200

5.2.6 Removal Process

Batch mode experiments were carried out randomly to study the influence of the three independent variables on the MO removal by the MLTA and MZP.

In the dye removal process, two adsorbents were utilized with different MLTA and MZP masses (200–1000 mg/L), at a fixed pH (3, 6, and 9), and an initial concentration of (20–100 mg/L) after the equilibrium was reached the adsorbents separating from the solution using a centrifuge.

The residual MO concentration in the solution was measured using the UV-visible (Cary 60, Agilent Technology, Germany) at 464 nm (λ_{\max} of MO).

The dye removal percentage was calculated by applying the following equation:

$$\% \text{ MO dye removal} = \frac{C_o - C_f}{C_o} \times 100 \quad (5-1)$$

where C_o and C_f are the initial and final MO concentration (mg/L). The details of the experiments are shown in Table 5.2.

Table 5.2. CCD for three independent variables and the obtained % dye removal.

Run No.	X ₁	X ₂	X ₃	% MO dye removal	
				(MZP)	(MLTA)
1	6.00	60.00	600.00	27.09	53.5
2	6.00	60.00	600.00	27.8	53.5
3	9.00	60.00	200.00	3.47	13.41
4	6.00	100.00	200.00	18.72	20.52
5	9.00	100.00	600.00	4.935	23.41
6	6.00	20.00	200.00	30.94	40.1
7	6.00	60.00	600.00	27.6	53.66
8	9.00	60.00	1000.00	21.74	86.28
9	6.00	60.00	600.00	27.1	53.96
10	3.00	60.00	1000.00	60.59	92.31
11	6.00	60.00	600.00	27.2	52.86
12	6.00	20.00	1000.00	91	99.9
13	6.00	100.00	1000.00	31.99	56.24
14	3.00	60.00	200.00	36.13	73.33
15	3.00	20.00	600.00	82.73	82.44
16	9.00	20.00	600.00	58.64	90.2
17	3.00	100.00	600.00	63.18	90.2

5.3 RESULTS AND DISCUSSION

Microwave heating (MW) is a volumetric heating process due to ionic conduction and dipolar nature of H₂O. Therefore, MW heating is preferable to conventional heating, since its two aforementioned characteristics shorten the reaction time, while increasing the yield and selectivity.⁽¹⁷⁾

CFA is converted to zeolite via three main steps.⁽¹⁸⁾ During the first step, Si and Al dissolve from CFA particles into the solution. In the second step, alumina-silicate gel is formed in the solution. In the last step, the zeolite nuclei that formed in previous stage are grown and crystallized to zeolite particles on the CFA surface. In the present study, exposing the mixture to MW irradiation assisted with dissolving the Si and Al from the CFA particles into the solution and enhanced the crystal growth. Thus, zeolite ZP and LTA were deposited on the CFA surface.⁽⁹⁾

5.3.1 Characterization of LTA and ZP

Figure 5.2 presents the nitrogen adsorption/desorption isotherms of the ZP and LTA. Both show isotherms of type IV based on the International Union of Pure Applied Chemistry (IUPAC) isotherm classification,^(19,20) typical of the mesoporous materials. This finding could be due to the presence of impurities trapped inside the pores and channels of the synthesized zeolite, which limit nitrogen adsorption inside the pores. Table 5.3 summarizes the textural properties of ZP, LTA and raw CFA. The Brunauer-Emmett-Teller (BET) surface area of ZP was found to be 378.07 m²/g higher than that of the raw CFA sample, which had a surface area of 15.47 m²/g. The surface area of LTA was 48.47 m²/g, which is less than the ZP surface area. The pore size of ZP and LTA was similar, as 118.9336 Å and 110.6834 Å, respectively, were measured. On the other hand, the micro pore volume of LTA was 0.134135 cm³/g greater than that of ZP (0.015059 cm³/g). The higher pore volume may be one of the main reasons for the higher removal efficiency of LTA compared to ZP. In both cases, however, the HCl acid treatment of CFA prior to the microwave-assisted synthesis step resulted in producing ZP and LTA with greater surface area and pore size.

Obviously, the pore volume of zeolite ZP is much lower than that of LTA, while its surface area is much higher than that of LTA. These characteristics could be attributed to the porosity of both zeolites. Based on their crystal structures—cubic structure for LTA and fiber structure for ZP—zeolites have various connective pores.⁽²¹⁾ In zeolites, pores grow from the radical crystalline structure, which follows configurational diffusion.⁽²²⁾ Zeolites comprise of primary tetrahedral units, whereby Si and Al atoms are located at the center of the tetrahedral and are surrounded by four oxygen atoms, located at the corners. As Si-O and Al-O cannot fill the space perfectly, cavities are produced.⁽²³⁾ These cavities could result in porosity, which increases the

zeolite surface area. Owing to this characteristic, the surface area of ZP is much higher than that of LTA, while the pore volume of ZP is much lower than that of LTA.

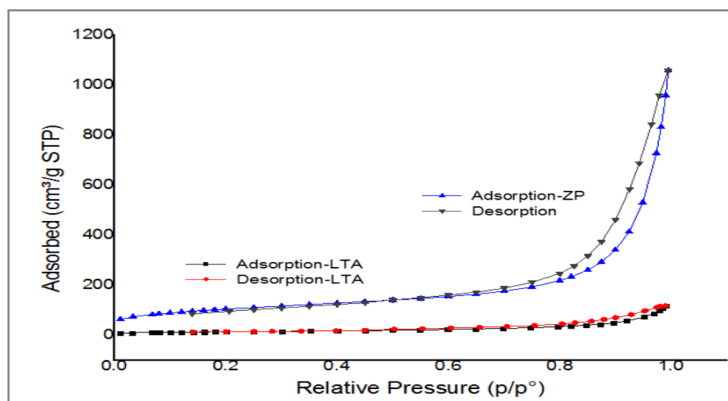


Figure 5.2. The adsorption /desorption of ZP and LTA synthesized from CFA.

Table 5.3. BET surface area of CFA and synthesized ZP and LTA

	Surface area (m ² /g)	Pore volume (cm ³ /g)	Pore size (Å)
CFA	15.47	-	-
LTA	48.47	0.134135	110.6834
ZP	378.07	0.015059	118.9336

The samples were analyzed by XRD after being subjected to microwave irradiation to determine the zeolite phases present. Figure 5.3 shows that CFA was successfully converted into zeolite ZP and LTA, and the main characteristic peaks were observed at 12.5°, 17°, 21.3°, 28°, 31.8°, and 33° 2-theta for ZP, and 7.25°, 10.26°, 12.56°, 16.2°, 21.8°, 24°, 27.2°, 30.1° and 34.3° 2-theta for LTA. Moreover, a major zeolitic phase was identified, namely zeolite Na-P (ZP) and Linde-Type A (LTA). The average crystalline size of ZP and LTA, as calculated using Scherrer's equation was found to be 31 and 43 nm, respectively.

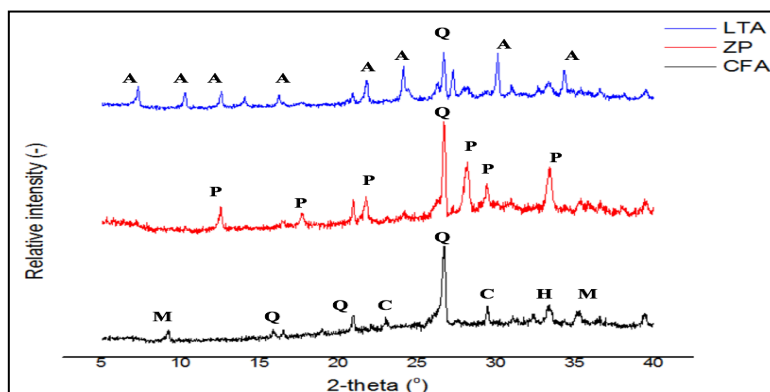


Figure 5.3. The XRD patterns of CFA, ZP and LTA. (A = zeolite Na-A, Q = quartz, M = mullite, H = hematite, M = magnetite, P = zeolite Na-P, H = hydroxy-sodalite and C= cristobalite)

The SEM images obtained for raw CFA and synthesized LTA and ZP zeolites are shown in Figure 5.4(a) – (c). Figure 5.4(b) shows one major structure observed, namely a fiber structure, associated with the Na-P zeolite.^(24,25) Figure 5.4(c) shows another major cubic structure, related to the Linde-Type A (LTA) framework.⁽²⁶⁾ These observations confirm the BET and XRD results. In addition, they concur with the findings reported in pertinent literature,⁽¹²⁾ confirming that ZP and LTA structures cover the undissolved CFA surface.

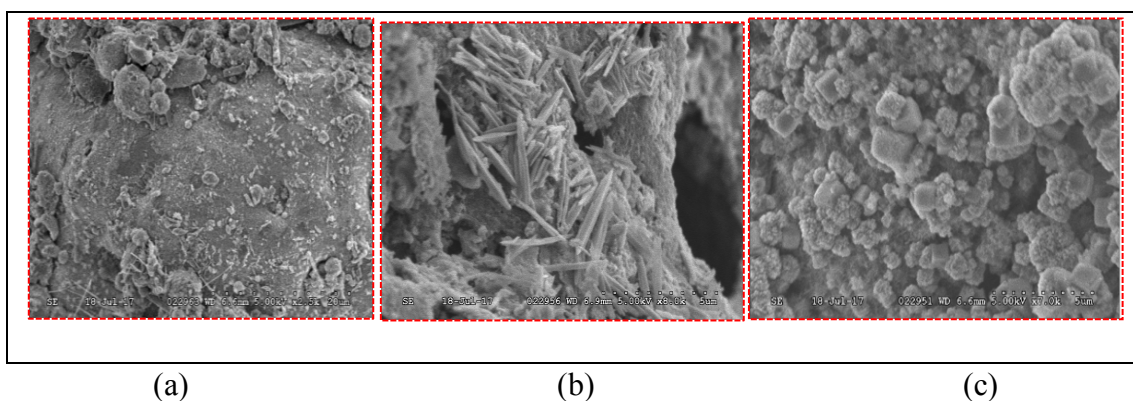


Figure 5.4. The SEM of (a) CFA, and synthesized (b) ZP and (c) LTA zeolites.

The TGA curves of the synthesized ZP and LTA zeolites are shown in Figure 5.5. Both samples exhibit a significant weight loss at approximately 105–128 °C, corresponding to ~ 14% and ~ 3 % of the initial ZP and LTA weight, respectively, while 5% was measured for the raw CFA. These findings demonstrate the high water holding capacity of synthesized ZP and LTA zeolite compared to the raw CFA, and confirm the BET results.

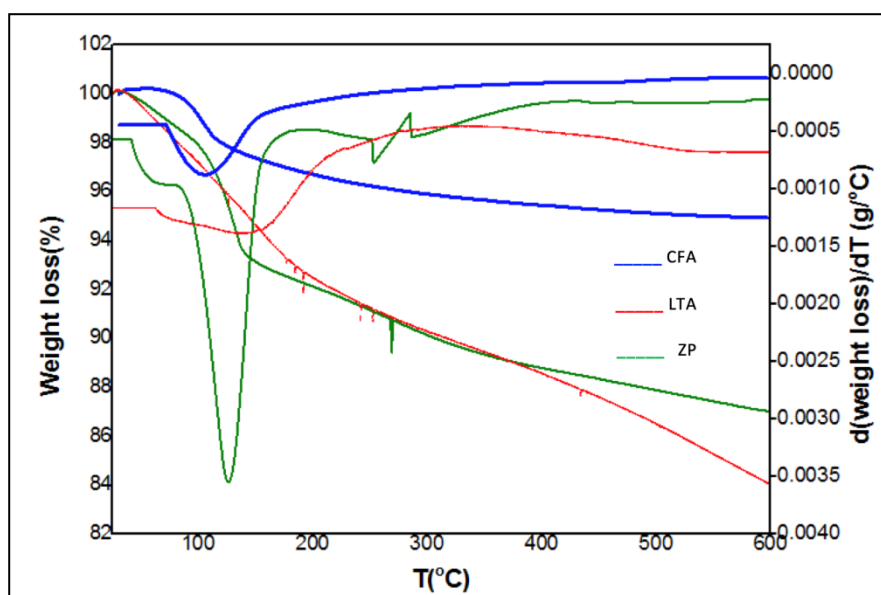


Figure 5.5. The TGA of CFA and synthesized ZP and LTA zeolite.

The zeta potential of MLTA and MZP versus the pH of the solution is shown in Table 5.4. The surface charges for both types of adsorbent were positive and had the highest value at pH 6.

Table 5.4. Zeta potential of modified zeolite (MLTA) and MZP vs pH

pH	MLTA (mV)	MZP (mV)
3	24	20
6	32.7	25
8	15.8	8
9	10	4

5.3.2 Dye Removal Regression Equations

The regression equations of %MO dye removal using LTA and ZP as adsorbent are shown below. The quadratic model equations were obtained by applying the Design Expert Software.

$$\begin{aligned} \% \text{ MO dye removal (ZP)} = & 27.36 - 19.23 \times X_1 - 18.06 \times X_2 + 14.51 \times X_3 - 8.54 \times X_1 \times X_2 \\ & - 1.55 \times X_1 \times X_3 - 11.70 \times X_2 \times X_3 + 6.17 \times X_1^2 + 18.85 \times X_2^2 - 3.04 \times X_3^2 \end{aligned} \quad (5-2)$$

$$\begin{aligned} \% \text{ MO dye removal (LTA)} = & 53.50 - 15.62 \times X_1 - 15.28 \times X_2 + 23.42 \times X_3 - 18.64 \times X_1 \times \\ & X_2 + 13.48 \times X_1 \times X_3 - 6.02 \times X_2 \times X_3 + 15.11 \times X_1^2 + 2.96 \times X_2^2 - 2.27 \times X_3^2 \end{aligned} \quad (5-3)$$

where X_1 is the pH of the solution, X_2 denotes the initial MO dye concentration (mg/L) and X_3 pertains to the adsorbent mass (mg/L).

Positive sign in the above equations reveal an increase in the value of the variable results in an increase in the % dye removal.

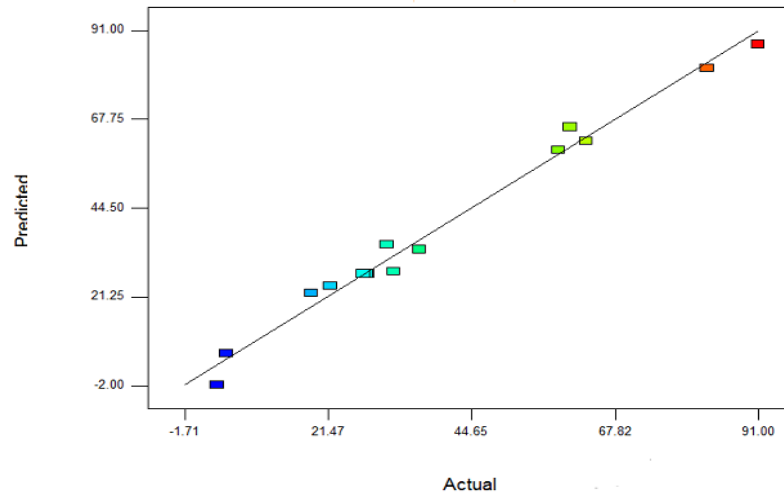
To study the adequacy and the significance of the current models, ANOVA test was performed and the results are shown in Table 5.5. The p value was set at < 0.05 and the F-value was high, at 57.59 and 847.10 for MZP and MLTA, respectively. These results confirm that the models are statistically significant.

The accuracy of the models fit was checked by calculating the correlation coefficient R^2 , which had the value of 98.60% and 99.91%, for MZP and MLTA, respectively. These values indicate that only 1.4% and 0.09% of the total data variations were not captured by the current models. Moreover, the high values of adjusted determination coefficients (Adj = 96.95%) and (Adj = 99.79%), which were close to R^2 , confirm the high statistical significance of these models.

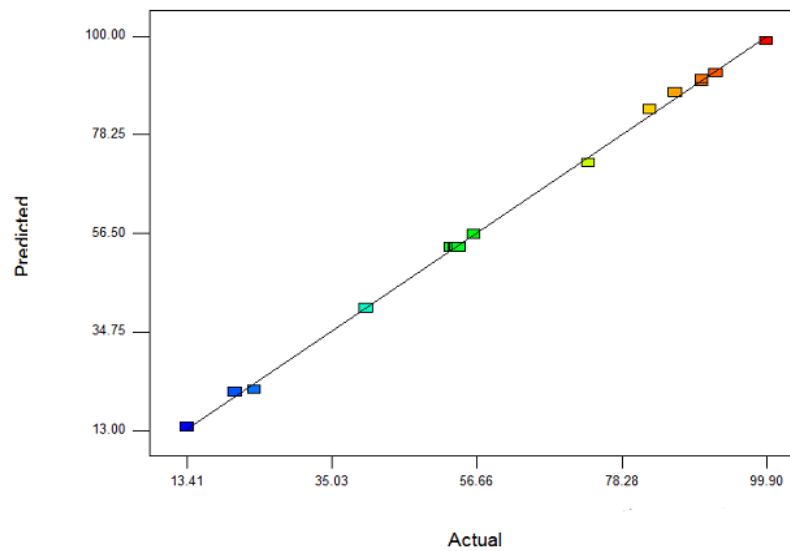
Table 5.5. The results of ANOVA analysis for MZP and MLTA.

Source	Sum of Squares		df	Mean Squares		F-Value		p-value prop>F		
	MZP	MLTA		MZP	MLTA	MZP	MLTA	MZP	MLTA	
Model	9824.5	11496.8	9	1091.61	1277.43	57.59	847.10	< 0.0001	< 0.0001	significant
X1	2958.5	1952.09	1	2958.52	1952.10	156.07	1294.5	< 0.0001	< 0.0001	
X2	2610.15	1868.36	1	2610.15	1868.36	137.70	1238.9	< 0.0001	< 0.0001	
X3	1683.7	4387.97	1	1683.69	4387.97	88.82	2909.8	< 0.0001	< 0.0001	
X1X2	291.8	1389.75	1	291.83	1389.75	15.40	921.59	0.0057	< 0.0001	
X1X3	9.6	726.34	1	9.59	726.34	0.51	481.66	0.5000	< 0.0001	
X2X3	547.4	145.08	1	547.40	145.08	28.88	96.21	0.0010	< 0.0001	
X1 ²	160.16	960.89	1	160.16	960.90	8.45	637.20	0.0228	< 0.0001	
X2 ²	1495.3	36.96	1	1495.32	36.96	78.88	24.51	< 0.0001	0.0017	
X3 ²	38.98	21.663	1	38.98	21.66	2.06	14.37	0.1947	0.0068	
Residual	132.69	10.56	7	18.96	1.51					significant
Lack of Fit	132.28	9.90	3	44.09	3.30	428.21	20.27	< 0.0001	0.0070	
Pure Error	0.41	0.65	4	0.10	0.16					
Cor Total	9957.2	11507.4	16							

The predicted and the actual values of the % dye removal are plotted in Figure 5.6(a) and 5.6(b). These plots % show that the predicted values provide a good fit for the experimental results pertaining to the %MO removal using LTA and ZP. Similar results were reported by Singh et al. ⁽¹⁶⁾



a)

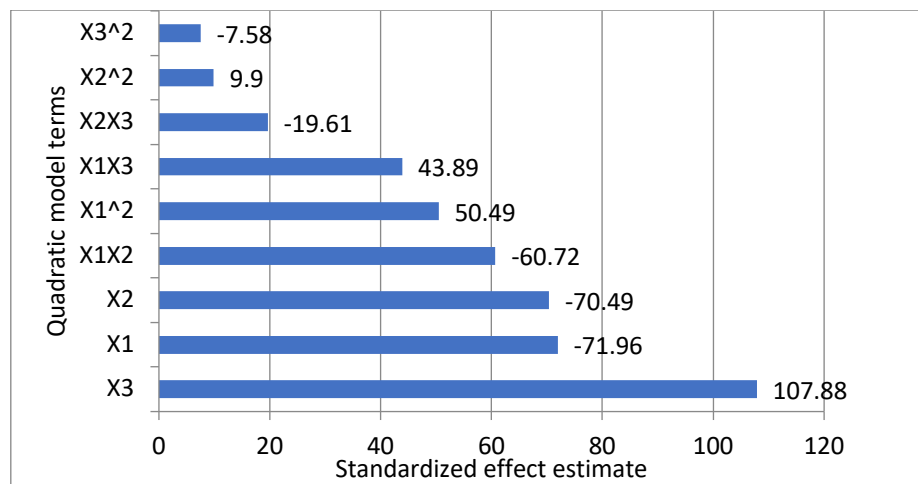


b)

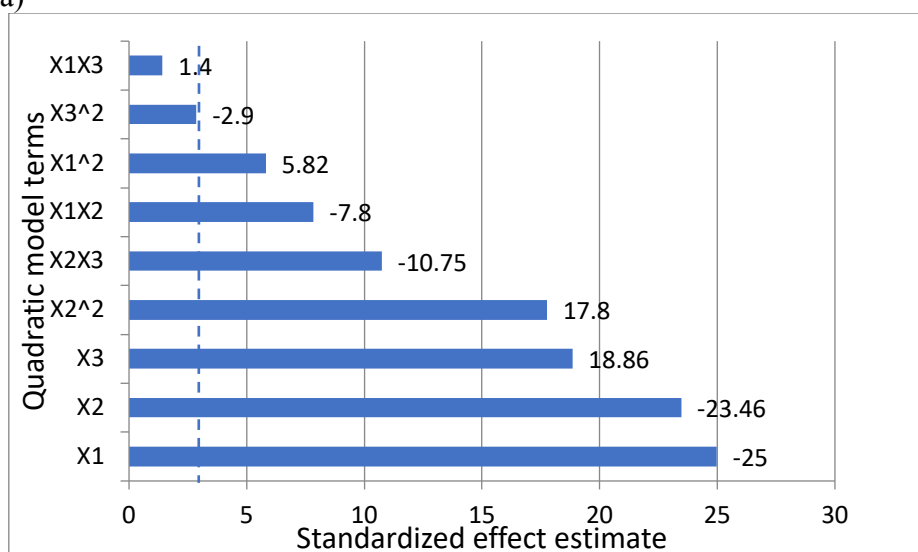
Figure 5.6. Actual vs. predicted values of %MO dye removal: (a) MLTA, and (b) MZP.

The influence of the independent variables and their joint effects are presented in Pareto charts, shown in Figure 5.7(a) and 5.7(b). In these graphs, the influence of the variables is denoted by the bar length. As can be seen in Figure 5.7(a), when MLTA was employed, the amount of the adsorbent (X_3) had the greatest and positive effect in the %MO dye removal followed by X_1 , X_2 , X_1 – X_2 interaction, $(X_1)^2$, X_1 – X_3 interaction, X_2 – X_3 interaction, $(X_2)^2$, and $(X_3)^2$. The terms X_1 , X_2 , X_1 – X_2 , X_2 – X_3 and $(X_3)^2$ had a

negative effect, while the remaining terms had a positive effect. For ZP, the Pareto chart shown in Fig7(b) suggests that the pH of the solution (X_1) had the greatest effect on the MO removal process, followed by the initial MO dye concentration (X_2), the amount of the adsorbent (X_3), $(X_2)^2$, X_2-X_3 interaction, X_1-X_2 interaction, and $(X_1)^2$, while $(X_3)^2$ and X_1-X_3 interaction had no effect. The negative sign of the terms in Pareto charts indicates that the increase in the term causes a decreases in %MO dye removal (antagonistic effect), which was the case for X_1 , X_2 , X_2-X_3 interaction, and X_1-X_2 interaction. Conversely, X_3 , $(X_2)^2$, and $(X_1)^2$ had a synergistic effect, as these terms increased the %MO dye removal.



a)



b)

Figure 5.7. Pareto chart for (a) MLTA and (b) MZP.

From the ANOVA results, the percentage contributions (PC) of each independent variable in the MO dye removal were calculated and the results are shown in Table 5.6, where SS is the sum of the squares of these terms, calculated using the equation below⁽²⁷⁾:

$$PC = \frac{SS}{\Sigma SS} \times 100 \quad (5-4)$$

As shown in Table 5.6, using ZP as the adsorbent, the pH of the solution (X_1) showed the highest effect on MO dye removal, as its contribution was 30.2%, while for LTD, the adsorbent mass exerted the highest effect, at 38.19%. These results confirm the findings reported in the Pareto charts.

Table 5.6. The percentage contributions (PC) for MZP and MLTA.

Source	PC%								
	X_1	X_2	X_3	X_1-X_2	X_1-X_3	X_2-X_3	X_1^2	X_2^2	X_3^2
MZP	30.20	26.65	17.19	2.98	0.098	5.59	1.64	15.27	0.398
MLTA	16.99	16.262	38.19	12.096	6.322	1.263	8.364	0.322	0.19

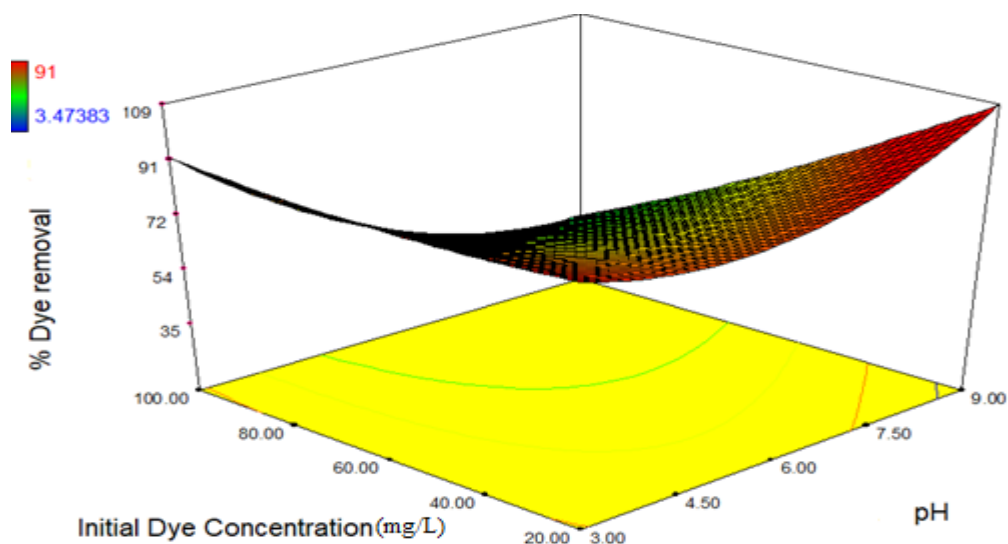
5.3.3 Three-Dimensional (3D) Response Surface and Contour Plots

In three-dimensional (3D) response surface plots, %MO removal, as the dependent variable, was plotted against two independent variables, while keeping the third independent variable constant. In addition, 3D response surfaces and their analogous 2D contour plots, which were constructed using the model equation, can assist in elucidating the influence of the independent variables on the response.⁽²⁸⁾

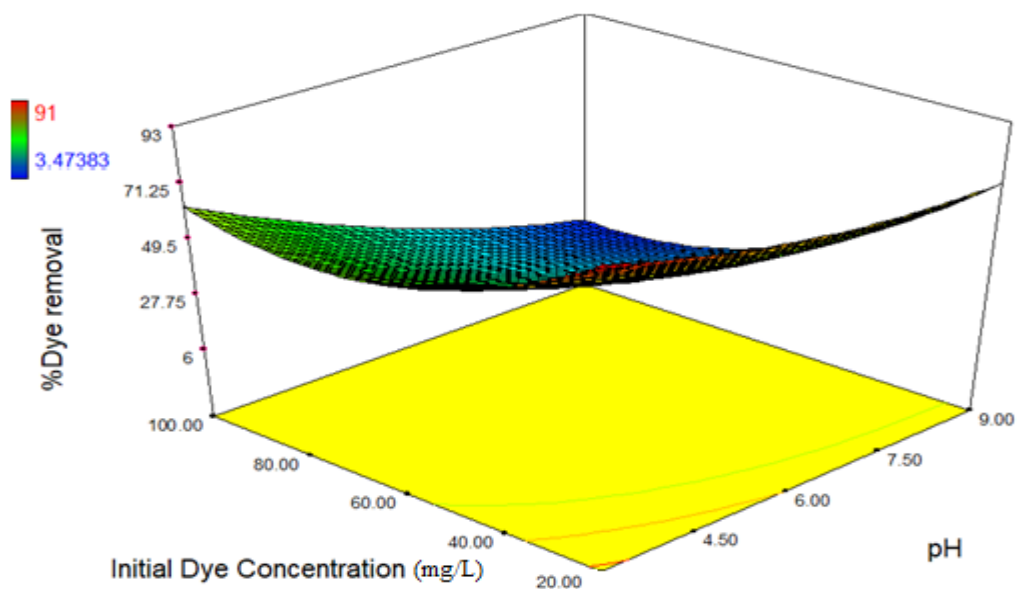
Based on the findings reported in extant literature, the removal of MO dye is highly dependent on pH of the solution.⁽²⁹⁾ Figure 5.8 (a) and 5.8 (b) show the interactive effect of the pH of the solution and the initial MO dye concentration on the % dye removal at a fixed mass of the adsorbent. It is obvious that the % dye removal decreases with the

increase in the solution pH as well as the initial MO dye concentration. A maximum % dye removal is observed at pH = 6, which may be attributed to the fact that the MO dye consists of the ($-\text{SO}_3\text{Na}$) group. Thus, in aqueous solution, it dissociates, whereby anionic form of the dye can emerge. Hence, because of the electrostatic attraction between positive charges of the modified LTA and ZP and MO, dye can be efficiently removed. As shown in Table 5.4, for both zeolites, the zeta potential increases as the pH increase until pH 6, when it starts to decrease. Hence, the % dye removal increases as the number of positive charge sites on the surface increases. Moreover, the modified LTA zeolite was found to be more effective when compared with modified ZP zeolite because its modified surface is more positive than that of ZP, yielding more positive active sites. In addition, the combined effect of initial dye concentration and the solution pH is shown in Figure 5.8(a) and 5.8(b), where it can be seen that maximum % dye removal as 100% and 91% is attained at pH 6.17 and 5.15 and initial MO dye concentration 20 and 20.24 mg/L for MLTA and MZP respectively adsorbents.

In addition, it is clearly demonstrated that the initial MO dye concentration had a negative effect on the % dye removal under these conditions, these is due to at low dye concentrations, there is a sufficient number of active sites on the surface of the adsorbed material for a reduced number of dye molecules. However, when the initial dye concentration is increased, the number of active sites is insufficient to adsorb the dye molecules. The contour curve placed down in the 3D plots gives an indication on the type of the interaction between the independent variables. If the shape is circular or a parallel plane, it suggests absence of interaction, whether the shape is elliptical or curved. ^(30, 31) Figure 5.8(a) and 5.8(b) depict an elliptical curve of contour plots, indicating a good interaction between the initial MO dye concentration and the pH of the solution for both adsorbents.



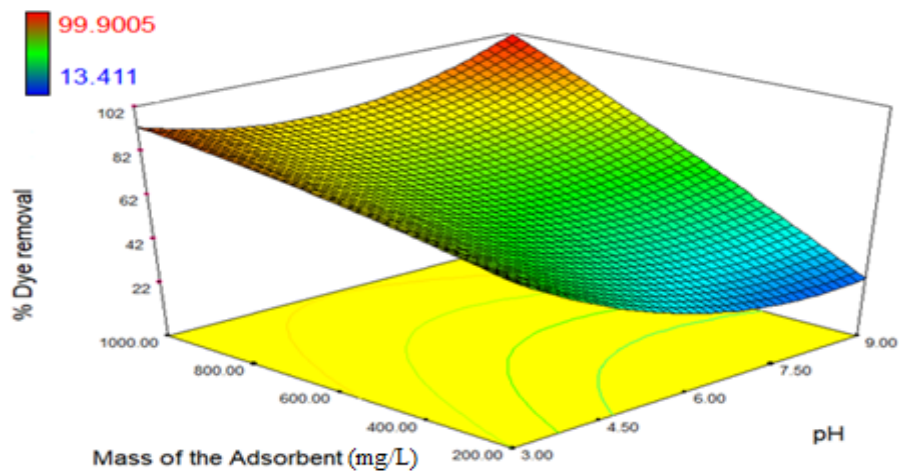
a) MLTA



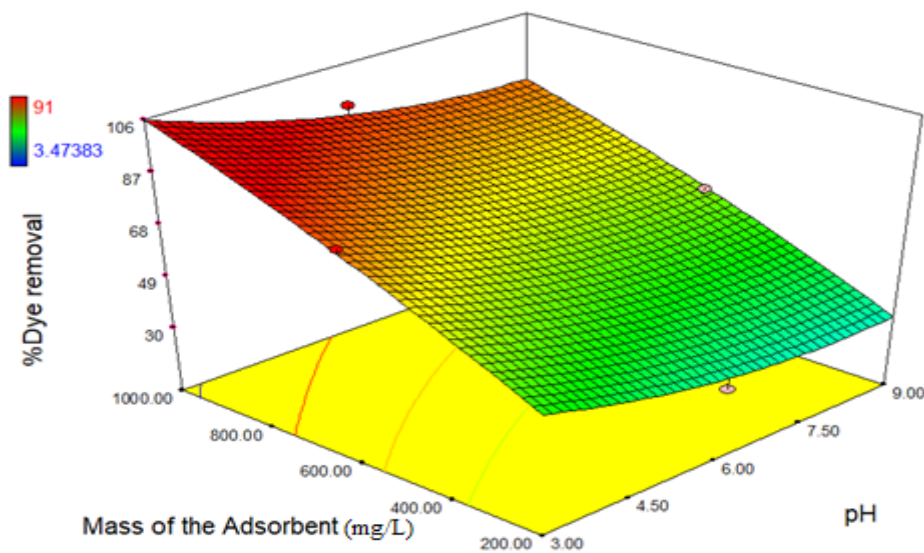
b) MZP

Figure. 5.8 Response surface for MO removal at constant mass of adsorbent (1000 mg/L) by (a) MLTA and (b) MZP, respectively.

Figure 5.9(a) and 5.9(b) depict the influence of the adsorbent mass and the solution pH at a constant initial MO dye concentration. It can be seen from the plots that the adsorbent mass had a positive effect on the dye removal. For both modified adsorbents, in the studied solution pH range, the dye removal increased with the increase in mass. This behavior can be attributed to the fact that, when adsorbent mass is high (1000 mg/L), the available active sites at the adsorbent surface are sufficient to interact with the MO ions, ensuring high dye removal rate. Conversely, at low adsorbent mass (200 mg/L), certain percentage of active sites will be occupied and the saturation state will be achieved, whereby the adsorbent is unable to adsorb more MO molecules. Similar findings were reported by Noorimotlagh et al. for the uptake of acid orange by activated carbon.⁽³²⁾ As can be seen in Figure 5.9(a) and 5.9(b), for LTA, there is interaction between the mass of the adsorbent and the pH of the solution due to the elliptical nature of the contour plots. However, for the ZP, there is no interaction in the effect of these variables due to the contour plot shape, which is a parallel straight line. These results are in good agreement with the Pareto charts.



a) MLTA



b) MZP

Figure 5.9. Response surface for MO removal at constant mass of adsorbent (20 mg/L) by (a) MLTA and (b) MZP, respectively.

Figure 5.10(a) and 5.10(b) show the joint effect of the MO initial dye concentration and the amount of the adsorbent on the %MO removal when the pH of the solution is kept constant. For both adsorbents, the positive effect of the amount of the adsorbent and the negative effect of the MO initial dye concentration on the %MO dye removal

is in agreement with the results yielded by Equation (2) and (3). In the entire range of the adsorbent mass examined in this study, the %MO removal decreases as the initial dye concentration increases. This trend can be explained by the fact that, at a low initial concentration (20 mg/L), the MO ions present in the solution can interact with accessible binding sites. However, at a high dye concentration (100 mg/L), due to the limited number of the energetic adsorption sites, the adsorbent cannot interact with all MO molecules in the solution.⁽³³⁾

Based on the above discussion, the trends in Figure 5.10(a) and 5.10(b) indicate that the interaction between the initial MO dye concentration and the mass of the adsorbent is in good agreement with the previous conclusion and the findings reported in Pareto charts for both adsorbents.

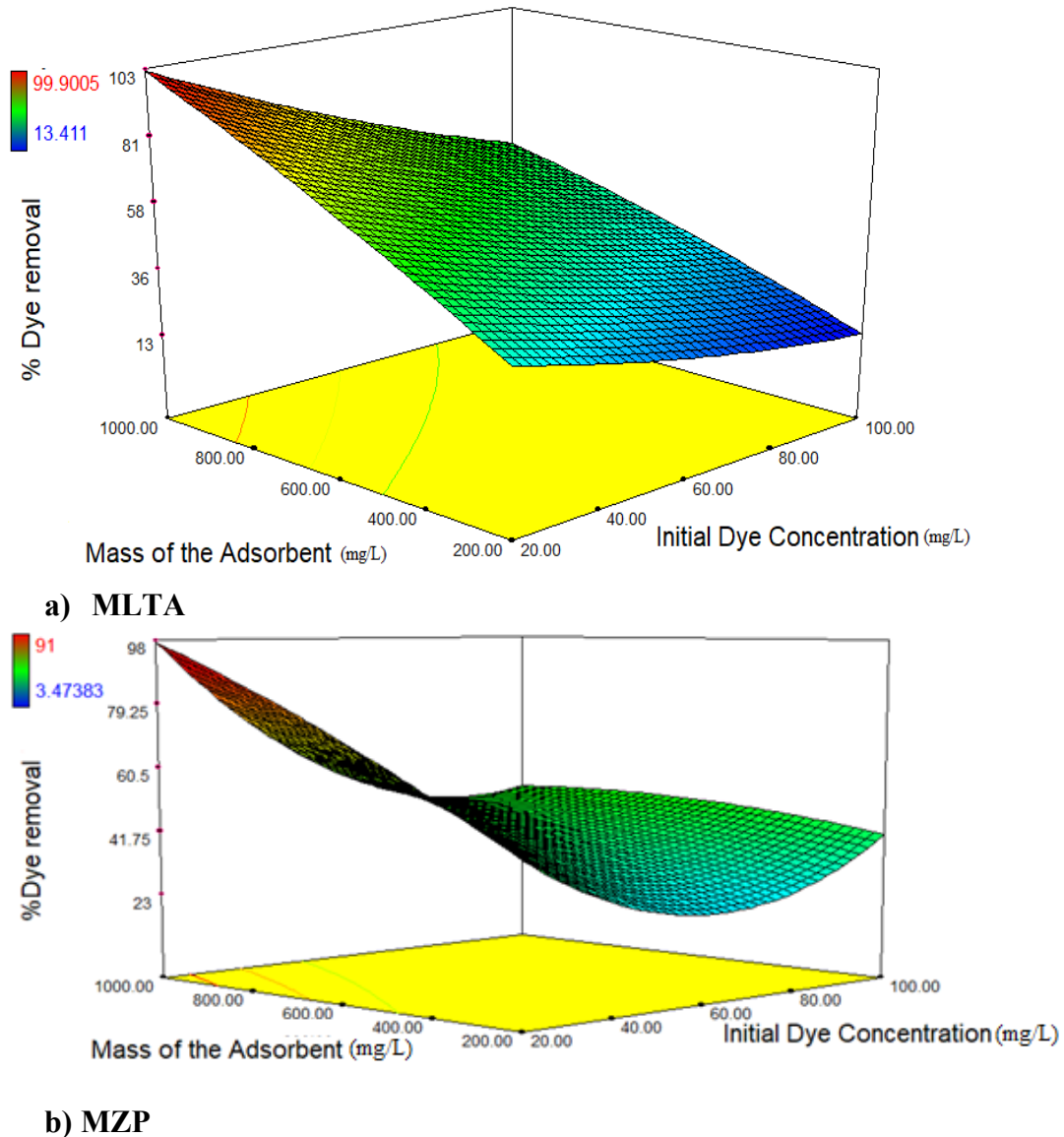


Figure 5.10. Response surface for MO removal at constant pH 6 by (a) MLTA and (b) MZP, respectively.

5.3.4 Selection of Optimum Conditions

The DESIGN EXPERT software was applied to optimize the %MO removal. The input variables were “within the range” and the response (% dye removal) for both adsorbents was chosen as "maximum". The desirability values of 0.960 and 0.986 were obtained for LTA and ZP (Figure 5.11), respectively. The maximum MO dye removal was obtained as 100% and 91% at pH 6.17 and 5.15, the initial MO dye concentration of 20 and 20.24 mg/L, and adsorbent mass of 1000 and 1000 mg/L, respectively. To

assess the validity of the quadratic models developed in this work, the corresponding experimental %MO dye removal values were determined at the optimum conditions as 100% and 91%, which was in good agreement with the predicted values. Therefore, the two models presented here may be used to optimize the dye removal process and predict the %MO removal.

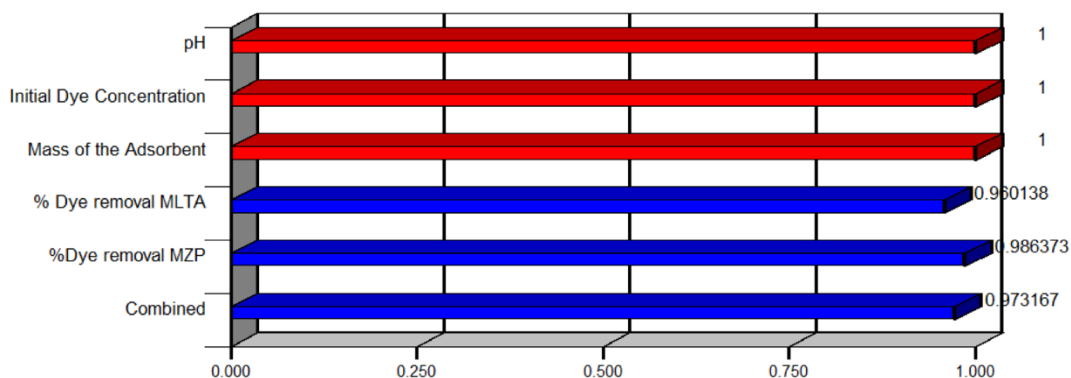


Figure 5.11. Bar-graph showing the desirability values of %MO dye removal for both adsorbents; MLTA and MZP.

5.3.5 The mechanism of MO removal

The Langmuir model was fitted into the developed kinetic model because the Langmuir equation can accurately describe the equilibrium data over the chosen concentration range of initial dye in the present study.

Based on Markandeya, et al. [34], precipitation is largely dependent upon the combination of three factors: mass of the adsorbent, the initial dye concentration, and pH. Figure 5.12 shows the mechanism of anionic dye adsorption onto modified zeolite.

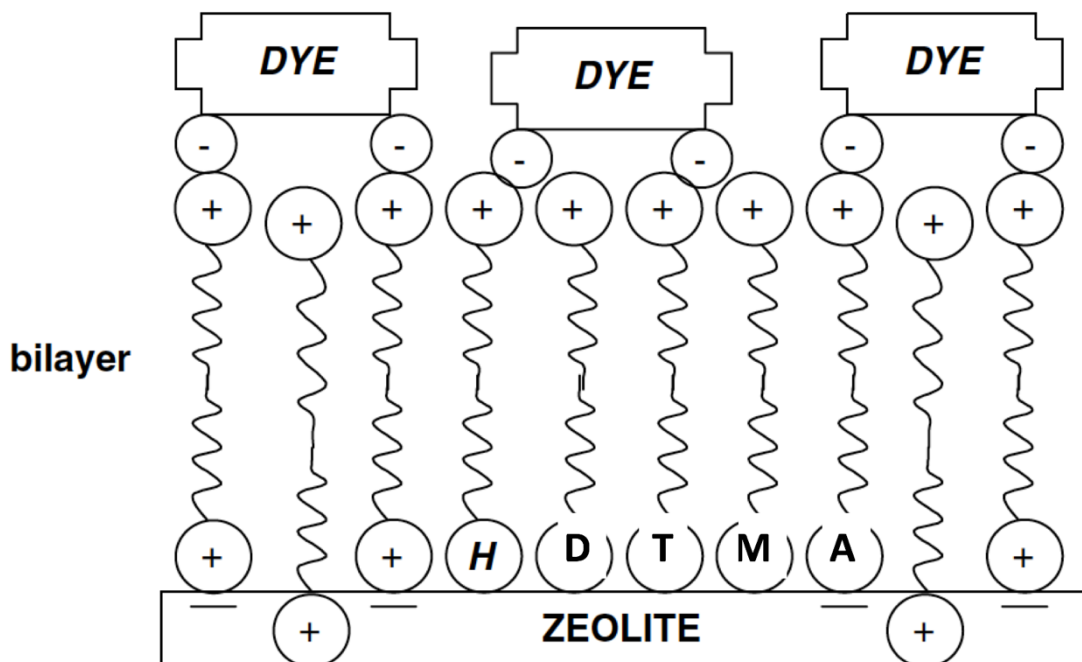


Figure 5.12. The mechanism of anionic dye adsorption onto modified zeolite

The adsorption isotherms with modified adsorbents indicate the three regions of interest, each corresponding to a different adsorption mechanism. In region I (at the minimum value of the initial dye concentration), the adsorption of dyes onto modified zeolite is governed initially by electrostatic attraction of anionic dye groups onto already adsorbed cationic head groups of the HDTMA molecules. The zeta potential results (Table 5.1) support this mechanism. Region II (at initial dye concentration value between the minimum and maximum) is ascribed to the precipitation of an anionic dye-cationic HTAB complex, and Region III (with initial dye concentration value at the maximum) is ascribed to the formation of solid phase of the dye [34].

5.4 CONCLUSION

In this study, two types of zeolite, namely Na-P and Linde type-A, were prepared by microwave-assisted synthesis of waste CFA. Acid pretreatment of raw CFA resulted in high-purity ZP and LTA zeolite, with high pore volume and surface area. The

synthesized zeolites were modified by cationic surfactant (HDTMA) bromide. The dependency of the MO removal process on the pH of the solution, the initial dye concentration, and the mass of the modified zeolites was studied utilizing the RSM. The CCD method was applied to develop a quadratic model in each case. The predicted values, calculated using the quadratic models, were in good agreement with the response (% dye removal) for LTA and ZP ($R^2 = 0.9991$ and 0.986 , respectively). The pH of the solution had the greatest effect when using ZP as an adsorbent, whereas the adsorbent amount had the greatest influence on the dye removal rate when LTA was employed.

ANOVA results indicate presence of interaction between all the variables, except pH and the initial dye concentration, when using ZP as an adsorbent.

The results obtained from the optimization of the MO removal process (100% at pH 6.17, the initial MO concentration of 20 mg/L, and 1000 mg/L adsorbent mass) and for LTA as adsorbent 91% at pH 5.15, with the initial MO dye concentration of 20.24 mg/L and adsorbent mass of 1000 mg/L for ZP as an adsorbent. Finally using waste CFA as a source for LTA and ZP production for dye removal from aqueous solutions is economically very attractive.

5.5 REFERENCES

- [1] S. Mondal .Methods of dye removal from dye house effluent: an overview. Environ. Eng. Sci. 25, 383 (2008).
- [2] S. Yadav, D. K. Tyagi, and O. P. Yadav. An overview of effluent treatment for the removal of pollutant dyes . Asian Journal of Research in Chemistry . 5, 1 (2012).
- [3] T. R. Das S, and Barman S. Removal of methyl orange and mythelene blue dyes

from aqueous solution using low cost adsorbent zeolite synthesized from fly ash. *J. Env. Sci. Eng.* 54, 472 (2012).

[4] M. Ghaedi, S. Hajati, M. Zaree, Y. Shajaripour, A. Asfaram, and M. K. Purkait. Removal of methyl orange by multiwall carbon nanotube accelerated by ultrasound devise: Optimized experimental design . *Adv. Powder Technol.* 26, 1087 (2015).

[5] D.Robati, B.Mirza, M.Rajabi, O.Moradi, I.Tyagi, S.Agarwa and V.K.Gupta .Removal of hazardous dyes-BR 12 and methyl orange using graphene oxide as an adsorbent from aqueous phase .*Chem. Eng. J.* 284, 687 (2016).

[6] D. Yuan, L. Zhou, and D. Fu, .Adsorption of methyl orange from aqueous solutions by calcined ZnMgAl hydrotalcite. *Appl. Phys. A.* 123,146 (2017).

[7] X. Querol, N. Moreno, J.C, Umaña A. Alastuey, E. Hernández, A. López-Soler and F. Plana . Synthesis of zeolites from coal fly ash: an overview. *Int. J. Coal Geol.* 50, 413 (2002).

[8] S. S. Bukhari, J. Behin, H. Kazemian, and S. Rohani. Conversion of coal fly ash to zeolite utilizing microwave and ultrasound energies: A review. *Fuel*, 140, 250 (2015).

[9] T. Aldahri, J. Behin, H. Kazemian, S. Rohani. Effect of microwave irradiation on crystal growth of zeolitized coal fly ash with different solid/liquid ratios. *Adv. Powder Technol.* 28, 2865 (2017).

[10] M. Ahmaruzzaman. A review on the utilization of fly ash . *Prog. Energ. Combust.* 36, 327 (2010).

- [11] A. M. Doyle, Z. T. Alismaeel, T. M. Albayati, and A. S. Abbas. High purity FAU-type zeolite catalysts from shale rock for biodiesel production. *Fuel* . 199, 394 (**2017**).
- [12] K. S. Hui and C. Y. H. Chao. Effects of step-change of synthesis temperature on synthesis of zeolite 4A from coal fly ash . *Micropor. Mesopor. Mat* . 88, 145 (**2006**).
- [13] X. Querol, A. Alastuey, A. López-Soler, F. Plana., J. M. Andrés, R. Juan, P. Ferrer and C.R. Ruiz . A Fast Method for Recycling Fly Ash: Microwave-Assisted Zeolite Synthesis . *Environ. Sci. Technol.* 31,2527 (**1997**).
- [14] M. M. J. Treacy and J. B. Higgins. Collection of simulated XRD powder patterns for zeolites . Fourth Revised Edition, Elsevier (**2001**).
- [15] G. R. Daham, A. A. Abdu IRazak, A. S. Hamadi, and A. A. Mohammed. Re-refining of used lubricant oil by solvent extraction using central composite design method. *Korean J. Chem. Eng.* 34, 2435 (**2017**).
- [16] K. P. Singh, A. K. Singh, S. Gupta, and S. Sinha. Optimizing adsorption of crystal violet dye from water by magnetic nanocomposite using response surface modeling approach . *J. Hazard. Mater* . 186, 1462 (**2011**).
- [17] K. Fukui, M. Katoh, T. Yamamoto, and H. Yoshida. Utilization of NaCl for phillipsite synthesis from fly ash by hydrothermal treatment with microwave heating, *Adv. Powder Technol.* 20 , 35 (**2009**).
- [18] M. Inada, H. Tsujimoto, Y. Eguchi, N. Enomoto, and J. Hojo. Microwave-assisted zeolite synthesis from coal fly ash in hydrothermal process. *Fuel* 84, 1482 (**2005**).

- [19] F. Rouquerol, J. Rouquerol, K. S. W. Sing, P. L. Llewellyn, and G. Maurin. Adsorption by powders and porous solids: principles, methodology and applications . Elsevier **(2014)**.
- [20] K. S. W. Sing , D.H. Everett, R. A. W. Haul, L. Moscou, R. A. Pierotti, J. Rouquerol and T. Siemieniewska . Reporting Physisorption Data for Gas/Solid Systems,” in Handbook of Heterogeneous Catalysis. Wiley-VCH Verlag GmbH & Co. KGaA, **(2008)**.
- [21] R. M. Barrer. Zeolites and clay minerals as sorbents and molecular sieves. London: Academic Press **(1978)**.
- [22] T. Masuda . Diffusion mechanisms in zeolite catalysts. Catalysis surveys from Asia. 7,133 **(2003)**.
- [23] K. Ramesh, K. Sammi Reddy, I. Rashmi and A. K. Biswas . Porosity distribution, surface area, and morphology of synthetic potassium Zeolites: A SEM and N₂ adsorption study. Commun. Soil Sci. Plan. 45, 2878 **(2014)**.
- [24] T. Aldahri, J. Behin, H. Kazemian, and S. Rohani. Synthesis of zeolite Na-P from coal fly ash by thermo-sonochemical treatment . Fuel .182, 494 **(2016)**.
- [25] P. Pal, J. K. Das, N. Das, and S. Bandyopadhyay. Synthesis of NaP zeolite at room temperature and short crystallization time by sonochemical method . Ultrason sonochem . 20, 314 **(2013)**.
- [26] S. S. Bukhari, J. Behin, H. Kazemian, and S. Rohani. Synthesis of zeolite NA-A

using single mode microwave irradiation at atmospheric pressure: The effect of microwave power,” *Can. J. Chem. Eng.* 93, 1081 (2015).

[27] K. Yetilmezsoy, S. Demirel, and R. J. Vanderbei. Response surface modeling of Pb(II) removal from aqueous solution by *Pistacia vera* L.: Box–Behnken experimental design . *J. Hazard. Mater.* 171,551 (2009).

[28] D. Wu, J. Zhou, and Y. Li . Effect of the sulfidation process on the mechanical properties of a CoMoP/Al₂O₃ hydrotreating catalyst . *Chem. Eng. Sci.* 64, 198 (2009).

[29] A. Mittal, A. Malviya, D. Kaur, J. Mittal and L . Kurup . Studies on the adsorption kinetics and isotherms for the removal and recovery of Methyl Orange from wastewaters using waste materials. *J. Hazard. Mater.* 148, 229 (2007).

[30] M. Rajasimman and P. Karthic. Application of response surface methodology for the extraction of chromium (VI) by emulsion liquid membrane . *Journal of the Taiwan Institute of Chemical Engineers* .41, 105 (2010).

[31] K. Anupam, S. Dutta, C. Bhattacharjee, and S. Datta. Adsorptive removal of chromium (VI) from aqueous solution over powdered activated carbon: Optimisation through response surface methodology . *Chem. Eng. J.* 173, 135 (2011).

[32] Z. Noorimotlagh, R. Darvishi Cheshmeh Soltani, A.R. Khataee , S. Shahriyar and H. Nourmoradi . Adsorption of a textile dye in aqueous phase using mesoporous activated carbon prepared from Iranian milk vetch. *J. Taiwan Inst. Chem. E.* 45, 1783 (2014).

[33] M. I. Mohammed, A. A. Abdul Razak, and D. A. Hussein Al-Timimi .Modified multiwalled carbon nanotubes for treatment of some organic dyes in wastewater . Adv. Mater. Sci. Eng. 2014, 1 (**2014**).

[34] Markandeya; S. Prasad Shukla; N. Dhiman; D. Mohan; G. C. Kisku; and S. Roy. An Efficient Removal of Disperse Dye from Wastewater using Zeolite Synthesized from Cenospheres. Journal of Hazardous, Toxic, and Radioactive Waste, vol. 21, no. 4, pp. 4017017 (**2017**).

Chapter 6

PREPARATION AND CHARACTERIZATION OF LINDE-
TYPE A ZEOLITE FROM COAL FLY ASH BY
MICROWAVE-ASSISTED SYNTHESIS METHODE: ITS
APPLICATION AS ADSORBENT FOR REMOVAL OF
ANIONIC DYES⁵

Abstract

The industrial dyes effluent poses serious concern to human health if it is discharged into water supplies system without treatment. Linde-type A zeolite (CFA-ZA) was prepared from coal fly ash (CFA) and used as an adsorbent to remove acidic dye (Acid red 66, AR66) from its aqueous solution. The (CFA) was converted to (CFA-ZA) by a single hydrothermal alkaline treatment process using microwave energy. The product was characterized by powder XRD, SEM, BET, ZP and TGA. The effectiveness of synthesized (CFA-ZA) in adsorbing (AR66) from an aqueous solution was studied using batch experiments. The effects of contact time, pH of the solution,

⁵ This chapter is under review by the Canadian J of Chem. Eng. Aldahri, T., AbdulRazak, A. A., Rohani, S. The Canadian J of Chem. Eng. (Submitted 2018).

initial dye concentration and adsorbent amount were investigated. It was found that 100% dye removal was achievable in 20 min for the following conditions; 25 mg/L initial dye concentration, 4 pH, and 250 mg/L adsorbent. The equilibrium data were studied using the Langmuir and Freundlich models and it was found that the data fit better to Freundlich model with a higher value of $R^2 > 0.998$. The maximum adsorption capacity of (AR66) for Langmuir equation was 416.67 mg/g. Kinetic adsorption studies were done in terms of intra-particle diffusion model, pseudo – first- order and pseudo-second-order models. The results showed that the data followed a pseudo-second order model. The present study demonstrates that the (CFA-ZA) prepared from (CFA) can be utilized for (AR66) dyes removal with high efficiency and therefore it may be considered as an alternative material to replace commercial and natural zeolite in this process.

Key words: Zeolite A, Coal fly ash, Microwave synthesis, Anionic dyes removal

6.1 Introduction

Azo dyes are the largest class of dyes. These dyes contain azo groups ($-N=N-$) in their chemical structure. Azo dyes are used to dye different materials such as leather, textiles, food and cosmetics. Nowadays azo dyes make 60-70 % among the other commercial types of dyes. Azo dyes are considered as a very serious health hazard to humans if they get into water supplies. They are harmful to ecosystems if discharged to water system [1, 2]. Current methods used to remove dangerous azo dyes from wastewater include physical and chemical treatment processes such as adsorption, precipitation, flocculation, flotation, coagulation, and electrochemical destruction

methods [3 – 6]. Biodegradation by fungi and bacteria [7], and photocatalytic degradation [8] have also been reported. Recent methods for removal of azo dyes include physical and chemical treatments due to high efficiency and low price compared with other methods. Various types of adsorbents are in use today to remove azo dyes from wastewater such as activated carbon [9], chitosan beads [10], and modified bentonite [11].

Coal-fired energy is a quite large sector in the market of the energy generation as a result of the fast growth in the world development and population. Coal fly ash (CFA) is a mixture of inorganic constituents that are generated by coal combustion in thermal power station as a waste. (CFA) has a negative environmental impact and should be discarded or utilized safely to diminish the possible risks [12]. (CFA) mainly consists of aluminum (Al) and silicon (Si) which can be used to produce zeolites. The unique microporous structure of zeolite, makes zeolite an excellent adsorbent with a high adsorptive capacity, ion-exchange capacity, and gas separation property [13]. Many studies have been carried out [14-16] and reviews written on the production of zeolites from CFA [17, 18].

Zeolite A has been successfully synthesized by the hydrothermal process utilizing the byproduct of the etching process of aluminum, sodium aluminate and sodium silicate. The results revealed that the reaction temperature and time and are directly proportional with the production of zeolite A [19]. Moreover, the synthesis of zeolites with the assist of microwave energy had been studied by many past works [14–16], and they found that to accelerate nucleation, reduce crystallization time, produce narrower particles size distributions, reduce undesirable phases, and obtain different morphologies [20].

A number of researches have used (CFA) as a low-cost adsorbent for removal of organic material [21-22] and heavy metals [23-24]. Many researchers have used different type of zeolite from (CFA) for removal of dyes [25] and heavy metals [26].

In this study, (CFA-ZA) synthesized from (CFA) by microwave-assisted method was used as adsorbent to eliminate anionic acid (acid red 66, AR66) from aqueous solution by applying various conditions for example contact time, pH of solution, adsorbent mass and dyes initial concentration through batch experiments.

6.2 Materials and Methods

6.2.1 Materials

Coal fly ash (CFA) was collected from (Ontario Power Generation, Nanticoke, Canada). The materials were stored in container before use. (Na_2SiO_3) Sodium meta-silicate, and (NaAlO_2) sodium aluminate anhydrous both brought from (Sigma-Aldrich, USA), NaOH Sodium hydroxide purchased from (Alphachem, Mississauga, Canada), and AR66 was supplied from (Alfa Aesar, USA). Molecular formula of (AR66) is $\text{C}_{22}\text{H}_{14}\text{Na}_2\text{O}_7\text{S}_2$, with a molecular mass of 556 g/mol and the following chemical structure:

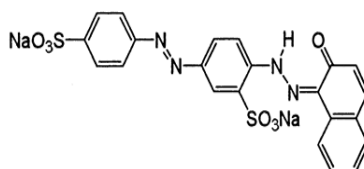


Figure 6-1: Acid red 66 chemical structures

6.2.2 Preparation of (CFA-ZA)

Linde-type A zeolite (CFA-ZA) was prepared by microwave-assisted synthesis method using (CFA) as raw materials, 2 g of (CFA) was dissolved in 20 mL of HCL solution (0.1 M). The mixture was agitated at 250 rpm and heated at 90 °C for 3 h. Subsequently, the sample was filtrated and the solid product was washed and dried overnight at room temperature. HCl treatment helps to remove impurities from the raw coal fly ash [27]. Zeolitization of coal fly ash involving a hydrothermal treatment step was conducted as follows: 1.5 molar of NaOH granules with 2 g of acid treated coal fly ash were dissolved in 20 mL of distilled water (CFA/NaOH ratio of 1.67). 0.4 g of the sodium aluminate and 1 g of sodium meta-silicate were added to the reaction solution. Thereafter, the mixture was introduced to microwave radiation energy for crystallization using microwave source (self-adjusting type) (2.45 GHz, single mode, CEM cooperation, USA), the experiment conducted at atmospheric pressure. A cylindrical tube PTEE, (28mmID X 108mm) where fixed at the microwave chamber equipped with a total reflux condenser. The radiation time was 30min and microwave power 250W. Later, the solid product was filtered and washed with distill water before dried at room temperature for overnight.

6.2.3 Characterization of (CFA-ZA)

Rigaku–Miniflex powder diffractometer (Japan) was used to collect XRD data of the synthesized zeolites using CuK_α (λ for $\text{K}_\alpha = 1.54059 \text{ \AA}$ over the range of $5^\circ < 2\theta < 40^\circ$ with a step width of 0.02°). The morphology of the zeolites were studied by scanning electron microscope (SEM); Hitachi S 2600N SEM (Tokyo, Japan) operating at 5 kV of acceleration voltage. The thermogravimetric analysis (TGA) of the sample carried out by using a Mettler Toledo TGA/SDTA 851e model (Switzerland) with

version 6.1 STARe software. The sample was heated from 25°C to 600°C at a heating rate of 10°C/min under nitrogen purge. Particle size distribution (PSD) analysis was also done by using Mastersizer 2000 (Malvern Instruments Ltd., UK), and a Zetasizer Nano ZS 3000 HSA (Malvern, Worcestershire, UK) was used to measure the zeta potential.

6.2.4 Adsorption Study of (AR66) on (CFA-ZA)

6.2.4.1 Batch experiments

In this study, batch experiments were conducted to study the influence of pH, initial concentration of the dye, adsorbent amounts, and contact time. A dye solution of 25mg/L initial concentration was prepared by dissolving 25 mg of dyes into 1 L distilled water. A 250 mL flask was used to add 100 mL (25 mg/L) of dye solution, 25 mg /100 mL of (CFA-ZA) at a fixed pH. The pH was fixed to 4 by adding either HCl or NaOH of 0.1M. The solution was mixed at 400 rpm speed at room temperature by a magnetic stirrer. Dyes concentration before and after adsorption was measured using UV spectrophotometer type ((Cary 60, Agilent Technology (Germany)) at 504nm wavelength which corresponds to the maximum absorbance wavelength of the dye. The dye concentration was calculated from previously ready calibration curves.

The initial dye concentration was in the range 25 to 100 mg/L, the pH of the solution was (4-9), and adsorbent amount range was 50 to 250 mg/L. The % dye removal and adsorption capacity of (CFA-ZA) were calculated by the following equations:

$$\% \text{ dye Removal} = \frac{C_o - C_f}{C_o} \quad (\text{Eq. 6-1})$$

$$\text{Adsorption capacity } (q) = \left(\frac{C_0 - C_f}{m} \right) \times V \quad (\text{Eq. 6-2})$$

Where C_0 and C_f are the initial and final (AR66) dye concentration (mg/L) respectively, (V) is the volume of dye solution (L), (m) is the adsorbent mass (g), and (q) is the amount of (AR66) dye adsorbed per weight of adsorbent (mg/g).

6.2.4.2 Adsorption isotherm

Adsorption isotherms were obtained at pH 4 using 100 mL (AR66) solution at (25, 50, 75 and 100, mg/L) initial concentration of the dye with 25 mg adsorbent, in a 250 mL conical flask at room temperature. A sample was withdrawn at a time interval of 10 min to calculate its concentration.

6.3 Results and Discussion

6.3.1 Characterization of (CFA-ZA)

The chemical analysis of the raw (CFA) shows in Table 3-1, this material was utilized as Al and Si main source in zeolitization process. The $\text{SiO}_2/\text{Al}_2\text{O}_3$ ratio was 2.13, this low ratio of silica was suitable for synthesis (CFA-ZA). The XRD data of (CFA) indicated that the main components of the (CFA) were amorphous aluminosilicate as well as mullite and quartz that appeared as crystalline structures in Figure 6-2.

The XRD analysis was performed for the sample after microwave irradiation to determine the zeolite phases existing. One main zeolitic phases was seen, that is zeolite A (CFA-ZA). The XRD patterns for the (CFA) and microwave-assisted zeolitized coal fly ash are shown in Figure 6-2.

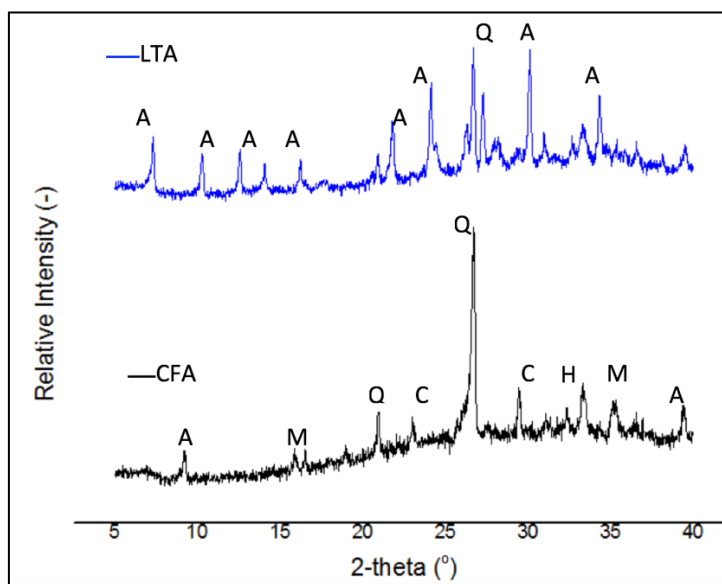


Figure 6-2: The XRD pattern of (CFA) and microwave-assisted zeolitized coal fly ash (LTA: CFA-ZA).

The (SEM) of (CFA) and (CFA-ZA) are displayed in Figure 6-3. In the entire SEM image, one distinct main structure can be observed, a cubic structure. The cubic structure is associated with (CFA-ZA) framework [20]. The zeolitic particles are deposited and crystallized on the surface of the undissolved (CFA) particles which agrees with an earlier suggested mechanism [28, 29].

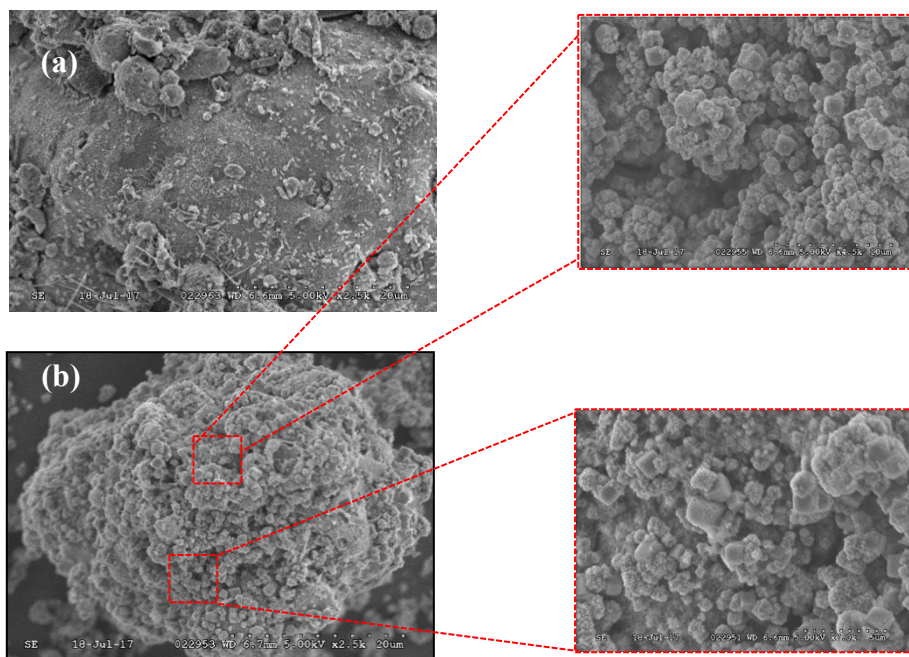


Figure 6-3. The SEM image of a) raw (CFA) and b) (CFA-ZA) from (CFA).

The BET surface area of the synthesized (CFA-ZA) from (CFA) by microwave-assisted synthesis method was $48.47 \text{ m}^2/\text{g}$ while that for the raw (CFA) was $15.47 \text{ m}^2/\text{g}$. The pore volume and the pore size were $0.134135 \text{ cm}^3/\text{g}$ and 110.6834 \AA , respectively. Obviously, the BET surface area of synthesized (CFA-ZA) was much higher than that of the raw (CFA). Figure 6-4 shows the nitrogen adsorption/desorption isotherm of the (CFA-ZA) which indicates an isotherm of type II. This type of isotherm is known for the micropores material based on Applied Chemistry (IUPAC) isotherm classification and the International Union of Pure [30, 31]. The reason could be related to the impurities that were trapped inside channels and pores of CFA-ZA and limited the nitrogen adsorption inside the pores.

The HCl treatment of (CFA) during preparation process had a significant effect on the of (CFA-ZA) structure, resulting in a pore size of 110.6834 \AA that can be considered appropriate for reducing the diffusional resistance of the dye ions. The dye ions transfer easily via the channels of the adsorbent lattice [32]. This may be one of

main reasons for the increase of the adsorption of dye anions on the adsorbent. In addition, the transformation of (CFA) to (CFA-ZA) increases the cation exchange capacity of the adsorbent, which also has a positive effect on increasing the dye adsorption [33].

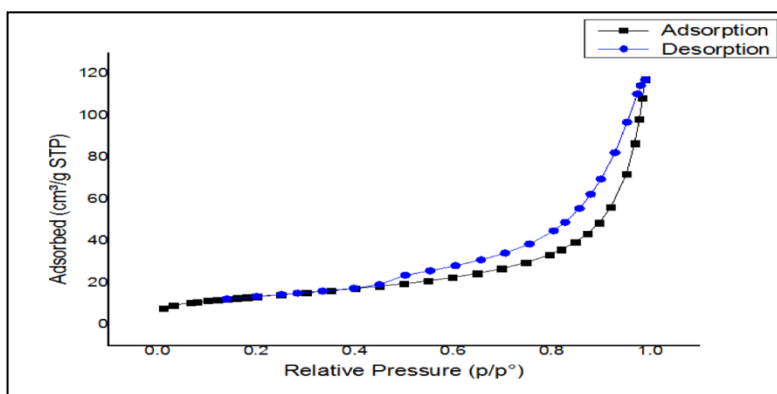


Figure 6-4: The adsorption and desorption isotherms of (CFA-ZA) from (CFA).

Particle size distribution curves for raw (CFA) and (CFA-ZA) are shown in Figure 6-5. The different size distribution indicates a significant change during the zeolitization of (CFA). Apparently, the microwave-assisted synthesis method has a strong effect on the particle size distribution. The maximum volumetric population of 4.5 vol % at $\sim 80 \mu\text{m}$ for raw (CFA) is shifted to $\sim 10 \text{ vol \%}$ for synthesized (CFA-ZA).

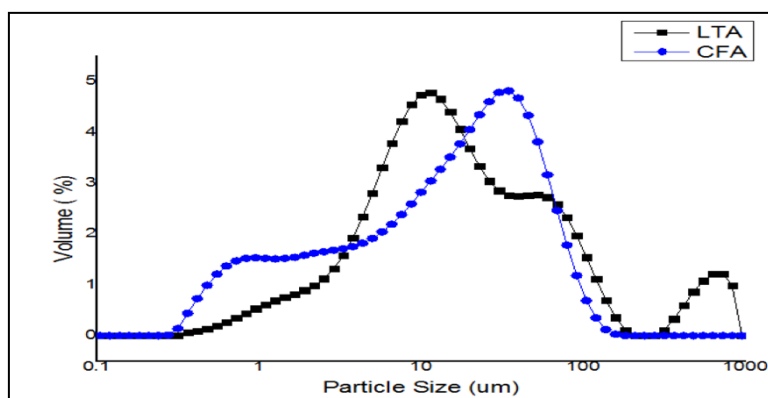


Figure 6-5: The (PSD) of raw (CFA) and (LAT: CFA-ZA) from (CFA).

6.4 Adsorption of (AR66)

6.4.1 Effect of pH on dye removal efficiency

The pH of solution is considered as one of most influential parameters affecting the adsorption process. Solutions with different pH values (4.0, 5.0, 6.0, 7.0, and 9.0), with initial dye concentration of 25 mg/L, 250 mg/L mass of adsorbent, and 1 h stirring time were prepared to study the influence of these parameters on (CFA-ZA) adsorption. The zeta potential (mV) versus the pH of the solution is shown in Figure 6-6. The point of zero zeta potential (pHzpc) of (CFA-ZA) is at 4.7 pH. The pHzpc of (CFA-ZA) shows that the surface of adsorbent is positively charged when the pH is less than 4.7 and negatively charged above 4.7 pH. At pH 4, 100 % removal of dye (AR99) was achieved due to high electrostatic attraction between positively charged (CFA-ZA) and sulfonate groups ($-\text{SO}_3^-$) of (AR66) dye [34]. For values of pH of the solution > 4.7 , there is a decrease in the positive charge and an increase in the number of negative charge, this condition does not favor the adsorption mechanism of the dyes. Hence the removal of dyes is decreased. A pH of 4 was fixed in the rest of experiments of this work to achieved high removal of dyes.

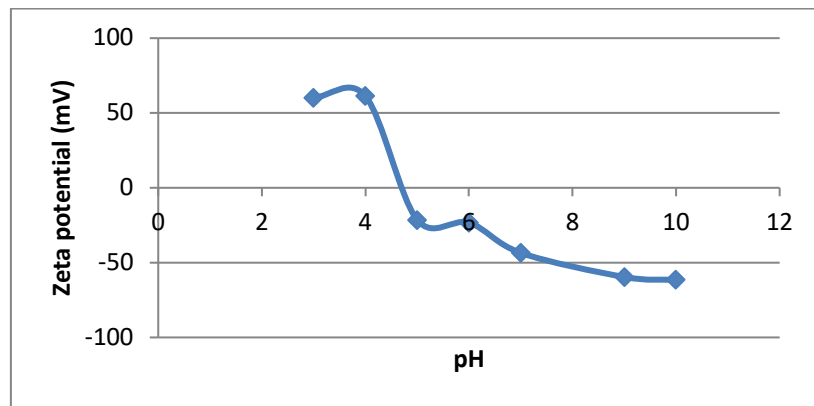


Figure 6-6: Zeta potential of (CFA-ZA) vs. the pH of solution.

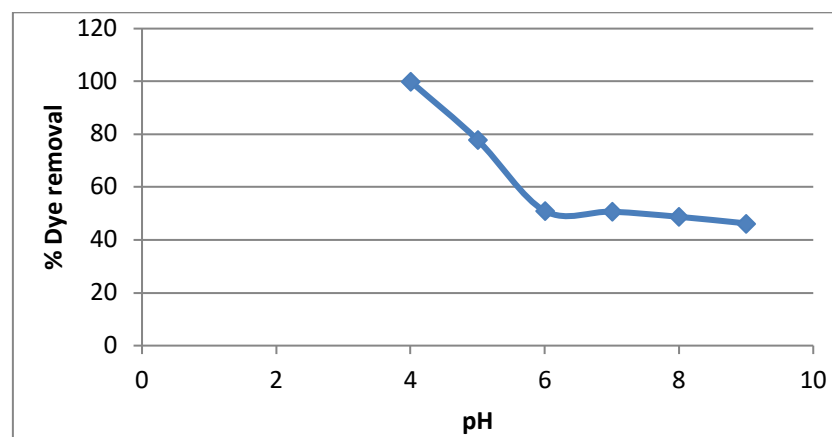
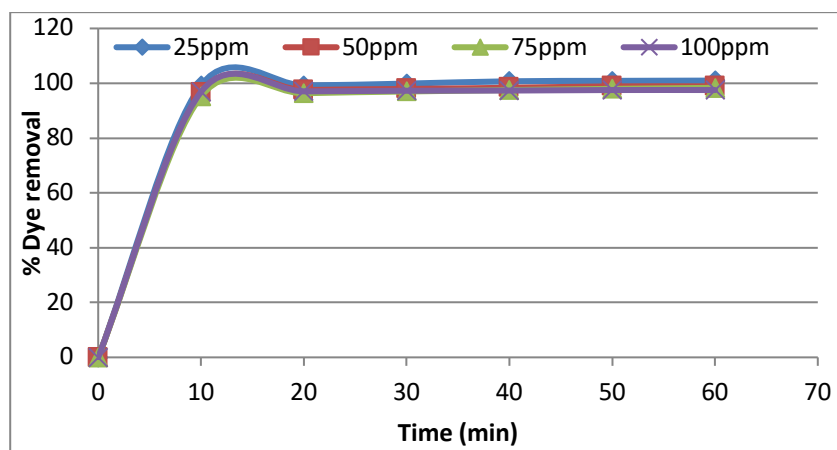


Figure 6-7: % dye removal vs. the pH of solution

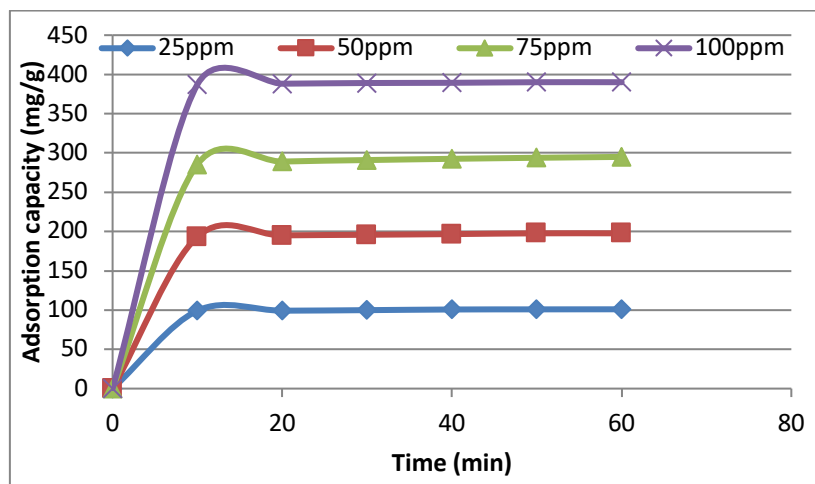
6.4.2 The effect of contact time and initial dye concentration

It is important to find the equilibrium adsorption of (AR66) over the adsorbent. The influence of time of contact on removal of (AR66) was studied at four initial concentrations of 25, 50, 75, and 100 mg/L, adsorbent mass 250 mg/L and 4 pH of the solution. The influence of time of contact on the (AR66) removal % is shown in Figure 6-8a and the effect of time of contact on adsorption capacity is illustrated in Figure 6-8b. It is clear that for all selected initial concentrations, at the beginning, the (AR66) adsorption is increased linearly at a very faster rate: 96-100% of dye removal was

reached in 10 min. The same time to reach equilibrium adsorption for all initial dye concentrations may suggest that the process of dye adsorption is second order as will be discussed in the next part of this paper [35, 36]. Note that the short contact time is useful in real applications. This behavior can be attributed to the fact that in the initial stage, the free surface sites are available in large numbers. Also, it is clearly illustrated that the maximum adsorption capacity of (AR66) dye increases from 100 mg/g to 390 mg/g as the initial concentration of the dye increased from 25 mg/L to 100 m/g. The increase in adsorption capacity of (AR66) with increased initial dye concentration may be due: 1) Greater driving force at higher (AR66) dye concentration as shown by Ranjusha et al. and Chen at al. [37, 38]. 2) The increased collisions between solid surface and dye molecules as the initial dye concentration is increased which augments the adsorption process.



a)



b)

Figure 6-8: The effect of contact time on a) % dye removal and b) adsorption capacity of (CFA-ZA)

6.4.3 Effect of (CFA-ZA) dosage on removal of dyes

The effect of (CFA-ZA) amount on (AR66) removal is shown in Figure 6-9, as (CFA-ZA) amount increases from 10 to 25 mg/100 mL, the % dye removal will increase from 96 to 100 %. An increase in (AR66) removal is due to the increased surface area of the adsorbent [39]. The dye removal remains unchanged as the (CFA-ZA) amount increases beyond 25 mg/100mL because no dye molecules are accessible for the adsorption.

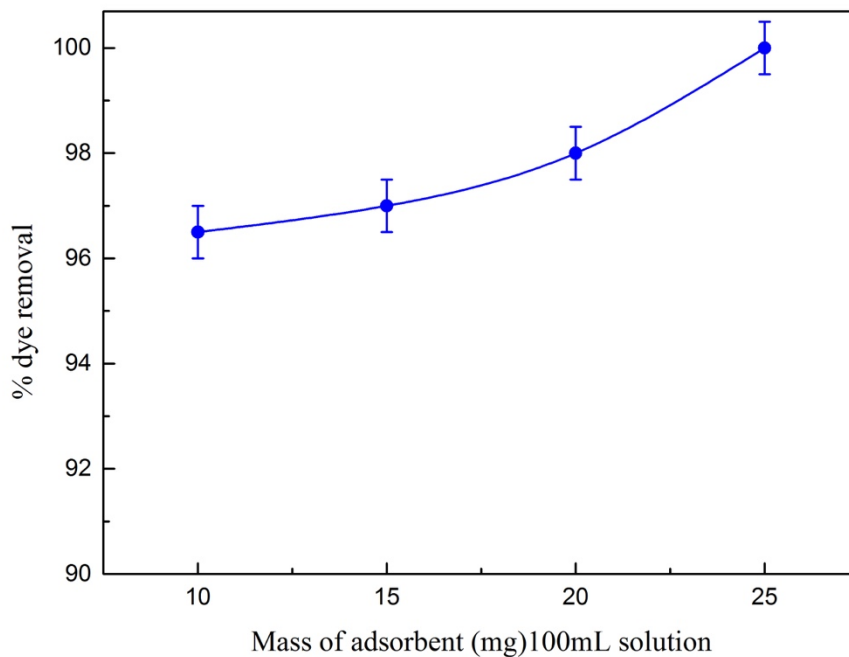


Figure 6-9: % Dye removal vs. mass of adsorbent.

6.5 Equilibrium isotherms

Equilibrium isotherms depict the interaction of adsorbents with adsorbates and therefore provide the basic tools in optimizing adsorption process. Commonly, isotherms of Freundlich [40] and Langmuir [41] are used to model experimental data. In this work these two important models are used to describe the experimental data of (AR66) dye.

The main assumptions of Freundlich model are dissimilar active sites with different adsorption energies, so this model can be applied to multilayer heterogeneous adsorption systems. The Freundlich equation is:

$$\text{Log } q_e = \frac{1}{n} \text{Log } C_e + \text{Log } k_f \quad (\text{Eq. 6-3})$$

Where n is a constant relating to the adsorption process intensity and k_f is Freundlich constant relating to the adsorption capacity, n and k_f values were estimated from the slope and the intercept of Figure 6-10 and appear in Table (6-2). The value of $n > 1$ demonstrates that the nature of adsorption is physical.

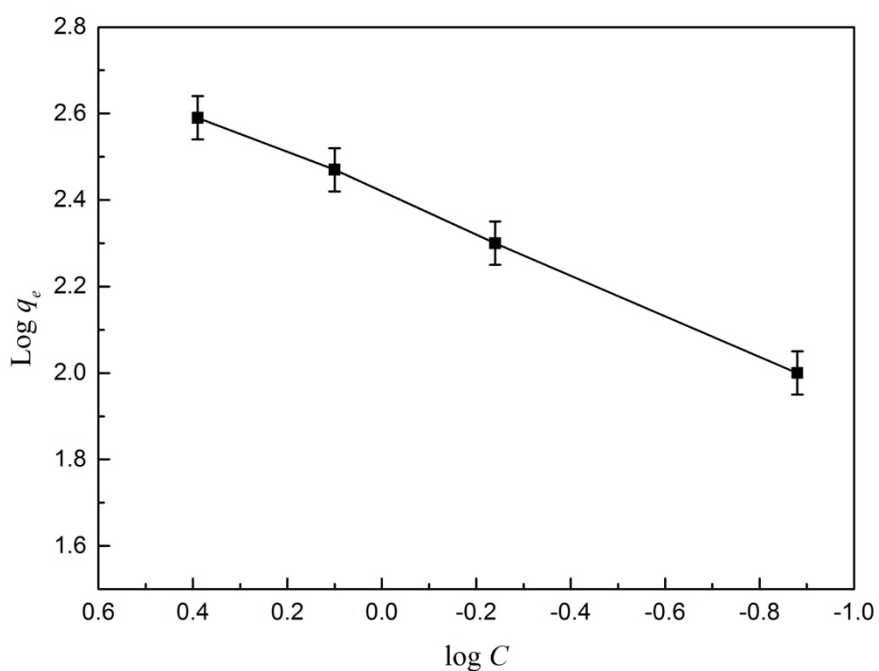


Figure 6-10: Freundlich isotherm of (AR66) on (CFA-ZA).

The assumption of the Langmuir model is that the adsorption occurs on a homogeneous monolayer covering the outer surface of the adsorbent. These sites have no interaction between them and when these sites are occupied by the dyes, no more adsorption can happen at those sites. The general linear form of Langmuir isotherm model is given below:

$$\frac{C_e}{q_e} = \frac{C_e}{q_m} + \frac{1}{k_L q_m} \quad (\text{Eq. 6-4})$$

Where k_L is the isotherm constant of Langmuir (L/mg) and q_m is the maximum adsorption capacity (mg/g). The plot of C_e/q_e against C_e for (AR66) dye is shown in Figure 6-11. The values of equilibrium constant k_L , monolayer adsorption capacity q_m and coefficients of correlation, R^2 , are presented in Table 6-1. Table (6-1) shows that the q_m of (AR66) is 416.67 mg/g. The nonlinearity and relatively low value of $R^2 < 92$ indicate that the equilibrium data of adsorption of this dye did not follow well the Langmuir model.

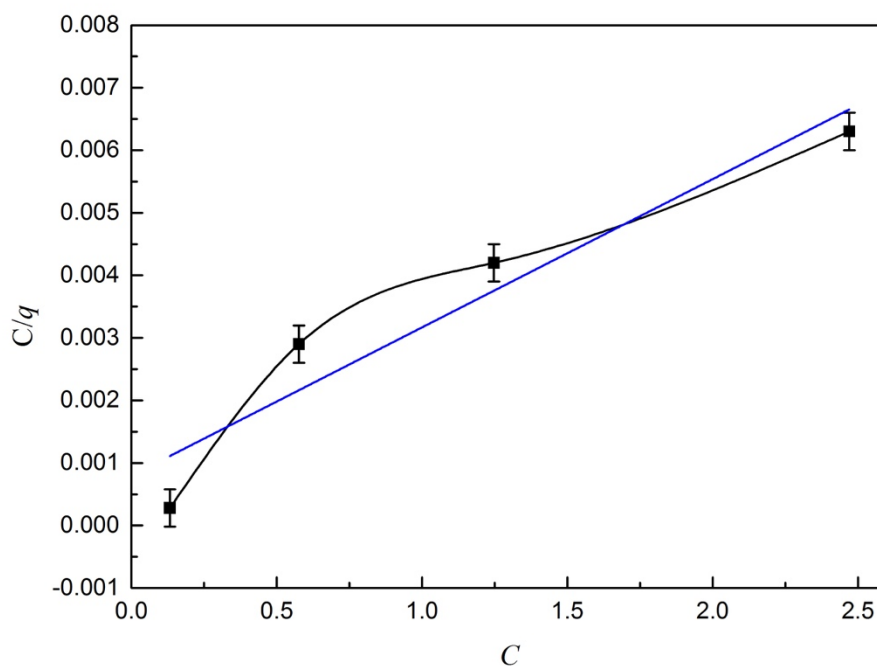


Figure 6-11: Langmuir isotherm of (AR66) on (CFA-ZA).

The equilibrium data had a better fit with the Freundlich model as shown by higher value of $R^2 > 0.998$ (Table 6-1). This proves that the (AR66) adsorption process takes place on the heterogeneous adsorbent surface, non-uniform and non-specific in nature.

Table 6-1: Langmuir and Freundlich constants for (AR66) dye adsorption isotherms on (CFA-ZA) at 25°C, 4 pH and 250 mg /L adsorbent dosage.

Freundlich parameters			Langmuir parameters		
k_f (mg/g)	n	R^2	q_m	k_L	R^2
2.41	2.13	1	416.7	3	0.92

Table 6-2 shows comparison of q_m of (AR66) on (CFA-ZA) of this work with other references. It is clearly concluded that (CFA-ZA) gives higher performance for removal of (AR66) dye from wastewater.

Table 6-2: Comparison of q_m appears in references with this work.

Adsorbent	Dyes	q_m (mg/g)	Isotherm model	References
Nymphaea rubra (biosorbent)	Reactive Red 2	66.67	Freundlich	[38]
Microalgae	(AR 66)	44.24 mg/g	Freundlich	[39]
Mg–Al–CO ₃ , (LDH)	(AR66)	102.7	Sips and Langmuir	[40]
Zeolite A from CFA	(AR 66)	416.7	Freundlich	This work

6.6 Kinetic models

The adsorption mechanism of (AR66) dye onto the (CFA-ZA) zeolite surface was investigated by a pseudo first order [Eq. 6-5], a pseudo second order [Eq. 6-6] and intraparticle diffusion kinetics models [Eq. 6-7]. The pseudo first order kinetic model is based on the concept that the change of quantity of the dye adsorbed with the time is related to the difference between saturation dye concentration and the quantity of dye adsorbed with time.

$$\ln(q_e - q_t) = \ln q_e - k_1 t \quad (\text{Eq. 6-5})$$

Where q_t and q_e refer to the amounts of (AR66) dye adsorbed (mg/g) at any time (t) and at equilibrium condition, respectively, and k_1 is the rate constant of a pseudo-first-order model (1/h) or (1/min). The intercept and slope of the linear plot of above equation render k_1 values at different initial dye concentrations. The R^2 (correlation coefficient) of this model had a low value.

The chemisorption of the dye on the adsorbents surface is the main assumption of a pseudo second- order kinetic model [45]. The following equation represents this model:

$$\frac{t}{q_t} = \frac{1}{k_2 q_e^2} + \frac{1}{q_e} t \quad (\text{Eq. 6-6})$$

Where k_2 is the rate constant of a pseudo-second-order model (g/mg h) or (g/mg min). The intercept and slop of a linear plot of t/q_t vs. time (t) provide the k_2 values at different initial dye concentrations (Figure 6-12). The k_2 and R^2 listed in Table 6-3. The value

of $R^2=1$ for this model confirms that the adsorption system of (AR66) dye by (CFA-ZA) zeolite follows a pseudo second-order model, based on the assumption that the limiting rate step could be chemisorption [36]. Also, the q_e values calculated are well close to experimental q_e values.

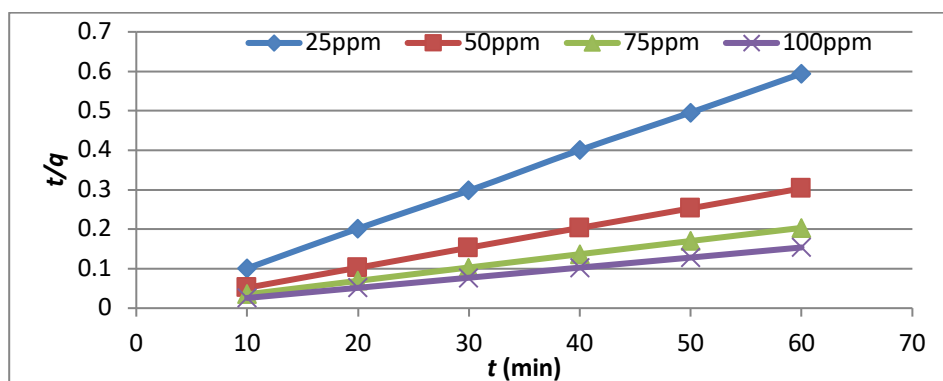


Figure 6-12: Pseudo second order model for (AR66) dye adsorption onto (CFA-ZA).

The intra particle model states that the adsorption rate depends essentially on the solid adsorbent properties such as size, surface area, shape, functional group, surface charge and porosity [46]. This model is expressed by the following equation: [47]

$$q_t = k_3 t^{1/2} + C \quad (\text{Eq. 6-7})$$

Where k_3 is the rate constant of intraparticle diffusion models. An adsorption process that follows this model should render a linear plot of q_t verses $t^{1/2}$, and the rate limiting step is the intra particle diffusion, if the plot passes through the origin [48]. If not, other mechanisms will also be involved [49]. As shown in Figure 6-13, the plot does not pass through origin, indicating that this model is not applicable to the adsorption of (AR66)

on (CFA-ZA) for all the dye concentrations. Also, as appears in Table 6-3, the R^2 value is lower than the pseudo second-order kinetic model.

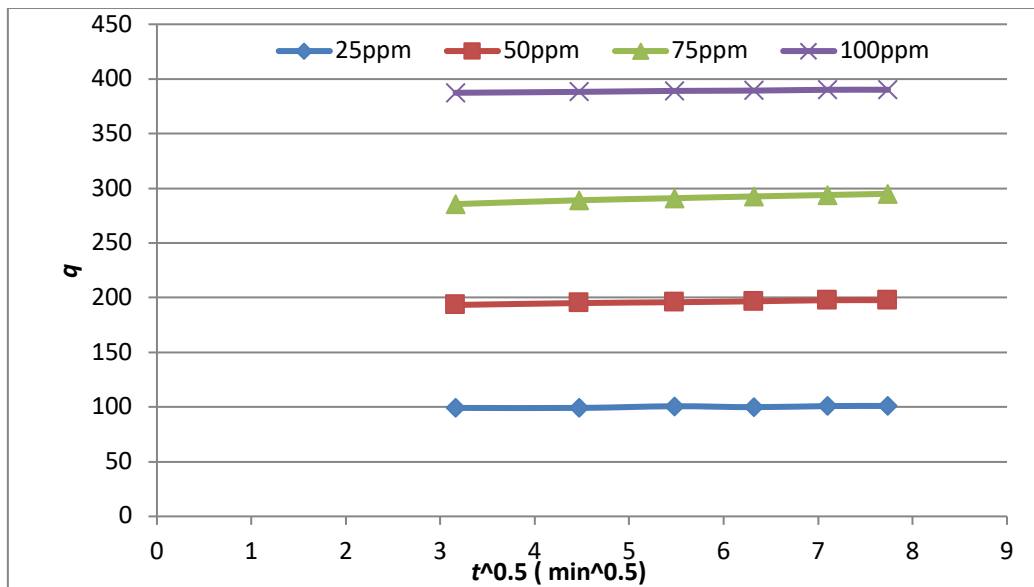


Figure 6-13: Intra- particle diffusion for (AR66) adsorption onto (CFA-ZA).

Table 6-3: The kinetic results of Intra- particle diffusion and Pseudo- second order.

C_o mg/L	Pseudo- second order				Intra- particle diffusion		
	q_e mg/g	q_c (mg/g)	k_2 (g/mg/min)	R^2	C (mg/ g)	k_3 (mg/g/min ^{-1/2})	R^2
25	99.9	101	0.033	1	97.8	0.414	0.72
50	197.7	200	0.014	1	190.5	0.979	0.98
75	295.0	294.1	0.006	1	279.65	2.014	0.99
100	390.1	384.6	0.022	1	385.44	0.631	0.98

6.7 Conclusions

(CFA-ZA) was successfully synthesized by microwave-assisted method from coal fly ash as a plentiful industrial waste. After the synthesis process, different characterizations were performed such as SEM, XRD, PSD and TGA. The XRD results show that utilizing microwave irradiation after acid treatment of the raw (CFA) results in producing a high purity (CFA-ZA). Microwave synthesis resulted in both higher crystallinity and production of (CFA-ZA). The PSD and TGA results confirmed with the SEM and XRD results. The SEM micrographs showed the CFA-ZA crystallites deposited on the undissolved (CFA) particles. This zeolite was used for the removal of (AR 66) from an aqueous solution. The removal process was affected by pH of solution, contact time, initial dye concentration, and the amount of adsorbents. The amount of (AR66) uptake on (CFA-ZA) was found to increase with a decrease of solution pH but increased with an increase in contact time, initial dye concentration, and the amount of adsorbents. The maximum removal efficiency of almost 100 % was achieved with an initial dye concentration of 25 mg/L, pH 4, dose adsorbent 250 mg/L, and 20 min contact time. The obtained adsorption data fit Freundlich isotherm better than Langmuir isotherm and (416.6 mg/g) adsorption capacity was attained. The adsorption kinetic process for (AR66) over (CFA-ZA) described by a pseudo second-order kinetic better than a pseudo first-order kinetic and the intraparticle diffusion models. (CFA-ZA) prepared from (CFA) has an extraordinary potential and effectiveness for the removal (AR66) from waste water. This zeolite can remove dyes from aqueous solutions with high efficiency about 100% and therefore it may consider as an alternative material to replace commercial and natural zeolite. Coal fly ash used to prepare the (CFA-ZA) in this work, is available in Canada in large amounts at zero cost. This adsorbent can be obtained from the power plants as waste material. The method of synthesis of (CFA-

ZA) from coal fly ash is simple. Therefore, from economic point of view, using this (CFA) as a source of production of (CFA-ZA) for removal of dyes from aqueous solutions is economically very attractive.

6.8 References

- [1] Reife, A., and Fremann, H.S., (1996)" Environmental Chemistry of Dyes and Pigments" Wiley, New York.
- [2] Neppolian, B., Choi, H.C., Sakthivel, S., Arabindoo, B., and Murugesan, V., (2002) "Solar/UV induced photocatalytic degradation of three commercial textile dyes" J Hazard Mater, 89, 303–317.
- [3] Robinson, T., McMullan, G., Marchant, R., and Nigam, P., (2001)"Remediation of dyes in textile effluent: a critical review on current treatment technologies with a proposed alternative" Bioresource Technol. 77, 247–255.
- [4] Zamora, P.P., Kunz, A., Moraes, S.G., Pelegrini, R., Moleiro, P.C., Reyes, J., and Dura, N. (1999)" Degradation of reactive dyes I. a comparative study of ozonation, enzymatic and photochemical processes" Chemosphere, 38, 835–852.
- [5] Ladakowic, L. z, Solecka, M., and Zylla, R., (2001)"Biodegradation, decolorization and detoxification of textile wastewater enhanced by advanced oxidation processes" J. Biotechnol. 89, 175–184.
- [6] Georgiou, D., Melidis, P., Aivasidis, A., and Gimouhopoulos, K., (2002)" Degradation of azo reactive dyes by ultraviolet radiation in the presence of hydrogen peroxide" Dyes Pigments, 52, 69–78.
- [7] Kapdan, IK, Kargi, F, McMullan, G, Marchant, R. (2002) "Effect of environmental conditions on biological decolourization of textile dyestuff by C.

versicolor." *Enzyme Microb Tech*, 26, 381–387.

[8] Kansal, S. K., Ali, A. H., and Kapoor, S. (2010)"Photocatalytic decolorization of bieberich scarlet dye in aqueous phase using different nanophotocatalysts" *Desalination*, 259, 147–155.

[9] Rodríguez, A., García, J., Ovejero, G., and Mestanza, M., (2009) "Adsorption of anionic and cationic dyes on activated carbon from aqueous solutions: Equilibrium and kinetics" *J Hazard Mater*, 172, 1311–1320.

[10] Chiou, M.S., Ho, P.Y., and Li, H.Y. (2004)"Adsorption of anionic dyes in acid solutions using chemically cross-linked chitosan beads" *Dyes Pigments*, 60, 69–84.

[11] Ma, J., Qi, J., Yao, C., Cui, B., Zhang, T., and Li, D. (2012)"A novel bentonite-based adsorbent for anionic pollutant removal from water" *Chem Eng J* , 200, 97–103.

[12] Fisher, GL, Chrisp, CE, and Raabe, OG. (1979) "Physical Factors Affecting the Mutagenicity of Fly Ash from a Coal-Fired Power Plant" *Science*, 204,879–81.

[13] Breck, D.W., (1974) "Zeolite Molecular Sieves" Wiley, New York.

[6] Abrishamkar, M., Azizi, S. N., and Kazemian, H., (2011)" The Effects of Various Sources and Templates on the Microwave-assisted Synthesis of BZSM-5 Zeolite" *Z Anorg. Allg. Chem.*, 637, 312.

[14] Gordon, J., Kazemian, H., and Rohani, S., (2012) " Rapid and efficient crystallization of MIL-53(Fe) by ultrasound and microwave irradiation" *Chem. Eng. J.*, 165, 966.

[15] Sabouni, R., Kazemian, H., Rohani, S., (2010)"A novel combined manufacturing technique for rapid production of IRMOF-1 using ultrasound and microwave energies" *Chem. Eng. J.*, 165, 966.

- [16] Querol, X, Moreno, N, Umaña, JC, Alastuey, A, Hernández, E, López-Soler, A, and Plana, F. (2002)"Synthesis of zeolites from coal fly ash: an overview" *Int. J. Coal Geol.*, 50,413–423.
- [17] Bukhari SS, Behin J, Kazemian H, Rohani S. (2015)"Conversion of coal fly ash to zeolite utilizing microwave and ultrasound energies: A review" *Fuel*, 140, 250–66.
- [18] Hussar, K, Teekasap, S, and Somsuk, N. (2011)" Synthesis of Zeolite A from By-Product of Aluminum Etching Process: Effects of Reaction Temperature and Reaction Time on Pore Volume" *Am. J. Environ., Sci*,7, 35.
- [19] Bukhari, SS, Behin, J, Kazemian, H, Rohani, S. (2015) "Synthesis of zeolite Na-A using single mode microwave irradiation at atmospheric pressure: the effect of microwave power. *Can. J. Chem. Eng.* 6, 93.
- [20] Janoš, P., Buchtová, H., Rýznarová, M., (2003) "Sorption of dyes from aqueous solutions onto fly ash" *Water Res* 37, 4938–4944.
- [21] Markandeya, G. C., Shukla, S. P., Sen Singh, D., and Murthy, R. C. (2015) "Characterization and adsorptive capacity of coal fly ash from aqueous solutions of disperse blue and disperse orange dyes" *Environ. Earth. Sci.*, 74,1125 –1135.
- [22] Cho, H., Oh, D., and Kim, K. (2005)"A study on removal characteristics of heavy metals from aqueous solution by fly ash" *J Hazard Mater* 127, 187–195
- [23] Mohan, S. and Gandhimathi, R. (2009) "Removal of heavy metal ions from municipal solid waste leachate using coal fly ash as an adsorbent" *J. Hazard. Mater.* 169, 1-3.
- [24] Sun, Z. , Li, C. ,and Wu, D. (2010)" Removal of methylene blue from aqueous solution by adsorption onto zeolite synthesized from coal fly ash and its thermal regeneration" *J. Chem. Technol. Biot.* 85, 6.

- [25] Apiratiku, R. I. and Pavasant, P. (2008) " Sorption of Cu²⁺, Cd²⁺, and Pb²⁺ using modified zeolite from coal fly ash" *Chem. Eng. J.*, 144, 2, 245-258.
- [26] Doyle, A. M., Alismaeel, Z. T., Albayati T. M., and Abbas A. S.,(2017) " High purity FAU-type zeolite catalysts from shale rock for biodiesel production", *Fuel*, 199 , 394–402.
- [27] Musyoka, NM, Petrik, LF, Balfour, G, Gitari, WM, Hums, E. (2011) "Synthesis of hydroxysodalite from coal fly ash using waste industrial brine solution. " *J Environ Sci Health Part A*, 46, 1699–1707.
- [28] Dehnavi, V, Luan, BL, Shoesmith, DW, Liu, XY, Rohani, S. (2013) "Effect of duty cycle and applied current frequency on plasma electrolytic oxidation (PEO) coating growth behavior" *Surf. Coat. Tech.*, 226,100–7.
- [29] Sing, K., Everett, D., Haul, R., Moscou, L., Peirotti, R., and Rouquerol, J., (1985) " Reporting Physisorption Data for Gas/Solid Systems with Special Reference to the Determination of Surface Area and Porosity " *Pure Appl. Chem.* 1985, 57, 603-619.
- [30] Rouquerol, F., Rouquero, J., Sing, K. S. W., Llewellyn, P. L, and Maurin, G, (1999) "Adsorption by powders and porous solids" Academic Press, Waltham, USA.
- [31] Akgu, M., Karabakan, A, Acar, O., and Yurum, Y. (2006) "Removal of silver (I) from aqueous solutions with clinoptilolite" *Micropor. Mesopor. Mat.* 94, 99–104.
- [32] Wang, S., Soudi, M., Li, L., and Zhu, Z.H. (2006) "Coal ash conversion into effective adsorbents for removal of heavy metals and dyes from wastewater" *J. Hazard. Mater.* B13,133, 243- 251
- [33] Banat, I.M., Nigam, P., Singh, D. and Marchant, R. (1996) " Microbial

Decolorization of Textile-Dye Containing Effluents: A Review" *Bioresource Technol.* 58, 217. [http://dx.doi.org/10.1016/S0960-8524\(96\)00113-7](http://dx.doi.org/10.1016/S0960-8524(96)00113-7)

[34] Gücek, A., Sener, S., Bilgen, S., and Mazmancı M. A. (2005) "Adsorption and kinetic studies of cationic and anionic dyes on pyrophyllite from aqueous solutions" *J. Colloid. and Interf. Sci.* 286, 53–60

[35] Jain, A.K., Gupta, V.K., Bhatnagar, A., and Suhas (2003)" Utilization of industrial waste products as adsorbents for the removal of dyes" *J. Hazard. Mater.* 101 ,31–42

[36] Ranjusha, V.P., Pundir, R., Kumar, K., Dastidar, M.G. and Sreekrishanan, T.R. (2010) " Biosorption of Remazol Black B Dye (Azo Dye) by the Growing *Aspergillus flavus*" *J. Environ. Sci. Health, Part A*, 45, 1256-1263. <http://dx.doi.org/10.1080/10934529.2010.493812>

[37] Chen, H. and Zhao, J. (2009)" Adsorption Study for Removal of Congo Red Anionic Dye Using Organo-Attapulgitite " *Adsorption*, 15, 381-389. <http://dx.doi.org/10.1007/s10450-009-9155-z>

[38] Mohammed, M. I., Abdul Razak, A. A., and Al-Timimi, D. A. H. (2014)" Modified Multiwalled Carbon Nanotubes for Treatment of Some Organic Dyes in Wastewater" *Adv Mater. Sci. Eng.*, Volume 2014, Article ID 201052, 10.

[39] Freundlich, H.M.F. (1906)." Over the adsorption in solution" *J. Phys. Chem.* 57–385. 470.

[40] Langmuir, I., (1918) "The adsorption of gases on plane surfaces of glass, mica, and platinum." *J. Am. Chem. Soc.* 40, 1361–1403.

[41] Renganathan, S., Kalpana, J., Kumar, M. D., and Velan, M. (2009)" Equilibrium and Kinetic Studies on the Removal of Reactive Red 2 Dye from an Aqueous Solution Using a Positively Charged Functional Group of the *Nymphaea*

rubra Biosorbent " Clean, 37 (11), 901 – 907

[42] Sarwa, P., Vijayakumar, R. and Verma, S.K. (2014) "Adsorption of Acid Red 66 Dye from Aqueous Solution by Green Microalgae *Acutodesmus obliquus* Strain PSV2 Isolated from an Industrial Polluted Site" Open Access Library Journal, 1: e712. <http://dx.doi.org/10.4236/oalib.1100712>

[43] Chebli, D., Bouguettoucha, A., Reffas, A., Tiar, C., Boutahala, M., Gulyas, H., and Amrane, A. (2016)" Removal of the anionic dye Biebrich scarlet from water by adsorption to calcined and non-calcined Mg–Al layered double hydroxides " Desalin Water Treat, 57, 22061–22073.

[44] Ho Y.S., and McKay G., (1999) "Pseudo-second order model for sorption processes" Process Biochem. 34, 451–465.

[45] Ahamad, R (2013) "Adsorption of dyes by non-conventional adsorbents. In: Bharati PK, Gajananda K (eds) Environmental health and problems "Discovery Publishing House Pvt Ltd., New Delhi, pp 107–140

[46] Weber, W.J. Jr., and Morris J.C., (1963)"Kinetics of adsorption on carbon from solution" J. Sanit. Eng. Div. ASCE 89 , 31–59.

[47] Hameed, B.H., Din, A.T.M., and Ahmad, A.L. (2007) "Adsorption of methylene blue onto bamboo-based activated carbon: kinetics and equilibrium studies" J. Hazard. Mater. 141(3):819–825.

[48] Cheung, WH, Szeto, YS, and McKay, G (2007) "Intraparticle diffusion processes during acid dye adsorption onto chitosan" Bioresource Technol. 98, 2897–2904.

Chapter 7

SYNTHESIS OF PURE ZEOLITE-X IN A FLOWSYNTH CIRCULATING BATCH MICROWAVE REACTOR FROM CLEAR SOLUTION EXTRACTED FROM COAL FLY ASH⁶

Abstract

The present work shows that pure phase of Na-X zeolite can be successfully synthesized via a microwave-assisted system in a flow process from a clear solution extracted from alkaline treated coal fly ash (CFA). The FlowSynth microwave reactor supplies continuous microwave irradiation for the circulating batch manufacturing of nanomaterials. The effect of crystallization time and temperature of circulating batch microwave on the yield and crystallinity of the produced zeolite was investigated. The synthesized crystalline zeolite Na-X was thoroughly characterized by XRF, XRD, SEM, EDX, and BET. The maximum crystallinity (99.13%) was achieved at an operating temperature of 85 °C, 124-W, and 4-h. Circulating batch flow microwave reactor enhances and accelerates the crystal growth of zeolite. The produced crystalline zeolite had a high purity.

⁶ This chapter is under review by Advance Powder Technology. Aldahri, T., Rohani, S. Adv. Powder Technol. (Submitted 2018).

Keywords: Coal fly ash, Synthesis, Microwave irradiation, Bench scale, Zeolite X, Extracted solution

7.1. Introduction

Coal fly ash (CFA), is a waste by-product of coal-fired power plants, that has serious and harmful effects on the environment [1]. To overcome this issue, investigations have been conducted on zeolitization of CFA as a raw source of silica (SiO_2) and alumina (Al_2O_3). Different types of zeolites have been synthesized such as Na-A [2, 3], Na-P [4, 5], ZSM-5 [6, 7], Na-X [8, 9, 10], and faujasite-Y [8, 9, 11]. One of the most interesting zeolites is Na-X because of its high cation exchange and adsorption capacity [13]. It is also used for removing and adsorbing gaseous emissions and for refining oil as a fluid catalytic cracking catalyst. [14, 15].

Successful conversion of coal fly ash (CFA) to Na-X zeolite was carried out utilizing different approaches [8, 9]. Hussar et al. [16] synthesized zeolite Na-A hydrothermally by using sodium silicate (Na_2SiO_4), sodium aluminate (Na_2AlO_3) and the by-product of an aluminum etching process. They found that high crystallinity of synthesized zeolite could be achieved under high reaction time and temperature. Also, ultrasound has been utilized to produce Na-X from CFA. According to Hums et al., pure phase of zeolites Na-X, Na-A, and sodalite (SOD) were synthesized via ultrasound-assisted prior to crystallization step, from the clear solution extracted from fused coal fly ash [17]. Moreover, microwave irradiation has been studied widely in batch mode to convert CFA into Na-X. Ansari et al. produced pure zeolite Na-X or a mixture of zeolites Na-A and Na-X by utilizing microwave-assisted hydrothermal heating in one step by controlling the reaction temperature and time [9].

Querol et al. [18] used a 10,000-L reactor to synthesize zeolite Na-P by conventional heating at ~ 150 °C, 0.35-MPa. with a solid/liquid ratio of 0.60-kg/L using a 2.4-M alkaline solution. In addition, Moriyama et al. [19], converted hydrothermally CFA into zeolite P in a 0.6-L reactor at temperature of 153 °C, a solid/liquid ratio of 0.91-kg/L, 0.48-MPa, and a 3-M alkaline solution. Although these approaches were used for the zeolitization of CFA, some economical and technical issues still exist at industrial scale. Remaining impurities (heavy and toxic metals) inside the produced zeolitic powder, and an expensive cost of processing are the most common issues at large scale [20]. To overcome these problems, extraction of SiO_2 and Al_2O_3 from coal fly ash followed by nucleation of zeolite in the clear phase could be considered as a potential solution. Under certain conditions of reaction time and temperature, additional sodium aluminate or sodium silicate must be added to adjust the Si/Al ratio. This approach shows a significant and remarkable result to produce a pure zeolite compared to the product produced via hydrothermal process from the CFA slurry. However, the yield from extracted solution is much lower than the hydrothermal process [17]. Although the conventional synthesis techniques have been conducted successfully at large scale, a quick, cheapen economically viable, and environmentally friendly process is desired for the conversion of CFA to zeolite. Microwave-assisted synthesis of zeolite from a CFA slurry was used [21] with a short reaction time [2, 4, 5]. The scale-up limitations related to the need of applying microwave irradiation to a large volume could be alleviated in a flow process. Circulating batch flow microwave-assisted synthesis is attractive as a potential technique for the production of zeolite from CFA. To the best of our knowledge, microwave-assisted zeolite synthesis from a clear solution in a bench FlowSynth circulating batch Microwave Reactor with a volume of 0.5-L, has not been reported.

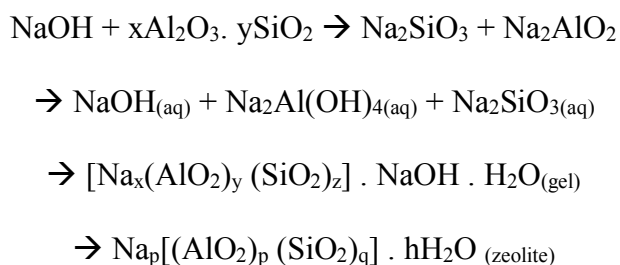
7.2. Materials and method

7.2.1 Materials

Raw coal fly ash (Class C) was obtained from a coal-fired power plant (OPG, Nanticoke) located in Ontario, Canada and stored in a sealed container before use. According to the American Society for Testing and Materials, ashes from bituminous coal combustion are known as class F with $\text{SiO}_2 + \text{Al}_2\text{O}_3 + \text{Fe}_2\text{O}_2 > 70\%$, while ashes from lignite coals are known as class C with $\text{SiO}_2 + \text{Al}_2\text{O}_3 + \text{Fe}_2\text{O}_2$ in the range 50 – 70% [22,23]. Analytical grade NaOH (Alphachem, Canada), Na_2AlO_3 anhydrous (Sigma-Aldrich, USA), and Na_2SiO_4 (Sigma-Aldrich, USA), were used as received. For the preparation of the solutions and washing, deionized water was used.

7.2.2 Method

The general reaction scheme for the alkaline treatment and zeolitization of CFA is given by [24]:



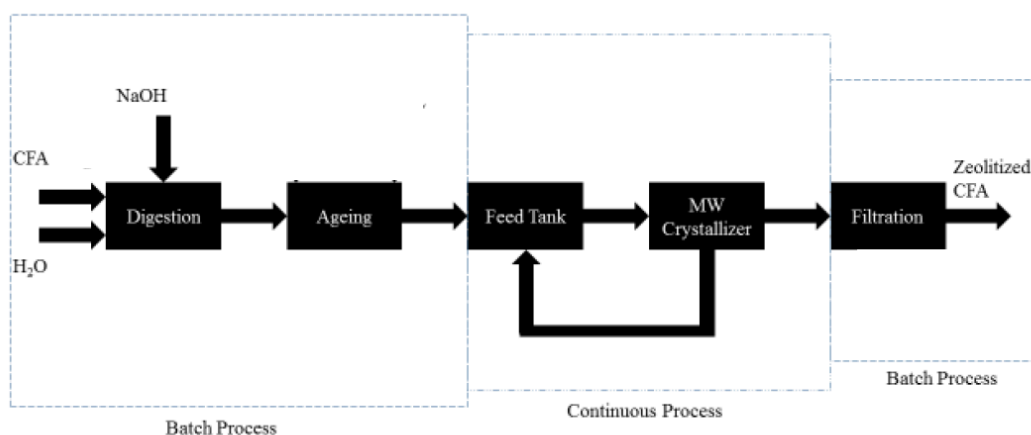
7.2.3 Extraction of silica (SiO_2) and alumina (Al_2O_3) from coal fly ash

A mixture of 14.0-g of raw CFA and 5.6-g of sodium hydroxide granules was dissolved in 140-mL deionized water to form an alkaline solution of 1-M. The alkaline hydrothermal process was applied to break down the fly ash crystalline phases and release the SiO_2 and Al_2O_3 content. Therefore, the mixture was subjected to conventional heating under atmospheric pressure at 90 °C for 4-h using a heater stirrer

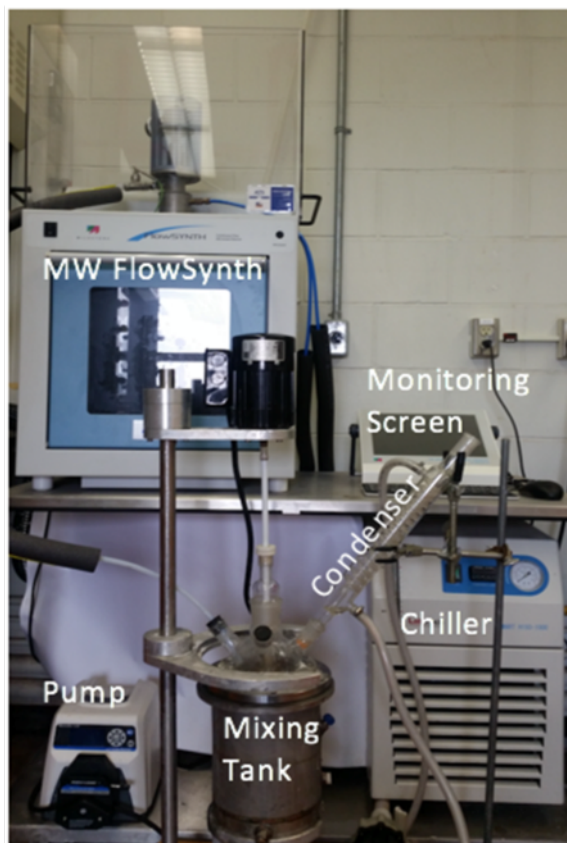
(Thermo Scientific, China). After hydrothermal treatment for 4-h in a 1000-mL glass flask reactor, SiO_2 and Al_2O_3 were dissolved into the liquid and extra deionized water was added while stirring the mixture at 200 rpm for 18-h. The mixture was filtered and the supernatant was collected as an aluminosilicate gel.

7.2.4 Circulating Batch Microwave Experiments (Crystallization stage)

An appropriate amount of filtrate solution was mixed with Na_2SiO_4 and Na_2AlO_3 to render a molar ratio of the sample: 3.0 Na_2SiO_4 : 0.5 Na_2AlO_3 : 192 H_2O . The resulting solution was left in an aging feed tank for 6-h at 85 °C. The aging feed tank was equipped with a heating jacket and a condenser for controlling reaction temperature. For the crystallization step, the mixture was then pumped into the microwave FlowSynth reactor for crystal growth at different temperatures; 78 °C, 85 °C, and 95 °C for 270-min. The reaction time was 4-h and the mixture flow rate was 5-mL/min. The system was kept at atmospheric pressure at 85 °C with the use of a reflux condenser and a recycle stream.



(a)



(b)

Figure 7-1: (a) The diagram [21] and (b) experimental setup of the microwave-assisted synthesis utilizing FlowSynth reactor

The solution was pumped into the FlowSynth MW reactor via a peristaltic pump (Masterflex L/S, Cole Parmer) with a tubing (L/S 15, Tygon Chemical) with an inner diameter of 4.8-mm and recirculated at a constant flow rate of 5-mL/min. The system took about 10-min to reach steady-state. After reaching the steady-state, 5-mL samples were withdrawn from the mixing/feed tank every hour. Mechanical mixer was used to control the level of mixing during the experiment. The goal of mixing is to either prevent or reduce temperature or concentration gradients, or to ensure good dispersion of multiple phases. Good mixing is preferable for several reasons, such as improving mass transfer in multi-phase systems, side-reactions or byproduct formation, or

ensuring fast heat transfer [25]. Less than 1000 ml of the mixture; 850 ml, from the Flow Synth MW reactor was recovered (Figure 7-1 (a)). 150 ml, was lost due to (1) the liquid content inside the Flow Synth MW reactor could not be completely removed, and (2) the liquid remained in the zeolitized CFA.

Microwave power was constant at 125 Watts during the experiments. Subsequently, the filtrate solid products were washed and dried overnight at room temperature. The experimental setup of the bench scale reactor; the Milestone FlowSynth circulating batch MW reactor (Milestone, Italy), with 1-L capacity is shown in Figure 7-1 (b) [21].

X-ray fluorescence spectroscopy (XRF) was used to determine the chemical composition of the raw CFA by using PANalytical PW2400 Wavelength Dispersive as shown in Table 3-1. To collect XRD data of the synthesized samples, Rigaku-MiniFlex powder diffractometer (Japan) was used; utilizing CuK_α ($\lambda = 1.54059 \text{ \AA}$) over the range of $5^\circ < 2\theta < 40^\circ$ with a step width of 0.02° . The XRD patterns of the synthesized zeolite samples were compared with the characteristic peaks of the standard Na-X from reference [26]. The specific characteristic peaks intensity of the synthesized zeolite X were determined by "peak fitting" algorithm in the MDI-Jade v 7.5 software. The characteristic peaks for the Na-X main peaks were found at 2θ of 6.12° , 10.0° , 15.34° , 23.31° and 30.94° . The crystallinity of the sample was determined from the characteristic peak areas of 111 (6.12°); by dividing the peak intensity of the product at $2\theta = 6.12^\circ$ by the peak intensity of the standard sample run for 48-h using conventional hydrothermal synthesis.

$$\text{Crystallinity (\%)} = \frac{\text{The peak intensity of the sample at } 2\theta = 6.10^\circ}{\text{The peak intensity of the standard sample at } 2\theta = 6.10^\circ} \times 100$$

(Eq. 7-1)

The average crystal dimension was calculated using Scherrer's equation [27]:

$$d = \frac{B\lambda}{\beta \cos\theta} ; \quad (\text{Eq. 7-2})$$

where d is the average crystal size (nm), B is the Scherrer's constant, λ is the wavelength of the X-ray (nm) and θ is the Bragg's angle (i.e. the angle of the maximum peak). β is the full width at half-maximum (FWHM) of the broad peak after correction for intrinsic instrumental line broadening and must be in radians [9].

Morphology of the produced zeolite was studied by scanning electron microscope (SEM) using a JSM 600F (Joel, Japan) operating at 10-keV of acceleration voltage. To measure the specific surface area, pore size and pore volume of selected Na-X, Burnauer-Emmett-Teller (BET) technique was used; using a Micrometrics Accelerated Surface Area and Porosimetry (ASAP 2010) surface area analyzer (Micrometrics, USA). Synthesized Na-X samples were degassed for 6-8 hours at 150°C, before the analysis. Percentage yield of synthesized zeolite Na-X was calculated by dividing the weight of the sample by the weight of the Na_2AlO_3 , and Na_2SiO_4 .

$$\text{Yield (\%)} = \frac{\text{Weight of synthesized Na-X}}{\text{Weight of (Na}_2\text{AlO}_3 + \text{Na}_2\text{SiO}_4)} \times 100 \quad (\text{Eq. 7-3})$$

7.3. Results and discussion

The chemical and mineral compositions of the raw CFA which was used as the main source of SiO_2 and Al_2O_3 are given in Table 3-1. The $\text{SiO}_2/\text{Al}_2\text{O}_3$ ratio was found to be 2.13, which is unsuitable for synthesis of zeolite Na-X under the medium concentration of NaOH solution. Therefore, extra aluminate or silicate precursors for adjusting the $\text{SiO}_2/\text{Al}_2\text{O}_3$ ratio were added [28].

Figure 7-2 presents the X-ray pattern of synthesis zeolite Na-X by a) microwave-assisted process from extracted solution of alkaline treated CFA in the circulating batch flow reactor, b) hydrothermally-synthesized at 75 °C for 48-h, and c) raw CFA. It can be noticed that hydrothermal and MW-assisted methods result in similar XRD patterns. Microwave-assisted synthesis zeolite Na-X had a very high crystallinity and purity with very sharp peaks. Also, the microwave-assisted synthesis reduced the reaction time compared to the conventional conversion which required 48-h at 75 °C [17]. Moreover, the purity and crystallinity of the synthesized zeolite X increased although the yield was lower as will be discussed later [17].

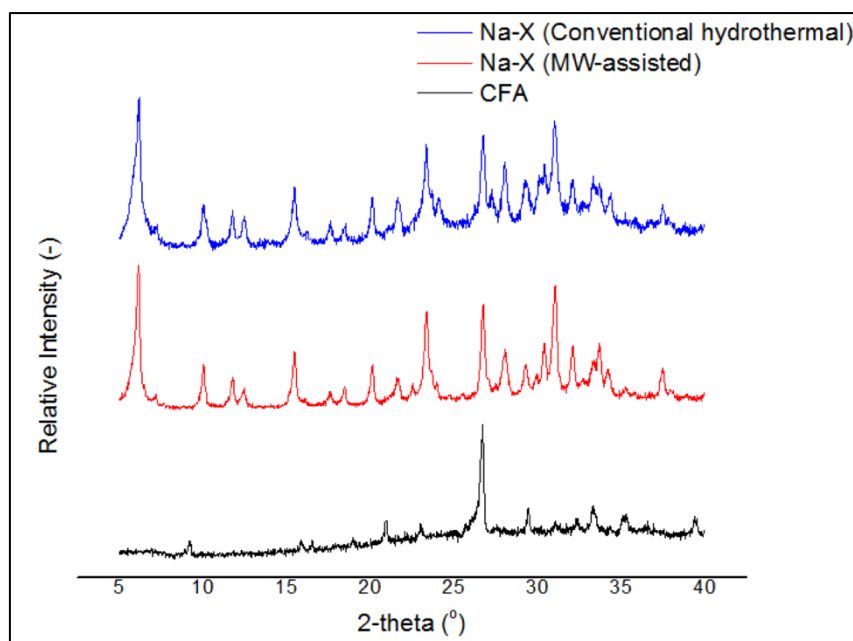


Figure 7-2: The XRD patterns of Na-X zeolite synthesized by MW-assisted in the circulating batch reactor, hydrothermally- synthesized, and raw CFA.

Aging process prior to the crystallization process for zeolitization of coal fly ash is a very important step. Figure 7-3 shows the XRD results of the sample with and without aging process. There are no characteristic peaks in the XRD results of the sample without aging step which means no zeolite Na-X was formed. In addition, a big

and strong hump appears which suggests the powder is still amorphous. However, XRD results of the sample with an aging step prior to crystallization step, shows characteristic peaks at 2θ of 6.12° , 10.0° , 15.34° , 23.31° and 30.94° as shown in Figure 7-2. For zeolite synthesis, there are three main steps: forming the building units, formation of zeolite nuclei during the aging step, and crystal growth by disposing the building units on the crystal's surface [29].

In present experiment to produce zeolites, I studied the effect of different independent variables on the crystallinity such as NaOH concentration, and MW irradiation power and time. Although mixing rate is considered as one of factors that has a strong effect on the quality of synthesized zeolite, I did not consider it as an independent variable in present work. However, Mainganye D. successfully synthesized zeolite P1 hydrothermally. He studied the effect of impeller design and agitation rates during the aging step of the synthesis process. His experimental results proved that the phase purity of zeolite Na-P1 was strongly affected by agitation and the type of impeller used during the aging step of the synthesis process [30].

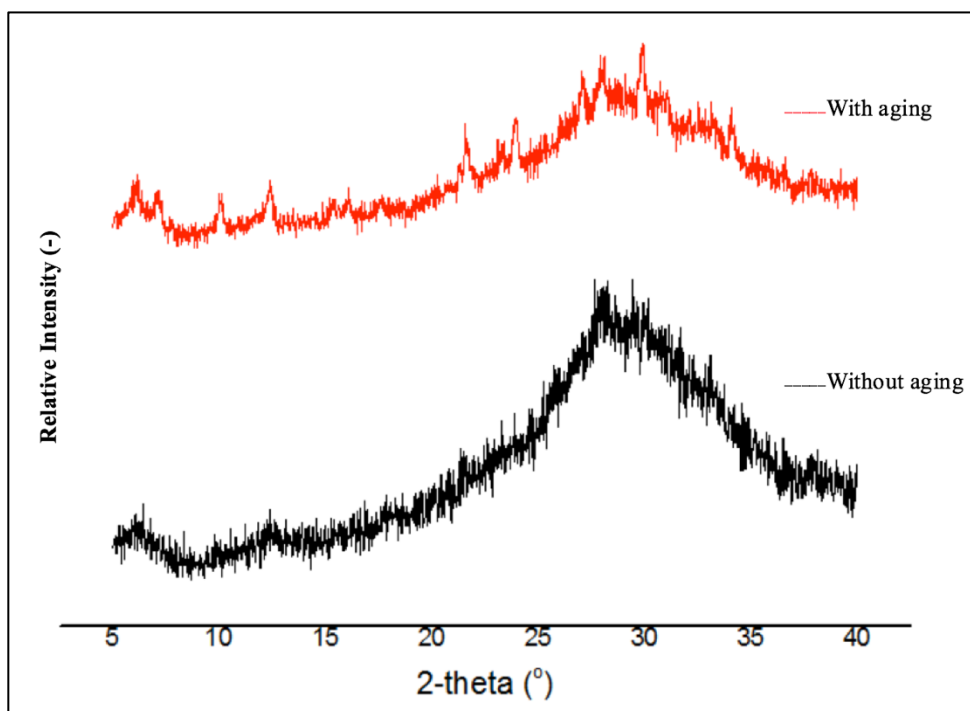


Figure 7-3: XRD patterns of the mixture after aging and without aging.

Adding extra Na_2SiO_4 and Na_2AlO_3 to the mixture is necessary to adjust the desired silica to alumina ratio. Na-X could not be formed without adding proper amounts of Na_2SiO_4 and Na_2AlO_3 to the extracted solution of CFA [4, 31].

The effects of crystallization temperature and time were investigated. Crystallization experiments were conducted at different crystallization temperature; 75 °C, 85 °C, and 95 °C. After 4-h of continuous microwave irradiation in the FlowSynth circulating batch flow microwave reactor, stable phases of zeolite Na-A, Na-X and Na-P with sharp and clear peaks as seen in Figure 7-4 were produced. According to Sang et al. [11], zeolite Y was transformed into zeolite P with increasing synthesis temperature. Also, transformation of zeolite A into zeolite X occurs by increasing reaction temperature. Building units of zeolite X, double 6-ring (D6R) and Sodalite (SOD), were formed with increasing synthesis temperature [29, 32]. Figure 7-5 shows

that up to 1-h no peaks appeared, however, after 2-h of crystallization, the characteristic peaks of zeolite Na-X started

to appear. With increasing the crystallization time, the characteristic peaks intensities increased and became sharper. Increasing crystallization time enhances crystallinity of zeolite Na-X which agrees with reference [9].

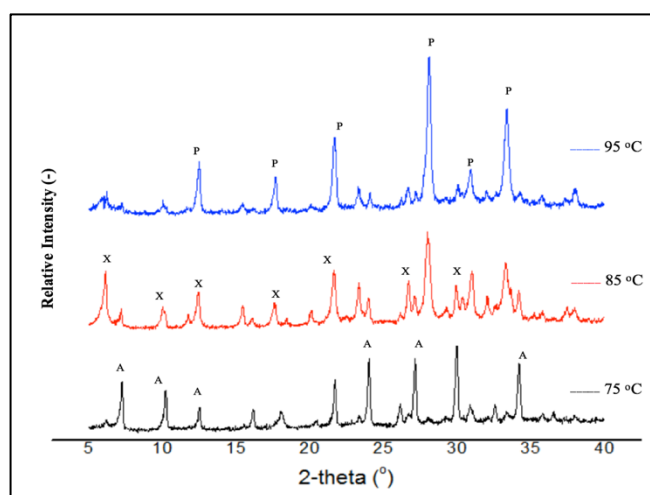


Figure 7-5: The XRD patterns of Na-X zeolites synthesized by the microwave heating at 85 °C after 1-h, 2-h, 3-h, and 4-h crystallization time.

SEM microphotographs of samples of zeolite at different crystallization temperatures; 85, and 95 °C, are presented in Figure 7-6. Figure 7-7 displays the Energy Dispersive X-ray spectroscopy (EDX) of chemical analysis. Observations were done at magnifications between 2.5 and 50,000. Figure 7-6 (a) displays SEM micrographs of synthesized Na-X from extracted solution of CFA. The product contains less impurities and heavy metals compared to the raw CFA, which has impurities as can be seen from the elemental composition analysis in Figure 7-7 and Table 3 -1 [5, 19]. Moreover, Figure 7-6 (b) shows the results of increasing synthesis temperature which produced zeolite Na-X with impurity of zeolite Na-P. This confirms the XRD results that were

mentioned in previous paragraphs. Also, Figure 7-7 (a, b) shows EDX results of the amount of impurities such as Ti, Mg, Fe, and Ca, in the final synthesized product. It is noted that the impurities in zeolite Na-X are significantly reduced compared to the starting raw CFA.

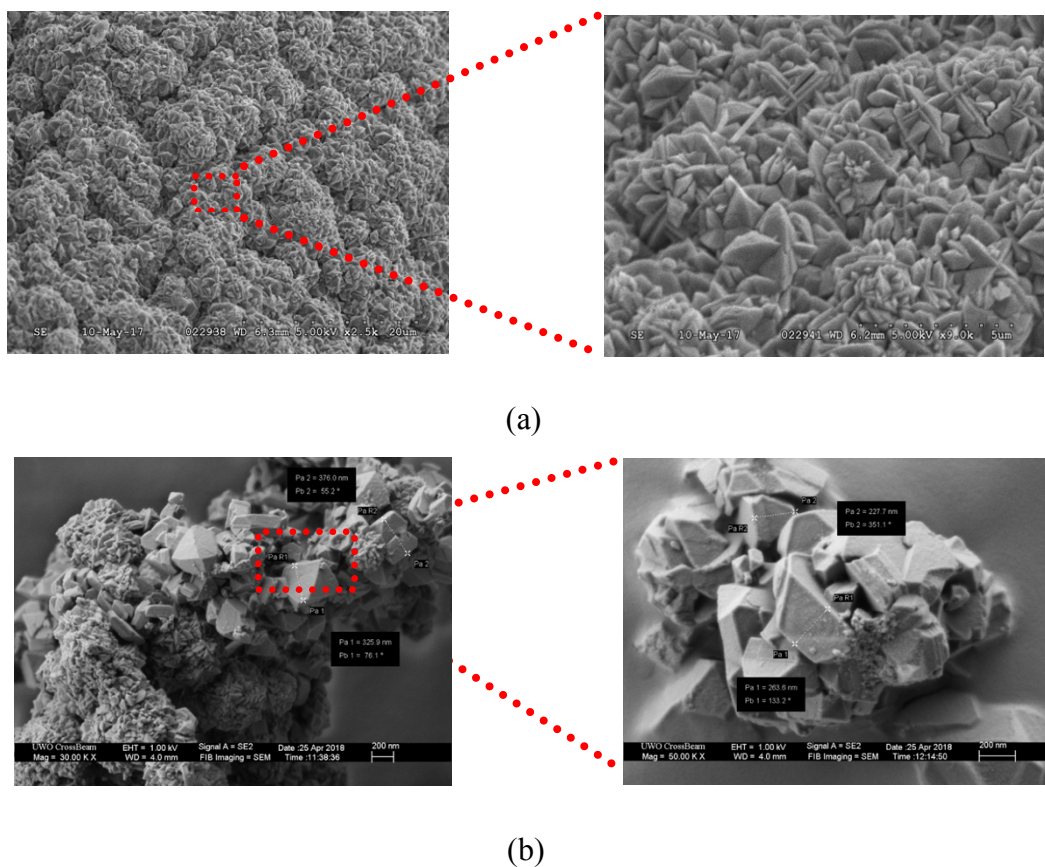
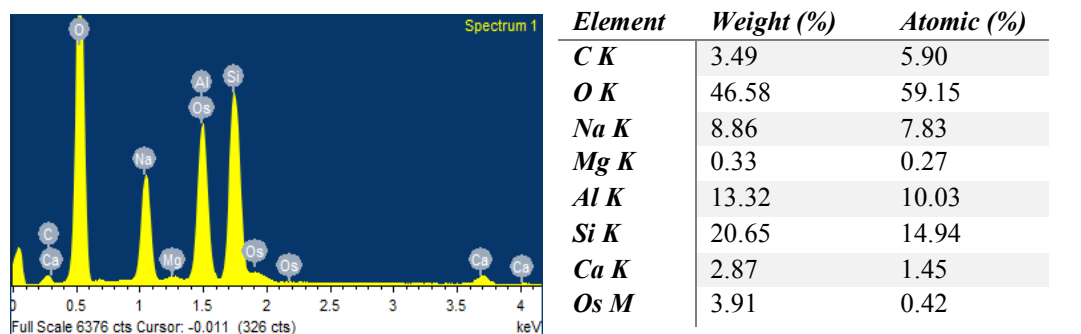
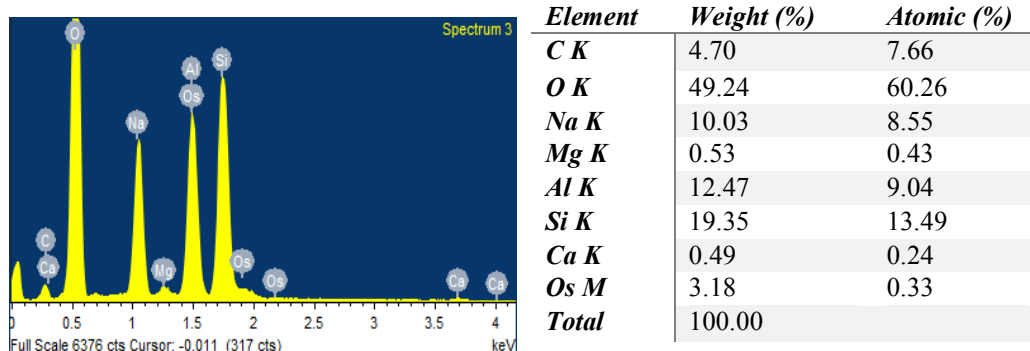


Figure 7-6: SEM images of the CFA and zeolite.



(a)



(b)

Figure 7-7: EDAX images and elemental composition of synthesized zeolite Na-X by MW-assisted synthesis a) 4-h, and b) 2-h of crystallization time.

Table 7-1 lists the BET surface area of the raw CFA, the Na-X zeolite synthesized hydrothermally, and by the microwave-assisted method. The proposed technique produced zeolite Na-X with surface area ($110.565 \text{ m}^2/\text{g}$), almost three times higher than that synthesized hydrothermally ($42.006 \text{ m}^2/\text{g}$). Nitrogen adsorption/desorption isotherms of the synthesized Na-X product are shown in Figure 7-8 and represent a type II isotherm. A type II isotherm is known for the nonporous aluminosilicate according to the Applied Chemistry (IUPAC) isotherm classification and the International Union

of Pure [33, 34]. Usually, the adsorption isotherm of type II is related to monolayer–multilayer adsorption on an open and stable external surface of a powder, which could be non-porous, macroporous, or to a limited extent microporous. The desorption isotherm is a distinct H₃-type hysteresis loop indicating mesoporous aluminosilicate [33]. The limited adsorption of N₂ inside the pores, could be attributed to the amorphous aluminosilicate that will block outside pores of the zeolite crystals.

Table 7-1: BET surface area of CFA and synthesized Na-X

	CFA	Zeolite Na-X	
		<i>Hydrothermally*</i>	<i>MW-assisted</i>
BET surface area (m ² /g)	15.47	42.006	110.565
Micropore volume (cm ³ /g)	3.3765	0.1110	0.0379

*[34]

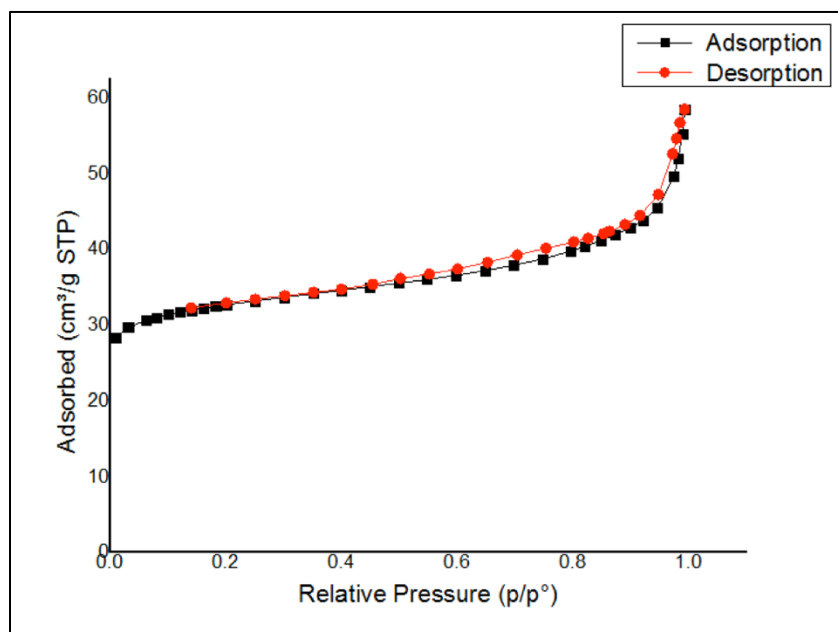


Figure 7-8: Isothermal plot of synthesized zeolite Na-X.

The average crystal size of the prepared zeolites at different synthesis times was calculated using Scherrer's from the peak at 2θ of 6.1° . The full width at half-maximum of the broad peak (FWHM), was calculated by "peak fitting" algorithm in the MDI-Jade v 7.5 software and the results are listed in Table 7-2. As can be seen in the Table 7-2, there is a proportional relationship between the average crystal size and synthesis time of synthesized Na-X. Increasing the average crystal size could be assigned to the increasing crystallization time that enhances the crystal growth and results in larger particles via agglomeration [9]. Also, the crystallinity of the synthesized product increases with increasing the synthesis time and this result agrees with reference [9]. In addition, the yield increases slightly with increasing synthesis time. As mentioned earlier, the yield of the proposed method is less than that of conventional hydrothermal method. However, optimizing the extraction condition could improve the extracted amounts of SiO_2 and Al_2O_3 from CFA and subsequently increase the yield of synthesized zeolite [17].

Table 7-2: Yield, crystallinity and crystal size of synthesized Na-X.

Synthesis Time (h)	Yield (%)	Crystallinity (%)	Crystal size (nm)
2	14.77	63.12	54.27
3	22.19	85.49	227.73
4	35.41	99.13	325.91

The mechanism for the formation of zeolite and microwave-assisted crystallization process is understood to a certain degree but not completely. However, it is known to provide volumetric heating, rather than conventional heating, which heats

by conduction and convection through a surface leading to a temperature profile within the reacting mixture.

Recent theory for zeolite synthesis from ash has been provided by Murayama et al., [35]. Their theory was based on the formation of amorphous aluminosilicate gel on the solid particles under high alkaline conditions followed by crystallization of zeolite due to the reaction between the gel and the alkali or dissolved species in the mother liquor solution. This theory advocated using the hydrothermal method for the zeolite synthesis process; it was based on type of zeolite produced as a function of time and by following the growth trend as observed in SEM images.

The general assumption is that the crystallization of zeolites proceeds via two steps: (1) nucleation of discrete particles of the new phase, and (2) growth of zeolite crystals. During the nucleation stage of zeolites, the smallest entities, “crystal nuclei,” with the identity of the new crystalline phase are formed. The crystal growth process of zeolites is classically described with typical S-shaped crystallization curves (Figure 7-9) [37].

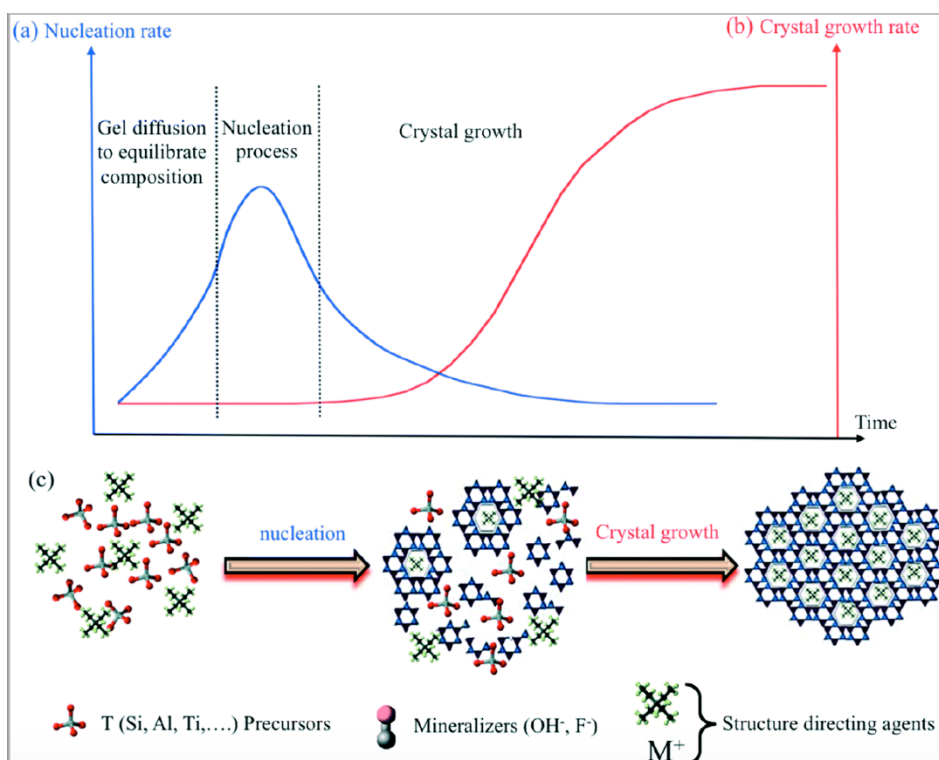


Figure 7-9 Schematic representation of the (a) nucleation rate and (b) crystal growth rate of zeolites described with a typical S-shaped curve, and (c) related rearrangements from amorphous particles into crystalline zeolite during the synthesis [37].

Even when the reaction mixture is stable, a large number of variables can impact zeolite crystallization. Among these variables, synthesis temperature and crystallization time used are the most influential due to the metastable nature of zeolites [38]. However, the type of raw materials (purities, reactivity), order of mixing, agitation, and aging each has a significant effect, too. It is common that the initial mixtures become gels with high viscosity due to the formation of amorphous aluminosilicate gel particles suspended in the basic medium.

In other words, zeolite crystals form on the CFA's surface via precipitation method as a result of fast homogenous heating of particles. Using microwave heating after the hydrothermal treatment at higher solid/liquid ratios increases the rate of crystal growth due to the surface activation characteristic of MW irradiation, which leads to a strong aggregation between zeolite particles and nuclei formed during the conventional heating step [39].

7.4 Conclusions

Pure zeolite Na-X was successfully synthesized from a clear solution containing SiO_2 and Al_2O_3 extracted from CFA, utilizing a FlowSynth circulating batch flow microwave reactor. The effects of crystallization time and temperature on the characteristics of the synthesized zeolite were investigated. Results of XRD data and SEM images showed that the highest percentage of crystallinity of the synthesized product was achieved after 4-h of continuous microwave irradiation at 85 °C in

circulating batch flow microwave reactor. Yield of zeolites obtained was lower than the conventional hydrothermal treatment, but the synthesis time was substantially reduced using microwave technology in the presented technique. The produced zeolite using the microwave-assisted circulating batch process was significantly more pure compared to the conventional hydrothermal. In conclusion, the pure zeolite-X could be synthesized in much shorter time using the circulating batch microwave heating method by controlling of the crystallization temperature and time.

7.5 References

- [1] I. Twardowska, J. Szczepanska, Solid waste terminological and long-term environmental risk assessment problems exemplified in a power plant fly ash study, *Sci. Total Environ.* 285 (2002) 29–51.
- [2] S.S. Bukhari, J. Behin, H. Kazemian, and S. Rohani, Synthesis of zeolite NA-A using single mode microwave irradiation at atmospheric pressure: The effect of microwave power, *Can. J. Chem. Eng.* 93 (2015b) 1081-1090.
- [3] X. Zhang, D. Tang, and G. Jiang, Synthesis of zeolite NaA at room temperature: the effect of synthesis parameters on crystal size and its size distribution, *Adv. Powder Technol.* 24 (2013) 689–696.
- [4] T. Aldahri, J. Behin, H. Kazemian, and S. Rohani, Synthesis of zeolite Na-P from coal fly ash by thermo-sonochemical treatment, *Fuel* 182 (2016) 494-501.
- [5] T. Aldahri, J. Behin, H. Kazemian, and S. Rohani, Effect of microwave irradiation on crystal growth of zeolitized coal fly ash with different solid/liquid ratios, *Adv. Powder Technol.* 28 (2017) 2865-2874.
- [6] X. Ou, S. Xu, J.M. Warnett, S.M. Holmes, A. Zaheer, A.A. Garforth, M.A. Williams, Y. Jiao, and X. Fan, Creating hierarchies promptly: Microwave-accelerated

synthesis of ZSM-5 zeolites on macrocellular silicon carbide (SiC) foams, *Chem. Eng. J.* 312 (2017) 1–9.

[7] N.L. Chauhana, J. Dasb, R.V. Jasrab, P.A. Parikha, and Z.V.P. Murthya, Synthesis of small-sized ZSM-5 zeolites employing mixed structure directing agents, *Mater. Lett.* 74 (2012) 115–117.

[8] P. Kunecki, R. Panek, M. Wdowin, and W. Franus, Synthesis of faujasite (FAU) and tschernichite (LTA) type zeolites as a potential direction of the development of lime Class C fly ash, *Int. J. Miner. Process.* 166 (2017) 69–78.

[9] M. Ansari, A. Aroujalian, A. Raisi, B. Dabir, and M. Fathizadeh, Preparation and characterization of nano-NaX zeolite by microwave assisted hydrothermal method, *Adv. Powder Technol.* 25 (2014) 722–727.

[10] B.Z. Zhan, M.A. White, M. Lumsden, J. Mueller-Neuhaus, K.N. Robertson, T.S. Cameron, and M. Gharghoury, Control of particle size and surface properties of crystals of NaX zeolite, *Chem. Mater.* 14 (2002) 3636–3642.

[11] Sh. Sang, Zh. Liu, P. Tian, Z. Liu, L. Qu, and Y. Zhang, Synthesis of small crystals zeolite NaY, *Mater. Lett.* 60 (2006) 1131–1133.

[12] B.A. Holmberg, H. Wang, and Y. Yan, High silica zeolite Y nanocrystals by dealumination and direct synthesis, *Micropor. Mesopor. Mater.* 74 (2004) 189–198.

[13] R. Szostak, *Handbook of Molecular Sieves*, Van Nostrand Reinhold, New York, (1992).

[14] A. Haas, D.A. Harding, and J.R.D. Nee, *Micropor. Mesopor. Mater.* 28 (1999) 325.

- [15] B. Liu, F. Chen, L. Zheng, J. Ge, H. Xi, and Y. Qian, Synthesis and structural properties of hierarchically structured aluminosilicates with zeolite Y (FAU), *RSC Adv.* 3 (2013), 15075–15084.
- [16] K. Hussar, S. Teekasap, and N. Somsuk, Synthesis of Zeolite a form by-product of aluminum etching process: Effects of reaction temperature and reaction time on pore volume, *Am. J. Environ. Sci.* 7 (2017) 35-42.
- [17] E. Hums, Synthesis of Phase-Pure Zeolite Sodalite from Clear Solution Extracted from Coal Fly Ash, *J. Thermodyn. Catal.* 8 (2017) 187.
- [18] X. Querol, J.C. Umaña, F. Plana, A. Alastuey, and A. Lopez-Soler, Synthesis of zeolites from fly ash at pilot plant scale. Examples of potential applications, *Fuel* 80 (2001) 857-865.
- [19] R. Moriyama, S. Takeda, M. Onozaki, Y. Katayama, and K. Shiota, Large-scale synthesis of artificial zeolite from coal fly ash with a small charge of alkaline solution, *Fuel* 84 (2005) 1455-1461.
- [20] E. Hums, Feasibility Study: Synthesis of zeolite from coal fly ash at a commercial scale in the context of fly ash leaching tests, part of ESKOM project: Feasibility of Application of Zeolites made from Fly Ash, (2008).
- [21] S. Bukhari, and S. Rohani, Continuous Flow Synthesis of Zeolite-A from Coal Fly Ash Utilizing Microwave Irradiation with Recycled Liquid Stream, *Am. J. of Environ. Sci.* 13 (2017) 233.244.
- [22] ASTM C618, Standard Specification for Coal Fly Ash and Raw or Calcined Natural Pozzolan for Use in Concrete, ASTM C618, (2015).

- [23] W. Franus, M. Wdowin, M. Franus, Synthesis and characterization of zeolites pre-pared from industrial fly ash, *Environ. Monit. Assess.* 186 (2014) 5721–5729.
- [24] S. Boycheva, D. Zgureva, and A. Shoumkova, Recycling of lignite coal fly ash by its conversion into zeolites, *CCGP* 7 (2014) 1–8.
- [25] E. Paul, *Handbook of Industrial Mixing, Science and Practice*. Wiley (2004).
- [26] M.M.J. Treacy, and J.B. Higgins, *Collection of simulated XRD powder patterns for zeolites*, Elsevier (2007).
- [27] M.M.J. Treacy, J.B. Higgins, and R.V. Ballmoos, *Collection of Particle Size is about 300 nm for the Sample Judged to Simulated XRD Powder Patterns for Zeolites*, third ed., New York, Elsevier (1996).
- [28] J.L.X. Hong, T. Maneerung, Sh. Nuo Koh, S. Kawi, and W. Chi-Hwa, Conversion of Coal Fly Ash into Zeolite Materials: Synthesis and Characterizations, Process Design, and Its Cost-Benefit Analysis, *Ind. & Eng. Chem. Research.* 56 (2017) 11565-11574.
- [29] T. Wakihara, A. Sugiyama, and T. Okubo, Crystal growth of faujasite observed by atomic force microscopy, *Micropor. Mesopor. Mater.* 70 (2004) 7–13.
- [30] Mainganye D. Synthesis of zeolites from South African coal fly ash: Investigation of scale-up conditions. At the CAPE PENINSULA UNIVERSITY OF TECHNOLOGY, Cape Town Campus. PhD Thesis, (2012).
- [31] J. Behin, S. Bukhari, H. Kazemian, and S. Rohani, Developing a zero liquid discharge process for zeolitization of coal fly ash to synthetic NaP zeolite, *Fuel* 171 (2016) 195-202.

- [32] J. Cejka, A. Corma, and S. Zones, *Zeolites and Catalysis, Synthesis, Reactions and Applications*, Wiley-VCH Verlag GmbH & Co. KGaA, Weinheim, 1 (2010).
- [33] F. Rouquerol, J. Rouquerol, and K.S.W Sing, *Adsorption by Powders and Porous Solids*, Academic Press. Waltham, USA, (1999).
- [34] Y. Liu, Q. Luo, G. Wang, X. Li, and P. Na, Synthesis and characterization of zeolite from coal fly as, *Materials Research Exp.* 5 (2018).
- [35] N. Murayama, H. Yamamoto, J. Shibata, Mechanism of zeolite synthesis from coal fly ash by alkali hydrothermal reaction, *Int. J. Miner. Process* 64 (2002) 1-17.
- [36] R. W. Thompson. *Synthesis Molecular Sieves*, Springer, 1 (1998) p. 1.
- [37] J. Grand, and S. Mintova. Mechanism of zeolites crystal growth: new findings and open. *Cryst. Eng. Comm.*, 18, 5 (2016) 650-664. DOI:10.1039/C5CE02286.
- [38] (a) D. W. Breck. *Zeolite Molecular Sieves*, Wiley-Interscience, New York, 1974. (b) S. P. Zhdanov *Adv. Chem. Ser.*, 101, 20.
- [39] J.R. Agger, N. Pervaiz, A.K. Cheetham, and M.W. Anderson, Crystallization in zeolite A studied by atomic force microscopy, *J. Am. Chem. Soc.*, 120 (1998) 10754-10759.

Chapter 8

RESEARCH FINDINGS AND RECOMMENDATIONS

8.1 Research findings

The research work of this thesis was focused on the synthesis of zeolite from coal fly ash utilizing a single-mode microwave unit and an ultrasound horn. The synthesis product samples were analyzed and characterized using XRD, SEM, BET, TGA, and CEC. The major conclusions from this research are as follows:

- 1) Results of this study have found that CFA was converted successfully to zeolite Na-P by using the thermo-sonochemical technique at low temperature ($\sim 100^{\circ}\text{C}$) and atmospheric pressure over 4 h. By applying the conventional heating for 1 h followed by 3 h of sonochemical treatment, Na-P zeolite was the major synthesized zeolitic phase with an impurity of hydroxysodalite. The crystallization of zeolite was hindered by introducing the ultrasound irradiation into the non-hydrothermal treated mixture. Thermo-sonochemical zeolitization of CFA increased its surface area and pore diameter. In conclusion, the ultrasound-assisted hydrothermal method facilitates the formation of Na-P zeolite from CFA by enhancing the rate of nucleation and shortening the crystallization time during the conversion process. The presented technique could be considered as a fast and eco-friendly zeolitization process with lower energy demands.

- 2) Utilizing MW irradiation at a high solid/liquid ratio was the next step of the initial conventional heating for a 6 h period. This is considered an eco-friendly technique to synthesize zeolite P from CFA, and it produced a higher yield of CFAZP, reducing the synthesis process time and energy consumption remarkably without affecting the zeolitic product quality. The XRD data and SEM images showed the product's relative peak intensity at 2θ : 28.1° and was comparable with the zeolite obtained hydrothermally with 24 h of conventional heating. Also, applying the MW irradiation has resulted in a narrower particle size distribution (PSD). Post-microwave heating enhanced the crystal growth of the existing nuclei formed during the initial 6 h of conventional heating.
- 3) An acid pre-treatment of raw CFA was applied prior to microwave irradiation to prepare two types of zeolite: Na-P (CFA-ZP) and Linde Type-A (CFA-ZA), which resulted in a synthesized, high-purity CFA-ZP and CFA-ZA zeolite with high pore volume and surface area.

The synthesized zeolites were modified by cationic surfactant (HDTMA) bromide. The Response Surface Method (RSM) was used to study the dependency of the Methyl Orange (MO) removal process on the pH of the solution, the initial dye concentration, and the mass of the modified zeolites. Also, the central composite design (CCD) method was applied to develop a quadratic model in each case. The predicted values, calculated using the quadratic models, were in good agreement with the response (% dye removal) for CFA-ZA and CFA-ZP ($R^2 = 0.9991$ and 0.986 , respectively). When the Na-P was used as an adsorbent, the pH of the solution had the strongest effect; whereas the adsorbent amount had the greatest influence on the dye removal rate when CFA-ZA was used. ANOVA results indicate the presence of interaction between all the variables, except pH and the

initial dye concentration, when using CFA-ZP as an adsorbent. The results obtained from the optimization of the MO removal process were 100% at pH 6.17, with initial MO concentration of 20 mg/L, and 1000 mg/L adsorbent mass. Results for CFA-ZA as an adsorbent were 91% at pH 5.15, with the initial MO dye concentration of 20.24 mg/L, and adsorbent mass of 1000 mg/L for CFA-ZP as an adsorbent. In conclusion, using CFA as a source for CFA-ZA and CFA-ZP production for dye removal from aqueous solutions can be economically viable.

- 4) Zeolite CFA-ZA was synthesized by a microwave-assisted method from coal fly ash as an abundant industrial waste. The synthesized product was characterized by XRD, SEM, TGA, and PSD. The XRD results show that an acid treatment of the raw CFA prior to a microwave irradiation produces a high purity zeolite CFA-ZA. Microwave-assisted synthesis resulted in both higher crystallinity and production of zeolite CFA-ZA. The PSD and TGA results confirmed this with the SEM and XRD results. This zeolite was used for the removal of Acid Red 66 (AR 66) from an aqueous solution. Different factors, such as pH of a solution, contact time, initial dye concentration, and number of adsorbents were affected by the removal process. The amount of AR 66 uptake on zeolite CFA-ZA was found to increase when the solution pH was lowered, but also increased with greater contact time, initial dye concentration, and the number of adsorbents used. The maximum removal efficiency of ~ 100% was achieved with an initial dye concentration of 25 mg/L, pH 4, dose adsorbent 250 mg/L, and 20 min of contact time. The obtained adsorption data fitted with the Freundlich isotherm better than the Langmuir isotherm, and 416.6 mg/g adsorption capacity was attained. The adsorption kinetic process for AR 66 over CFA-ZA described by a pseudo-second-order kinetic was better than a pseudo-first-order kinetic and the intraparticle diffusion models.

Zeolite CFA-ZA prepared from CFA has shown extraordinary potential for the removal of AR 66 from waste water. This zeolite can remove dyes from aqueous solutions with a high efficiency of about 100%, and therefore it may be considered as an alternative material to replace commercial and natural zeolite. Coal fly ash used to prepare the CFA-ZA in the present study is available in Canada in large amounts at zero cost. This adsorbent can be obtained from power plants as waste material. The method of synthesis of CFA-ZA from coal fly ash is simple and, from an economic point of view, using CFA as a source of CFA-ZA production for the removal of dyes from aqueous solutions is economically very attractive.

- 5) Utilizing a FlowSynth circulating batch microwave reactor resulted in the synthesis of pure zeolite Na-X successfully from a clear solution containing SiO_2 and Al_2O_3 extracted from CFA. The effects of crystallization time and temperature on the characteristics of the synthesized zeolite were investigated. Results of XRD data and SEM images showed that the highest percentage of crystallinity of the synthesized product was achieved after 4 h of circulating batch microwave irradiation at 85 °C. Although the yield of zeolites obtained was lower than the conventional hydrothermal treatment, the synthesis time was substantially reduced using microwave technology. The zeolite produced using the microwave-assisted circulating batch process was of significantly higher purity than the one synthesized by the conventional hydrothermal method. The pure zeolite-X can be synthesized in a much shorter time frame using the circulating batch microwave heating method by controlling the crystallization temperature and synthesis time.

S.S Bukhari et al. who were worked in my group, synthesized zeolite Na-A utilizing microwave-assisted and ultrasound-assisted methods from coal fly ash in small scale (~ 20 ml) and bench scale (~ 500 ml) using both batch and continuous systems [1- 4]. They needed to add extra Al_2O_3 to adjust the $\text{SiO}_3/\text{Al}_2\text{O}_3$ ratio and synthesized zeolite Na-A. To compare, in my thesis, I synthesized different types of zeolites, such as Na-P and Na-X, utilizing microwave-assisted and ultrasound-assisted methods from coal fly ash in small scale (~ 20 ml) and bench scale (~ 500 ml) using both batch and batch circulating systems. Moreover, I synthesized zeolite Na-P from CFA without add chemicals to adjust the $\text{SiO}_3/\text{Al}_2\text{O}_3$ ratio. The $\text{SiO}_3/\text{Al}_2\text{O}_3$ ratio of the raw CFA was suitable to synthesize zeolite, ~ 2.13, as shown in Table 3-1.

8.2 Recommendations for further research

8.2.1 Extraction of SiO_2 and Al_2O_3 from CFA

The amount of SiO_2 and Al_2O_3 extracted from CFA through the digestion step is an important factor in the zeolite synthesis process. The calculated yield of zeolitic product during the indirect conversion and during the direct hydrothermal conversion (as seen in data from Chapter 7) was different. Optimizing the extraction conditions, such as NaOH concentration, stirring speed, and extraction time, could improve the extracted amounts of SiO_2 and Al_2O_3 from CFA and subsequently increase the overall yield of synthesized zeolite.

8.2.2 Aging step of CFA prior to crystallization process for zeolitization

Regarding the XRD data seen in Chapter 7, the aging process of CFA plays the main role in zeolite synthesis. Without the aging step, the final product is amorphous

and no zeolite crystal is formed. Optimizing the aging conditions, such as aging temperature and time, could improve the yield of synthesized zeolites.

However, there is an aspect concerning the synthesis process which was not within the objectives of this thesis that need to be investigated such as the effect of agitation during the hydrothermal treatment/crystallisation step for all zeolite Na-P, X, and zeolite A.

8.2.3 Bench-scale FlowSynth circulating batch Microwave Reactor

For future work, this novel approach for zeolite crystallization in a FlowSynth circulating batch Microwave reactor still has much scope for optimization. It could be of benefit to study the effect of the resident time of the mixture inside a circulating batch MW flow reactor on the conversion rate (i.e. yield of synthesized zeolite). Also, conduct the experiment for zeolite crystallization in a MW circulating batch reactor under a certain pressure and investigate the effect of the pressure on the rate of conversion; yield of synthesized zeolite.

8.2.4 Filtration of CFA prior to zeolitization

The SEM data from Chapter 4 shows that, via microwave-assisted synthesis of zeolite from CFA, zeolite particles are formed on the surface of the undissolved CFA particles. Thus, the zeolitized (CFAZ) has a core of unreacted CFA particles; however, the work in Chapter 6 has shown that the undissolved CFA particles could be separated from the clear solution after the digestion step and zeolites are formed using the extracted aluminum and silicon in the clear solution. The zeolites formed in the clear solution are of high purity and do not have heavy metals that may exit in the CFA. Therefore, they can be used for a variety of applications compared to the CFAZ.

8.2.5 Other applications of zeolitized CFA

The results of this thesis offer a significant contribution to synthesizing zeolite at low cost that is eco-friendly with useful applications, such as dye adsorbents in wastewater treatment. In addition, it could be use the synthesized zeolite A as a dishwasher and laundry detergents in water softeners field. The zeolite A traps Mg^{2+} and Ca^{2+} and releases Na^+ , so the water become softer. Also, since the synthesized zeolite X has a relative large surface area, it could be used for catalytic cracking in petrochemical field. Moreover, these synthesized zeolites could be use at gas separation, odor controlling, and removing radioactive particles from nuclear waste.

8.3 References

- [1] Bukhari S., and Rohani S.; Continuous Flow Synthesis of Zeolite-A from Coal Fly Ash Utilizing Microwave Irradiation with Recycled Liquid Stream. *American Journal of Environmental Sciences* 2017, 13 (3): 233.244. DOI: 10.3844/ajessp.2017.233.244
- [2] Bukhari S.S., Rohani S., and Kazemian H.; Effect of ultrasound energy on the zeolitization of chemical extracts from fused coal fly ash. *Ultrason. Sonochem.* 2016; 28:47–53. doi: 10.1016/j.ultsonch.2015.06.031.
- [3] Bukhari S.S., Behin J., Kazemian H., Rohani S.; A comparative study using direct hydrothermal and indirect fusion methods to produce zeolites from coal fly ash utilizing single-mode microwave energy. *J. Mater. Sci.* 2014; 49:8261–71.
- [4] Bukhari S.S., Behin J., Kazemian H., Rohani S.; Synthesis of zeolite NA-A using single mode microwave irradiation at atmospheric pressure: The effect of microwave power. *Can. J. Chem. Eng.* 2015; 93:1081- 90.

Appendix A

A HIGHLY EFFICIENT LOW-COST ADSORBENT FOR
ANIONIC DYE USING A SYNTHESIZED ZEOLITE P
FROM WASTE COAL FLY ASH⁸

Abstract

In this work, the CFA collected from a Canadian generation power was converted into a zeolitic material following a new three step preparation method. The XRD analysis was used to determine that the type of the zeolite synthesized was a zeolite P (CFA-ZP). CFA-ZP was also characterized by SEM. The CFA-ZP was applied to remove the anionic dye Congo Red (CR) from waste water. The effect of the different factors on the adsorption of CR have been studied: pH (3-10), initial concentration (250-2000mg/L), adsorbent dosage (0.1-0.5g/L) and contact time (0-20min). The modeling study indicates that the pseudo second order and Freundlich models fitted well the kinetic and equilibrium data respectively. An extremely high capacity of adsorption was found for the adsorption of the CR on CFA-ZP with a maximum of 7819mg/g.

⁸ This Appendix has been published in the conference ISERD- 493rd International Conference on Chemical and Biochemical Engineering (ICCBE), I. Harizi, T. Aldahri, S. Rohani, D. Chebli, and A. Bouguettoucha, 2018-2019, Stockholm, Sweden.

A.1 Introduction

The water pollution has always been an increasing problem for the environment and the human wellbeing. The waste water, coming from the different human activities: agricultural, commercial, industrial and others is known to be the source of large types of pollutants. Dyes of all kinds, especially azo dyes, are considered to be one of most harmful contaminants that are contained in the waste water. The use of azo dyes in the different industries is indispensable, principally in textile industries [1]. Azo dyes constitute a large class of synthetic dyes that are identified by the presence of at least one functional azo group in their chemical structure [2]. Azo dyes, found in the industrial waste water discharges, are renowned by their visibility, water solubility, degradability, toxicity, carcinogenicity and mutagenicity which cause serious and severe health and environmental problems [3]. Studies reported that around 10-15% of the dyes used for industrial purposes are ending up being released to the nature [4]. Therefore, in a tentative to reduce the harmful impact of the waste water, a wide range of research has been devoted to the treatment of the waste water effluents. For this purpose, several techniques have been applied: coagulation, filtration, degradation by means of special fungi, oxidation, ozonation, ion exchange, neutralization and photocatalysis [5], sonochemical degradation [6]. Due to its low cost, ease of operation and reliability, the adsorption is one of the most popular techniques used in colors elimination. It has shown, through the countless studies carried out, very effective results and great yields of removed dyes. The activated carbon was the most ordinarily used adsorbent. Later, tens of materials of different natures have been applied as alternative low-cost sorbents such as alumina, polysaccharide, biopolymers, clays [7],

layered double hydroxides [8], zeolites, graphene oxides [3]. Recently, there has been growing interest in the use of industrial waste to synthesis ecofriendly materials used as effective adsorbents [9]. The valuation of these unused sources (industrial waste) is of great interest since it contributes to diminish environmental pollution by reducing the pile of industrial waste and, then, exploiting that waste for water treatment purposes. The coal fly ash is a byproduct generated from coal burning in combustion power plants. It constitutes more than 70% of the combustion solid residues [10]. One of best ways to recycle the coal fly ash collected after combustion process is to use it for the synthesis of new materials useful in other fields such as pollutants removal. Many studies have proved that coal fly ash can be transformed to valued compounds efficient for dyes removal essentially zeolites, mesoporous silica [11], silica aerogels [12]. Zeolites are microporous, aluminosilicate minerals, which have a three-dimensional structure formed of alumina and silica interconnected with each other in crystalline way [13]. Generally, the main components of the coal fly ash collected from pulverized combusted coal are silica and alumina [14]. For that reason, a large range of research have investigated the possibility to convert the coal fly ash into zeolitic materials considering the coal fly ash as a good resource of the raw materials needed for the synthesis of zeolite. Following different ways of synthesis, studies have reported considerable number of zeolites of different types that have been successfully synthesis from coal fly ash: zeolite X [15], Zeolite A [16], Zeolite P [17], Zeolite Y [18], Chabazite [19]. Most of these zeolites synthesized from the CFA have found great applications in different fields basically for water contaminants removal from waste water such as heavy metals [20] and dyes [21]. Lot of efforts has been spent in order to find a synthetic method that maximize the conversion yield of the raw CFA to zeolite. In this work, a multi-step synthesis method has been adapted to convert raw coal fly

ash into zeolite P (CFA-ZP). The obtained zeolite was used as an adsorbent for the dye Congo Red. The influence of the pH, mass of adsorbent, the concentration of the solution and temperature were investigated. Kinetics and isotherm data were also obtained to understand the mechanism of the adsorption.

A.2 Materials and methods

In this section a description of the chemical materials used (Coal fly ash, Dye...) was provided. The preparation process of the adsorbent (CFA-ZP) and some characterization methods were also explained. In addition, preliminary adsorption experiments were presented in order to test the susceptibility of using the obtained product for valuable applications such as water treatment.

A.2.1 Materials

The Coal fly ash used in this work, as a starting material for zeolite preparation, is a Canadian waste collected from coal-fired power plant (OPG, Nanticoke) in Ontario, Canada. The main composition of the Coal fly ash has been defined by X ray fluorescence analysis to have an idea about the amount of silica and alumina that have direct relation with the formation of the zeolite. The coal fly ash is composed of 41.8w% of silica (SiO_2) and 19.6w% of alumina (Al_2O_3) and other oxides. High purity Hydrochloric Acid and Sodium Hydroxide products were supplied by Alphachem, Canada.

The pollutant chosen in this study to test the adsorption capacity of the obtained zeolite was a dye, since in the literature the most applications of zeolite were as heavy metal adsorbents. The adsorbent was the azo dye Congo Red (CR) is known by its multi uses, stability and its toxicity [22]. The chemical structure of the dye is shown in Figure A-1.

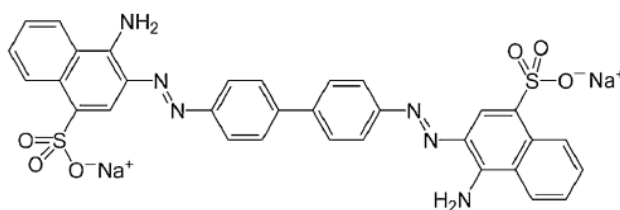


Figure A-1: Chemical structure of Congo red molecule.

A.2.2 Preparation of the adsorbent

Though the conventional hydrothermal conversion method, usually used to convert coal fly ash to zeolite, allows to obtain zeolite successfully [23], it gives generally a product of low quality in term of structural properties such as pore size and surface area and, also, low purity; Since it consumes only a small part of the alumina and silica contained in the coal fly ash used at the beginning. Recently, in addition to the conventional method, several ways have been followed in order to maximize the yield of conversion and ameliorate the quality of product by obtaining purer zeolite powder and well crystalline. New sources of energy such as microwave radiation [24], ultrasound [25] fusion followed by microwave [26] fusion followed by ultrasound [27] have been involved in the preparation mode to exploit as much alumina and silica found in the Coal Fly Ash as possible. In this study, the preparation of the zeolite from coal fly ash has been done in 3-step process. Firstly, a given mass of coal fly ash, passed trough 600um-seive, was subjected to hydrothermal treatment under high temperature of 800°C inside the furnace for 1h. The second step consisted on an acid treatment of the calcined coal fly ash. The calcined coal fly ash was added to a volume of 20ml of 0.1M hydrochloric acid solution and heated for 180 min at 65°C under slow stirring. Then the mixture was filtered, the solid phase is recovered, washed by deionized water

and has been let to dry. This two steps aim to get rid of the impurities which cover the external the surface and the internal pores of the coal fly ash particles, also they allow a faster and better access to the alumina and the silica [28]. the last step is the conversion phase or what is called the coal fly ash zeolitization. The solid particles dried were mixed with to 20ml of 1M NaOH solution in Teflon tube which was introduced into a single mode microwave irradiation (2.5-GHz, CEM cooperation, Discover, USA) at 250-W for 45-min. The mixture was filtered, and solid particles were collected and washed with deionized water. Finally, the powder was dried overnight at room temperature and the synthesized product zeolite P (CFA-ZP) was obtained.

A.2.3 Characterization

In order to identify the nature of the obtained product; the X-Ray diffraction was an indispensable analysis to be done. The XRD data were collected using MiniFlex powder diffractometer (Rigaku, Japan) under $\text{CuK}\alpha$ radiation ($\lambda = 1.54059\text{\AA}$) and at 2θ ranging from 3° to 40° with 0.02° increment. The scanning electron microscopy was also done to see the morphology of the product. SEM images has been obtained using Hitachi S 2600N microscope (Tokyo, Japan) at 5 kV. The zeta potential measurement has also been applied to define the point of zero charge of the product used as adsorbent in order to get an idea about the surface charge to better understand the adsorption mechanism. For the zeta potential measurements, equal masses of CFA-ZP were dispersed in equal volumes of DI water. HCl and NaOH solutions were used to adjust the pH of the suspension. 3000 zeta-analyzer was used to measure the zeta potential of CFA-ZP.

A.2.4 Sorption experiments

The CFA-ZP obtained has been applied as an adsorbent for the azo dye Congo Red.

The bath mode was followed to manipulate the adsorption experiments. In a 50ml flask, 20 mg of zeolite powder was added to 50ml of prepared dye solution of a known initial concentration. The mixture has been magnetically agitated, at room Temperature ($T \approx 23 \pm 2^\circ\text{C}$), with a speed of 200rpm and until the equilibrium is reached. The effect of several parameters on the adsorption yield has been studied to find the best condition in which zeolite is more effective. The effect of pH has been obtained by changing the pH of the CR solution between 3 and 10. pH was adjusted at the wanted values using drops of 1M HCl and NaOH solutions. We didn't go under pH value of 3 because for lower pH the control of the dye maximal wave length λ_{max} is quite difficult since it is different from λ_{max} at $\text{pH} \geq 3$. The effect of the adsorbent mass is also investigated where the mass of the zeolite has been changed in the range of 0.2g/L – 0.5g/L. The initial dye concentration has been explored for different initial concentrations 250mg/L - 2000mg/L. the effect of the temperature has also been examined by fixing the temperature degree at different values between 10°C and 40°C using a thermostat.

Kinetics data were collected as well. An adsorbent dosage of 0.4mg/L was added to 200mL of CR solution at different initial concentrations (250mg/L, 500mg/L, 1000mg/L and 2000mg/L). The mixture was put under stirring speed of 200rpm at room temperature. After each period of time a sample was taken until the equilibrium is installed.

Finally, the isotherm experiments were manipulated at room temperature $T = 23 \pm 1^\circ\text{C}$. Dye solutions of different concentrations were prepared: 50mg/L- 5000mg/L, a volume of 50mL was taken from each solution. The mixtures were put under a medium speed. After the equilibrium time is reached the suspensions were collected and analysed to determine the dye concentration after the adsorption.

The concentration of the suspensions after adsorption were centrifugated to separate

the solid from the liquid. The liquid phase of the samples was analysed using UV spectrometer (UV-1601Shi-madzu, Japan) at $\lambda_{\max} \approx 497\text{nm}$ to find the final concentration of the dye in the solution. The capacity of adsorption and the removal efficiency were, then, calculated using the following forms respectively:

$$Q_t \left(\frac{\text{mg}}{\text{g}} \right) = \frac{C_0 - C_t}{m} \times V \quad \text{(Eq. A-1)}$$

$$\eta(\%) = \frac{C_0 - C_e}{C_0} \times 100 \quad \text{(Eq. A-2)}$$

Where Q_t : Capacity of adsorption (mg/g), C_0 : Initial concentration (mg/L), C_t final concentration (mg/L), V : the volume of the dye solution (L), m : the mass of adsorbent (m), η : removal efficiency (%).

A.3 Results and discussions

A.3.1 Characterization of the materials

The XRD analysis was performed in order to identify the nature of the product, the crystal phases present in the material and to define which type of zeolite if the zeolite was successfully synthesised. The XRD patterns of the starting CFA and the obtained powder were presented in Figure A-2. The main crystalline phases that formed the raw CFA are Quartz Q, mullite M, Hematite H and cristobalite C. Their corresponding peaks are presented in Figure A-2. at specific angles. The main peaks of the phases M, Q, C and H forming the CFA appear at $2\theta = 9.4^\circ$, 26.77° , 29.54° and 33.48° respectively. The XRD pattern of the final product obtained after CFA conversion confirms that the CFA was successfully converted into zeolite. The comparison of the main peaks of the obtained zeolite (Figure A-2) with JCPDS data base of zeolites revealed that the main characteristic peaks appeared for the obtained zeolite matched well to a zeolite of type P. The characteristic peaks of CFA-ZP were, respectively, observed at $2\theta = 12.68^\circ$,

17.78°, 21.86°, 28.26°, 31.08° and 33.56°.

Figure A-3 shows the SEM images of the CFA and the synthesized CFA-ZP. The SEM picture of CFA (Figure A-3a) shows a spherical morphology where the CFA particles are spherically shaped with smooth surfaces. Figure A-3b shows noisy surfaces instead of the smooth surfaces confirming the conversion of the CFA and the formation of new particles. It could be seen that the particles formed are basically plates homogeneously distributed on the surface.

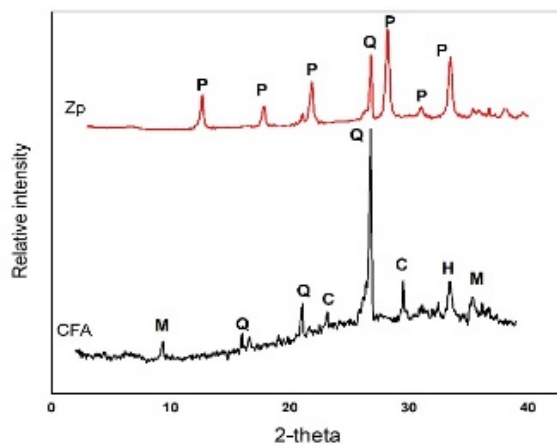


Figure A-2: The XRD patterns of CFA and P: CFA-ZP (Q: Quartz, M: mullite, H: Hematite, C: cristobalite, P: CFA-ZP)

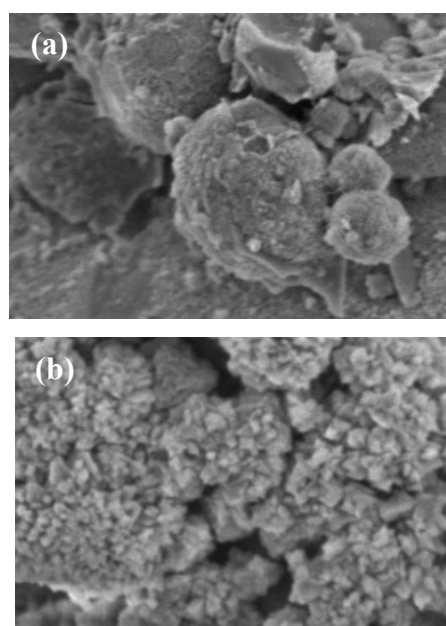


Figure A-1: SEM images of (a) Raw CFA (b) CFA-ZP

A.3.2 Adsorption results

A.3.2.1 The effect of the pH solution on dye adsorption

The capacity of dye adsorption on the different adsorbents is extremely dependent on the pH, as the adsorption has direct relation with the surface charge and the molecules ionization. The influence of the pH solution on the CR adsorption has been investigated. The results are displayed in Figure A-5. From Figure A-5 it could be observed that the CR removal by CFA-ZP is highly affected by the pH of the medium, where we can see a sharp drop in the capacity of adsorption when pH changes from acid to basic value. The best removal efficiency is obtained for pH value in the range 3-5. The more the solution is acidic the better removal is reached. For pH values, higher than 5, the adsorption capacity is less than 10%.

The explanation of this behavior can be done by referring to Figure A-6. Figure A-6 that exhibits the results of the zeta potential analysis shows that the point of zero charge (where the surface is of nil charge) is $pH_{zpc} = 5.37$. The positive values of zeta potential at $pH \leq pH_{zc}$ imply that the surface of the adsorbent carried a positive charge in this region due to the surface protonation. For pH values above the point of

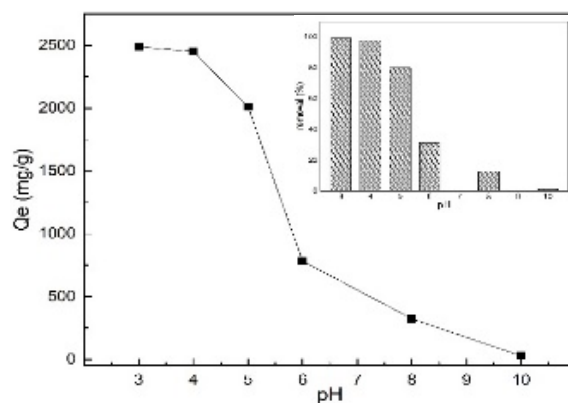


Figure A-3: pH effect on CR adsorption onto CFA-ZP

zero charge $\text{pH} \geq \text{pH}_{\text{zc}}$ the surface gained a negative charge due to its deprotonation. This electrostatics attraction phenomenon explains the adsorption of negatively charged dyes on a positively charged surface at pH values lower than P_{zc} of the zeolite which corresponds here to a value of 5,37. the pH chosen in this study was $\text{pH}=4$.

A.3.2.2 The effect of the adsorbent dosage

The adsorbent mass put in contact with the dye solution has a strong effect on the capacity of adsorption and the removal efficiency. The availability of a larger contacting surface allows to fix more dye molecules and then remove more dye from the liquid phase giving higher removal percentage. However, the capacity of adsorption decreases with the increase of the adsorbent mass due to the fact that it is calculated per unit of mass. The results of this study were presented in Figure A-6. It could be observed that a small dosage of 0.4g/L was very efficient to remove more than 99% of dye with a starting concentration of 1000 mg/L. less dosages are susceptible to remove more than 80% of the dye. For the adsorption experiments, the dosage of 0.4g/L was considered.

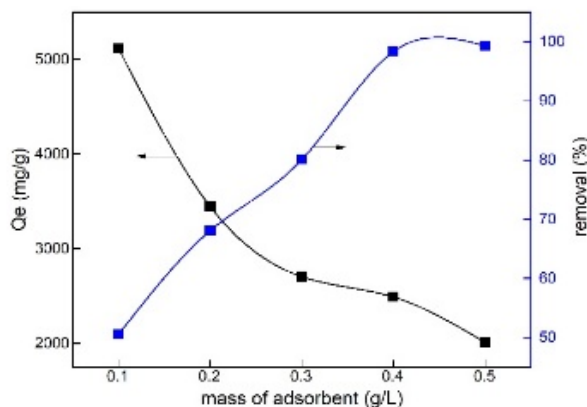


Figure A-4: The Adsorbent dosage effect on the adsorption of CR

A.3.2.3 The effect of the Initial concentration and the contact time

Figure A-5 shows the effect of the contact time and the initial concentration of the dye solution on the capacity of adsorption of CR on CFA-ZP. It could be seen that a larger contact time allows to adsorb more dye from the aqueous solution. The adsorption process is relatively fast where it could be observed that the equilibrium was reached in less than 30 minutes for all the concentrations. For the lowest concentrations, 6 minutes were enough to reach the maximum of adsorption with a removal efficiency of 99%. For the higher concentrations, the adsorption process would take more time to reach the equilibrium since the adsorption area is more occupied in the presence of extra dye molecules.

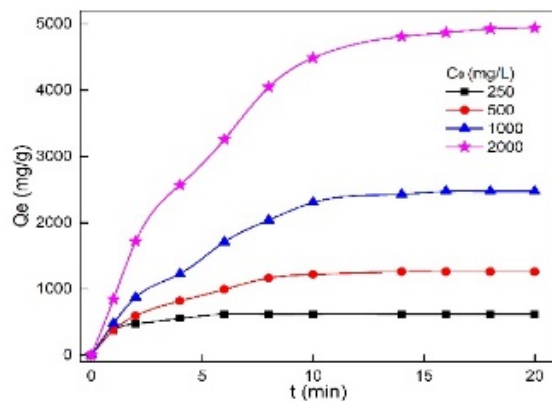


Figure A-5: The effect of the contact time and the initial concentration on the adsorption of CR on CFA-ZP

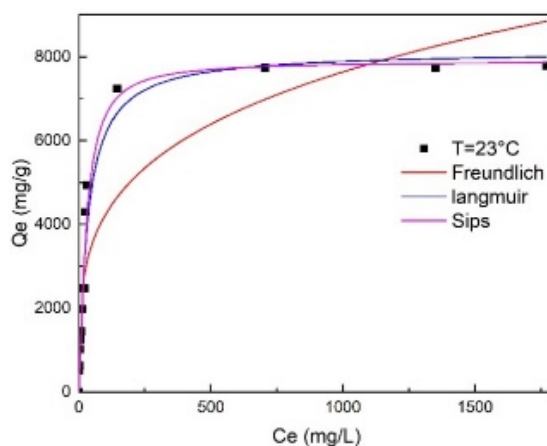


Figure A-6: Experimental and modeling data of the adsorption isotherm of Cr on CFA-ZP

A.3.2.4 The effect of temperature

The study of the temperature effect on the adsorption process allows to know if the adsorption is endothermic or exothermic. The results of this study are shown in Figure A- 7. The Figure A- 7 indicates that the adsorption of CR on CFA-ZP is slightly negatively affected by the temperature. When increasing temperatures, the capacity of adsorption of the dye on CFA-ZP is slightly decreasing.

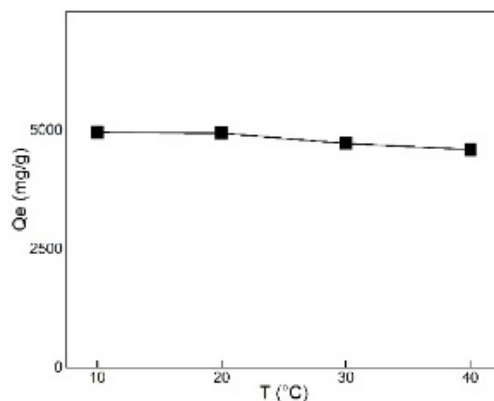


Figure A- 7: The effect of the temperature on the adsorption of CR on CFA-ZP

To determine the maximum of adsorption capacity of CR onto CFA-ZP, the isotherm of adsorption was performed at room temperature ($T=23^{\circ}\text{C}$). The results are displayed in Figure A-9. It could be observed that the capacity of adsorption of CR on CFA-ZP increases with the concentration until it stabilizes at an extremely high value estimated by more than 7500g/g .

A.3.3 Kinetic and equilibrium Modeling

To better understand the mechanism of the adsorption of CR on CFA-ZP, the modeling of the kinetics and isotherms data points were performed. Different models were tested to find the best one to fit the experimental data (pseudo first order, pseudo second order, Elovich...). The correlation coefficient of each model and their corresponding parameters were calculated and presented in Table A-1. The best model found to fit the kinetics was the pseudo second order (Table A-1) with $R_2 \geq 0.98$ and a good linear regression Figure A-10. As a consequence, the adsorption of CR on CFA-ZP is a chemisorption process.

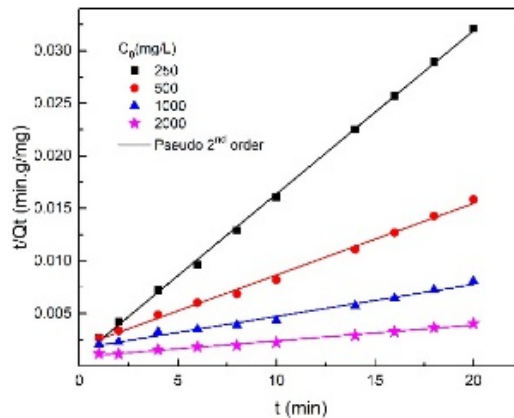


Figure A-8: Kinetics data points regression with pseudo second order model

Table A-1: Pseudo second order fitting results to kinetics data

Pseudo 2 nd order:		$\frac{t}{Q_t} = \frac{1}{k_2 Q_e^2} + \frac{1}{Q_e} t$			
C_0	250	500	1000	2000	
k_2 (g/mg.min)	$2.92 \cdot 10^{-3}$	$2.51 \cdot 10^{-4}$	$5.53 \cdot 10^{-5}$	$2.55 \cdot 10^{-5}$	
Q_e (mg/g)	645.16	1467.35	3279.66	6633.06	
R^2	1	1	0.99	0.99	

The non-linear regressions of the isotherm data obtained using MATLAB are represented in Figure A-6. It could be seen that the Langmuir and Sips models represent the highest correlation coefficients $R^2 \geq 0.978$ (Table A-2) and the closest capacity of adsorption from the experimental data. This can be explained by a favorable monolayer adsorption.

Table A-2: The parameters of the Langmuir and Sips model of the isotherm modeling of CR adsorption on CFA-ZP

Langmuir: $\frac{Q_e}{Q_m} = \frac{K_L C_e}{1 + K_L C_e}$	Sips: $\frac{Q_e}{Q_m} = \frac{(K_S C_e)^m}{1 + (K_S C_e)^m}$
Q_m (mg/g): $7.94 \cdot 10^3$	Q_m : $7.90 \cdot 10^3$
K_L (L/mg) :0.0309	K_S : 0.015
R^2 : 0.973	m : 0.7912
	R^2 : 0.978

The effect of the temperature has been explored to determine the thermodynamic parameters Gibbs free energy change (ΔG°), enthalpy (ΔH°) and entropy (ΔS°), of the CR adsorption on CFA-ZP. the results are reported Table A-3. the negative value of the ΔH° and ΔG° indicate that the CR is isothermally and spontaneously adsorbed on CFA-ZP, while the positive ΔS° suggests a rising randomness at the adsorption interface level.

Table A-3: Thermodynamic parameters of the adsorption of CR on CFA-ZP

ΔH° (kJ.mol ⁻¹)		ΔS° (J.K ⁻¹ mol ⁻¹)	
-56.82		97.00	
ΔG° (kJ.mol ⁻¹)			
10°C	20°C	30°C	40°C
-13.40	-14.08	-14.76	-15.43

A.4 Conclusion

In conclusion, this study demonstrated that the wasted coal fly ash collected from the power plants can be used to synthesis new materials that have great applications. The Coal fly ash has been successfully converted CFA-ZP by means of a developed method. The acid treatment of the CFA allows to obtain a well crystalline structure as confirmed by XRD analysis. The results of this research showed that the CFA-ZP is an efficient absorbent for anionic dyes. The capacity of adsorption of CR is remarkably high and it exceeded 7000mg/g, to our knowledge, it was the highest capacity of adsorption reported for CR removal. The pH of the solution was found to strongly affect the capacity of adsorption. The possessing temperature affected slightly the adsorption mechanism. The Pseudo second order model fits well the kinetics data. The Laugmuir and sips equations were the best models to describe the equilibrium adsorption of CR

on CFA-ZP. the thermodynamic study showed that the adsorption of CR on CFA-ZP is an isothermal spontaneous process. BET, TGA and more characterization analysis are under current investigations.

A.5 References

- [1] T. Robinson, G. McMullan, R. Marchant, and P. Nigam, "Remediation of dyes in textile effluent: A critical review on current treatment technologies with a proposed alternative," *Bioresour. Technol.*, vol. 77, no. 3, pp. 247–255, 2001.
- [2] E. Akceylan, M. Bahadir, and M. Yilmaz, "Removal efficiency of a calix[4]arene-based polymer for water-soluble carcinogenic direct azo dyes and aromatic amines," *J. Hazard. Mater.*, vol. 162, no. 2–3, pp. 960–966, 2009.
- [3] E. Mijowska, W. Konicki, and D. Moszyn, "Adsorption of anionic azo-dyes from aqueous solutions onto graphene oxide : Equilibrium , kinetic and thermodynamic studies," *J. Colloid Interface Sci.*, vol. 496, pp. 188–200, 2017.
- [4] F. Rafii, J. D. Hall, and C. E. Cerniglia, "Mutagenicity of Azo Dyes Used in Foods , Drugs and Cosmetics Before and After Reduction by Clostridium Species from the Human Intestinal Tract," vol. 35, pp. 897–901, 1997.
- [5] Y. M. Slokar and A. M. Le Marechal, "Methods of Decoloration of Textile Wastewaters," vol. 37, no. 4, pp. 335–356, 1998.
- [6] M. Abbasi and N. R. Asl, "Sonochemical degradation of Basic Blue 41 dye assisted by nanoTiO₂ and H₂O₂," *J. Hazard. Mater.*, vol. 153, pp. 942–947, 2008.
- [7] E. Errais *et al.*, "Efficient anionic dye adsorption on natural untreated clay : Kinetic study and thermodynamic parameters," *Desalination*, vol. 275, no. 1–3, pp. 74–81,

2011.

[8] I. Harizi, D. Chebli, and A. Bouguettoucha, "A New Mg – Al – Cu – Fe-LDH Composite to Enhance the Adsorption of Acid Red 66 Dye : Characterization , Kinetics and Isotherm Analysis," *Arab. J. Sci. Eng.*, 2018.

[9] I. Akin, G. Arslan, A. Tor, M. Ersoz, and Y. Cengeloglu, "Arsenic (V) removal from underground water by magnetic nanoparticles synthesized from waste red mud," *J. Hazard. Mater.*, vol. 235–236, pp. 62–68, 2012.

[10] R. William, R. G. Thiery, R. M. Schuller, and J. J. Subway, "ash : a review of the and proposed classification system with emphasis on environmental impacts," *Environ. Geol. NOTES*, vol. 96, 1981.

[11] J. Pizarro *et al.*, "Adsorption of Cu²⁺ on coal fly ash modified with functionalized mesoporous silica," *Fuel*, vol. 156, pp. 96–102, 2015.

[12] I. Smirnova, J. Mamic, and W. Arlt, "Adsorption of Drugs on Silica Aerogels," *Langmuir*, vol. 19, no. 20, pp. 8521–8525, 2013.

[13] I. Humelnicu and B. Adriana, "The removal of Basic Blue 41 textile dye from aqueous solution by adsorption onto natural zeolitic tuff: Kinetics and thermodynamics," vol. 5, pp. 274–287, 2016.

[14] F. Goodarzi, "Characteristics and composition of fly ash from Canadian coal-fired power plants," *Fuel*, vol. 85, pp. 1418–1427, 2006.

[15] J. D. C. Izidoro, D. A. Fungaro, J. E. Abbott, and S. Wang, "Synthesis of zeolites X and A from fly ashes for cadmium and zinc removal from aqueous solutions in single and binary ion systems," *Fuel*, vol. 103, pp. 827–834, 2013.

[16] N. Koshy and D. N. Singh, "Fly ash zeolites for water treatment applications," *J. Environ. Chem. Eng.*, vol. 4, no. 2, pp. 1460–1472, 2016.

[17] A. M. Cardoso, M. B. Horn, L. S. Ferret, and C. M. N. Azevedo, "Integrated

synthesis of zeolites 4A and Na – P1 using coal fly ash for application in the formulation of detergents and swine wastewater treatment,” vol. 287, pp. 69–77, 2015.

[18] M. Ahmaruzzaman, “A review on the utilization of fly ash,” *Prog. Energy Combust. Sci.*, vol. 36, no. 3, pp. 327–363, 2010.

[19] J. Dêdêcêk *et al.*, “Effect of Al/Si Substitutions and Silanol Nests on the Local Geometry of Si and Al Framework Sites in Silicone-Rich Zeolites: A Combined High Resolution ^{27}Al and ^{29}Si NMR and Density Functional Theory/Molecular Mechanics Study,” *J. Phys. Chem. C*, vol. 113, no. 32, pp. 14454–14466, 2009.

[20] W. Qiu and Y. Zheng, “Removal of lead, copper, nickel, cobalt, and zinc from water by a cancrinite-type zeolite synthesized from fly ash,” *Chem. Eng. J.*, vol. 145, no. 3, pp. 483–488, 2009.

[21] D. Mohan, K. P. Singh, G. Singh, and K. Kumar, “Removal of Dyes from Wastewater Using Flyash , a Low-Cost Adsorbent,” *Ind. Eng. Chem. Res.*, vol. 41, no. 15, pp. 3688–3695, 2002.

[22] V. Vimonses, S. Lei, B. Jin, C. W. K. Chow, and C. Saint, “Kinetic study and equilibrium isotherm analysis of Congo Red adsorption by clay materials,” vol. 148, pp. 354–364, 2009.

[23] N. Murayama, T. Takahashi, K. Shuku, H. Lee, and J. Shibata, “Effect of reaction temperature on hydrothermal syntheses of potassium type zeolites from coal fl y ash,” *Int. J. Miner. Process.*, vol. 87, pp. 129–133, 2008.

[24] M. Inada, H. Tsujimoto, Y. Eguchi, N. Enomoto, and J. Hojo, “Microwave-assisted zeolite synthesis from coal fly ash in hydrothermal process,” vol. 84, pp. 1482–1486, 2005.

[25] A. Sirkeciog, “Effects of ultrasound on zeolite A synthesis,” vol. 79, pp. 225–233, 2005.

- [26] S. Salman and B. Jamshid, "A comparative study using direct hydrothermal and indirect fusion methods to produce zeolites from coal fly ash utilizing single-mode microwave energy," *J. Mater. Sci.*, pp. 8261–8271, 2014.
- [27] S. Salman, J. Behin, H. Kazemian, and S. Rohani, "Conversion of coal fly ash to zeolite utilizing microwave and ultrasound energies : A review," *FUEL*, vol. 140, pp. 250–266, 2015.
- [28] A. M. Doyle, Z. T. Alismaeel, T. M. Albayati, and A. S. Abbas, "High purity FAU-type zeolite catalysts from shale rock for biodiesel production," *Fuel*, vol. 199, pp. 394–402, 2017.

Curriculum Vitae

Name: Tahani Hassan Aldahri

Place of birth: Kingdom of Saudi Arabia

Post-secondary Education and Degrees: 2018, Ph.D. Engineering Science
Faculty of Engineering
The University of Western Ontario
London, Ontario, Canada

Post-secondary Education and Degrees: 2012, Master of Science
Faculty of Science
The University of Western Ontario
London, Ontario, Canada

1998-2002, Bachelor of Science
Faculty of Science
King Abdul Aziz University
Jeddah, Kingdom of Saudi Arabia

Employment Lecturer, Taibah University, Saudi Arabia 2008-present.

Publications:

- [1] T. Aldahri, "The Behavior of a Falling Particle in a Funnel.", School of Graduate and Postdoctoral Studies, Western University, M.Sc. dissertation, 2012
<https://ir.lib.uwo.ca/etd/929>.
- [2] T. Aldahri, J. Behin, H. Kazemian, S. Rohani, (2016). "Synthesis of zeolite Na-P from coal y ash by thermosonochemical treatment". *Fuel*, 182: 494-501.
DOI: 10.1016/j.fuel.2016.06.019
- [3] T. Aldahri, J. Behin, H. Kazemian, S. Rohani, (2017) "Effect of microwave irradiation on crystal growth of zeolitized coal y ash with different solid/liquid ratios" *Adv Powder Technol*, ISSN 0921-8831, <https://doi.org/10.1016/j.appt.2017.08.013>.
- [4] T. Al-dahri, A. A. AbdulRazak, I. H. Khalaf, and S. Rohani, "Response surface modeling of the removal of methyl orange dye from its aqueous solution using two types of zeolite synthesized from coal y ash", *Mater. Express* 8, 234244 (2018).
- [5] I. Harizi, T. Aldahri, S. Rohani, D. Chebli, and A. Bouguettoucha, "Highly Efficient Low-Cost Adsorbent for Anionic Dye Using a Synthesized Zeolite P from Waste Coal Fly Ash", the conference ISERD- 493rd International Conference on Chemical and Biochemical Engineering (ICCBE), 2018-2019, Stockholm, Sweden.

Submissions under review:

- [1] T. Al-dahri, A. A. AbdulRazak, and S. Rohani, "Preparation and Characterization of Linde-Type A zeolite (LTA) From Coal Fly Ash by Microwave-Assisted Synthesis Method: its Application as Adsorbent for Removal of Anionic Dyes.", (*The Canadian J of Chem. Eng.*), 2018.

[2] T. Al-dahri, and S. Rohani, "Synthesis of Pure Zeolite-X in a FlowSynth circulating batchMicrowave Reactor from Clear Solution Extracted from Coal Fly Ash.", (Advance Powder Technology Journal), 2018.